ABSTRACT

Title of dissertation: MINIMAL LEFT-RIGHT SYMMETRIC MODEL,
                           NEUTRON ELECTRIC DIPOLE MOMENT
                           AND DARK MATTER

                           Haipeng An, Doctor of Philosophy, 2011

Dissertation directed by: Professor Xiangdong Ji
                           Department of Physics

In a class of other beyond-standard-model theories, CP-odd observables, such as the neutron electric dipole moment, receive significant contributions from flavor-neutral P-odd and CP-odd four-quark operators. However, considerable uncertainties exist in the hadronic matrix elements of these operators strongly affecting the experimental constraints on CP-violating parameters in the theories. Here we study their hadronic matrix elements in combined chiral perturbation theory and nucleon models. We first classify the operators in chiral representations and present the leading-order QCD evolutions. We then match the four-quark operators to the corresponding ones in chiral hadronic theory, finding symmetry relations among the matrix elements. Although this makes lattice QCD calculations feasible, we choose to estimate the non-perturbative matching coefficients in simple quark models. We finally compare the results for the neutron electric dipole moment and P-odd and CP-odd pion-nucleon couplings with the previous studies using naive factorization and QCD sum rules. Our study shall provide valuable insights on the present

hadronic physics uncertainties in these observables.

Using an effective theory approach, the neutron electric dipole moment in the minimal left-right symmetric model with both explicit and spontaneous CP violations is recalculated systematically. Using the state-of-the-art hadronic matrix elements, nEDM as a function of right-handed W-boson mass and CP-violating parameters is obtained. The most stringent constraint yet on the left-right symmetric scale in the minimal version of left-right symmetric model is obtained to be $M_{W_R} > (10 \pm 3)$ TeV.

Light WIMP (weakly interacting massive particle)-like signals were reported by dark matter direct detection experiments. WIMP candidates in this energy range can be constrained by various collider experiments. We show that colliders can impose strong constraints on models of low mass dark matter, in particular in the case that the direct detection interaction depends on the momentum of dark matter. We also find in the case of low mass dark matter, there are tensions between the observed relic abundance and collider constraints. Putting the constraints from collider physics, relic abundance and direct detection experiments, a large part of parameter space in different models can be ruled out.

MINIMAL LEFT-RIGHT SYMMETRIC MODEL, NEUTRON ELECTRIC DIPOLE MOMENT AND DARK MATTER

by

Haipeng An

Dissertation submitted to the Faculty of the Graduate School of the
University of Maryland, College Park in partial fulfillment
of the requirements for the degree of
Doctor of Philosophy
2011

Advisory Committee:
Professor Xiangdong Ji, Chair/Advisor
Professor Thomas D. Cohen
Professor Carter R. Hall
Professor Rabindra N. Mohapatra
Professor Da-Lin Zhang

To My Parents.

Acknowledgments

These five years as a graduate student has been becoming a special and important period of time in my life. I own my sincere appreciation to the people for their support and understanding.

First and foremost I'd like to thank my advisor, Professor Xiangdong Ji for giving me an invaluable opportunity to work on challenging and interesting projects in particle physics, nuclear physics and even experimental physics over the past five years and encouraging me to work not only with himself but also with other outstanding physicists. Prof. Ji sent me to UCLA to study dark matter direct detection experiment technologies. Although I finally decided to stay in the theoretical community, the valuable experience helps me build up a feeling in my mind of how to realize the theoretical models in the lab and how to think of a theoretical idea in an experimental way. Prof. Ji is not only an outstanding physicist, but also an excellent mentor. His influence on me is in every aspect of my life.

I would also like to thank Prof. Rabi Mohapatra from whom I have learned a lot of model building skills, including left-right symmetric models and supersymmetric models which are the main subjects of this thesis, as well as mirror symmetry model and leptogenesis. Prof. Rabi Mohapatra is also an outstanding teacher, from his 624 and 851 I learned not only the knowledge but also how to give lectures about quantum field theory.

I would also like to thank Prof. Lian-Tao Wang for guiding me into the field of collider physics and his hospitality when I was visiting University of Chicago.

the letters she made up for me, I might not be able to come back to Maryland to defend my thesis.

During these five years my friends Yongle Wu, Daohong Yao, Jing Li, Ming Du, Shihua Wen, Hua Chen, Xingshuo Zhao, Shuo Huang, Junfeng Huang have brought me so many happiness which will be printed in my mind forever.

I owe my deepest thanks to my family. My beloved mother passed away when I was in high school. My father supported me throughout my undergraduate life all by himself. Without the support from him I could not have the chance to study in Maryland. I would also like to thank my step mother and her lovely daughter for what they have been doing for the family.

Table of Contents

List of Figures

xi

List of Abbreviations

SM	Standard Model
vev	vacuum expectation value
CKM	Cabibbo-Kobayashi-Maskawa
LRSM	Left-Right Symmetric Model
LRS	Left-Right Symmetry
MSSM	Minimal Supersymmetric Standard Model
EDM	Electric Dipole Moment
nEDM	Neutron Electric Dipole Moment
χPT	Chiral Perturbation Theory
CP	Combined Charge Conjugation and Parity
WIMP	Weakly Interacting Massive Particle
BAU	Baryon-anti-baryon Asymmetry in the Universe
BBN	Big Bang Nucleosynthesis
$0\nu\beta\beta$	Neutrinoless Double Beta Delay Process
EW	Electroweak
d.o.f	Degrees of Freedom
SI	Spin-Independent
SD	Spin-Dependent
MI	Momentum-Independent
MD	Momentum-Dependent

Chapter 1

Introduction

1.1 Some Basic Features of Standard Model of Particle Physics

The known strong, weak and electromagnetic interactions can be described by the gauge interactions in the Standard Model (SM) of Particle Physics. The gauge group of SM is $SU(3)_C \times SU(2)_L \times U(1)_Y$. The quantum numbers of the fermion fields including quarks and leptons are shown in Table 1.1.

	$SU(3)_C$	$SU(2)_L$	$U(1)_Y$
$Q_L = \begin{pmatrix} u_L \\ d_L \end{pmatrix}$	3	2	1/3
u_R	3	1	4/3
d_R	3	1	$-2/3$
$L = \begin{pmatrix} \nu_L \\ e_L \end{pmatrix}$	1	2	1
e_R	1	1	-2

Table 1.1: Representations SM fermions in each gauge group of SM, where flavor indices are omitted.

At low energy scale, the $SU(2)_L \times U(1)_Y$ electroweak symmetry is spontaneously broken into $U(1)_{\rm em}$ by the Higgs mechanism. To break the electroweak symmetry, the Higgs boson is chosen to be a doublet under $SU(2)_L$ transformation and a singlet of $SU(3)_C$, and its $U(1)_Y$ charge is 1. The potential of the Higgs field can be written as

$$V(H) = \mu^2 |H|^2 + \lambda |H|^2 \ . \tag{1.1}$$

With a negative μ^2 the vacuum expectation value (vev) of Higgs can be nonzero and can be written as

$$\langle H \rangle = \begin{pmatrix} v/\sqrt{2} \\ 0 \end{pmatrix} \ , \tag{1.2}$$

where $v = \sqrt{-\mu^2/(2\lambda)}$.

In SM, the mass of quarks are also assumed to originate from the vev of Higgs through the following Yukawa couplings

$$\mathcal{L}_{\rm Yukawa} = -Y_u \bar{Q}_L H u_R - Y_d \bar{Q}_L \hat{H} d_R - Y_e \bar{L} \hat{H} e_R \ , \tag{1.3}$$

where $\hat{H} = (-i\sigma_2) H^*$, where σ_2 is the second Pauli matrix defined in Appendix A. The Yukawa couplings may not be diagonal. So the mass eigenstates of quarks may not be the same as flavor eigenstates. Since a squared matrix can be diagonalized by two Hermitian matrices, one can redefine the quark fields as

$$u'_L = V_L^u u_L \ , \quad u'_R = V_R^u u_L \ , \quad d'_L = V_L^d d_L \ , \quad d'_R = V_R^d d_R \ , \tag{1.4}$$

where the fields with a prime are mass eigenstates. Since the gauge interactions contain either lefthanded fermions or righthanded fermions, the redefinition of quark

2

fields bothers only those interactions containing different flavors. After the redefinition, the coupling between quarks and W-boson can be written as

$$\mathcal{L}_W \sim \bar{u}'_L W^+ V_{CKM} d_L \ , \qquad (1.5)$$

The combination $V_{CKM} \equiv V_L^u V_L^{d\dagger}$ is the famous Cabibbo-Kobayashi-Maskawa (CKM) matrix, and it is the only combination which can be observed in the quark rotation matrices. In SM, there is only one lefthanded charged gauge bosons, so one can only get the information of lefthanded quark rotations.

It is easy to see that V_{CKM} is a 3×3 unitary matrix which can be parameterized by three rotational angle plus six complex phases. However, some of the complex phases can be removed by redefinition of quark fields, and only one physical complex phase is left after the redefinition, this phase is usually called Dirac phase.

Righthanded neutrinos are not required to be present in the framework of SM, they are neutral under all gauge transformations in the SM gauge group. Therefore, a natural consequence of SM is that the mass of neutrino should be zero. However, the discovery of neutrino oscillation indicates the presence of non-vanishing tiny neutrino masses. How to understand the origin of neutrino masses is still a question.

1.2   Minimal Version of Left-Right Symmetric Model

Parity is violated in the electroweak sector of SM. The reason for parity violation is still mystery. The left-right symmetric model (LRSM) was motivated by the hypothesis that parity is a perfect symmetry at high-energy, and is broken spontaneously at low-energy due to the asymmetric vacuum [1]. Asymptotic restoration

3

of parity has a definite aesthetic appeal [2]. The model has a number of additional attractive features, including a natural explanation of weak hyper-charge in terms of baryon and lepton numbers, existence of right-handed neutrinos and entailed seesaw mechanism for neutrino masses, possibility of spontaneous CP (charge-conjugation-parity) violation, and natural solution for the strong CP problem. The model can be constrained strongly by low-energy physics and predicts clear signatures at colliders. It so far remains a decent possibility for new physics.

The LRSM is best constrained at low-energy by flavor-violating mixing and decays, particularly CP violating observables. In making theoretical predictions, the major uncertainty comes from the unknown right-handed quark mixing matrix, similar in spirit to that of the left-handed quark CKM mixing. The new mixing is a unitary matrix, depending on 9 real parameters: 6 CP violation phases and 3 rotational angles. All are physical after the left-handed CKM mixing is rotated into a standard 4-parameter form.

In Ref [3], we reported a systematic approach to analytically solving the right-handed quark mixing in a minimal version of LRSM (mLRSM), where the only requirement of parity invariance is the imposed prior to symmetry breaking, leaving automatically only one CP phase in the Higgs potential and one in the Yukawa couplings and leading to a theory with both explicit and spontaneous CP violations. This model therefore falls in-between the above two extreme cases and is free of the problems described above. Our approach is based on the observation that in the absence of any fine tuning, $m_t \gg m_b$ implies that the ratio of the two vev's of the Higgs bi-doublet, $\xi = \kappa'/\kappa$, is small and is of the order of m_b/m_t. In the leading-order

4

in ξ, we find a linear equation for the right-handed quark mixing matrix which can be readily solved. We present an analytical solution of this equation valid to $\mathcal{O}(\lambda^3)$, where $\lambda = \sin\theta_C$ is the Cabibbo mixing parameter. The leading right-handed quark mixing is nearly the same as the left-handed CKM matrix, except for additional phases which are fixed by ξ, spontaneous CP phase α, and the quark masses.

In mLRSM, after neglecting the contributions from FCNH and the charged higgs boson exchange, nEDM depends only on three parameters, $r \equiv (m_t/m_b)(\kappa'/\kappa)$, α, and M_{W_R}, where α is the new source of CP-violation. If $\alpha = 0$, nEDM predicted by the mLRSM will be the same as that predicted by SM, about five orders of magnitude smaller than the upper bound given by the current experiment [4]. Whereas for ϵ, there are two new contributions in mLRSM [3], the Dirac phase in the righthanded CKM matrix inherited from the lefthanded CKM matrix, and the spontaneous CP phase α. The new contribution from the Dirac phase is enhanced compared to the similar contribution in SM due to the chiral enhancement in the hadronic matrix element (see Ref. [5] for a good review). The contribution of the spontaneous CP-phase α must be adjusted to cancel the contribution of the Dirac phase. Therefore, in mLRSM there is a tension between nEDM and ϵ that one cannot only adjust α to suppress all the new CP-violation sources, and a large M_{W_R} is needed. As a result, nEDM and ϵ together give a lower bound on M_{W_R}, which turns out to be the most stringent to date in mLRSM.

1.3 Neutron Electric Dipole Moment

Neutron electric dipole moment (nEDM) has attracted considerable attention over more than half a century. For an elementary particle to have non-vanishing intrinsic EDM, simple analysis shows that parity-violating as well as time-reversal-violating interactions must be present. [T-violation is equivalent to CP-violation (combined charge-conjugation and parity) in local quantum field theory.] However, in the standard model (SM) of particle physics, such interactions arise only from flavor-changing Cabbibo-Kobayashi-Moskawa (CKM) matrix elements, which are strongly suppressed phenomenologically, yielding a very small neutron EDM of order 10^{-31} ecm. Therefore, an experimental observation of a large-size neutron EDM is an unambiguous signal for new physics, widely expected to exit somewhere between the electroweak symmetry breaking and TeV scales.

An efficient way to calculate the neutron EDM is to use the methodology of effective field theories (EFT). In this approach, one generates P-odd and CP-odd quark and gluon operators after integrating out the heavy particles (including heavy quarks, gauge bosons and new particles) and run these operators to a scale around 1 GeV where non-perturbative QCD physics becomes important. The effective degrees of freedom involves the light quarks (up, down and strange) and gluons. The CP-odd part of the lagrangian is generally written as a sum of CP-odd operators of different mechanical dimensions,

$$\mathcal{L}_{\text{CP-odd}} = \sum_{d=3}^{\infty} \sum_{i} C_{di}(\mu) \hat{O}_{di}(\mu) \ , \tag{1.6}$$

where $d = 3, 4, 5$, etc, is the mechanical dimension of the operators, μ is the renor-

malization scale (taken as $4\pi F_\pi$ in this paper) and i sums over operators of the same dimension. The dim-3 operator is the usual CP-odd quark mass term $\bar{q}i\gamma_5 q$, which can be rotated away through chiral rotations apart from the $U_A(1)$ anomaly. The dim-4 operator is the usual θ term $G\tilde{G}$. Dim-5 operators include quark electric and chromoelectric dipole operators. Dim-6 operators contain various four-quark operators and Weinberg three-gluon operator. The matrix elements of dim-4 and, to less extent, dim-5 operators have been studied extensively in the literature [6, 7, 8, 9, 10, 11, 12, 13, 14, 15], and the uncertainty of the estimates are typically at the level of factor 2. The contributions of these operators have also been studied extensively in the context of various new physics models (see Refs. [16, 17] for good reviews).

However, the matrix elements of dim-6 operators have been a challenge to estimate. In some beyond-SM theories such as the left-right symmetric model, dim-6 four-quark operators dominate the contributions to nEDM. In the literature, the only serious approach that has been proposed to calculate their matrix elements is the naive factorization method: breaking the four-quark matrix elements into the product of two-quark matrix elements between the nucleon states and between pion and vacuum [18, 19, 20]. While the factorization involving mesons can be and has been tested using lattice QCD [21] and the results may be trustable to within a factor of 2, the same is not known for matrix elements involving the nucleon states. The goal of this paper is to develop a chiral perturbation method combined with simple quark models to estimate the four-quark contribution to the nEDM with hopefully an improved accuracy.

7

The approach we are going to take is the standard chiral perturbation theory (χPT) (see, for example, Ref. [22, 23]) which has been used to calculate the contribution of θ-term to nEDM [8]. One of the successes of the chiral approach can be illustrated by the polarizabilities of the nucleon. The electric polarizabilities of the proton and neutron have been extracted from experimental data, $\alpha_p^{\text{exp}} = (10.4 \pm 0.6) \times 10^{-4} \text{fm}^3$, $\alpha_n^{\text{exp}} = (12.3 \pm 1.3) \times 10^{-4} \text{fm}^3$. The leading contribution in χPT comes from the pion-nucleon intermediate states,

$$\alpha_p = \alpha_n = \frac{5\alpha_{\text{em}}g_A^2}{96\pi F_\pi^2 m_\pi} \approx 11 \times 10^{-4} \text{fm}^3 \,, \tag{1.7}$$

which diverges linearly as $m_\pi \to 0$ and agrees well with the experimental data. One would expect then a similar pion dominance in the neutron EDM because the latter also involves the intermediate electric dipole excitations. Indeed a pioneering calculation by Crewther et al. found that the dominant contribution from the charged-pion chiral-loop diverges logarithmically as m_π goes to zero, and is proportional to the CP-odd pion-nucleon-nucleon coupling $\bar{g}_{\pi NN}$ [7]. In this work, we take this contribution as dominating and consider the four-quark operator contribution to $\bar{g}_{\pi NN}$. Of course, there are chiral-regular contributions to the nEDM which are of the same order in chiral power counting and numerically competitive or even dominating in the real world [17]. We will consider these contributions as well, although the model-dependence becomes unavoidable.

In the chiral approach, one first writes down the CP-odd and even lagrangian

in terms of meson and nucleon fields,

$$\mathcal{L} = \mathcal{L}_{\text{Goldstone-boson CP-odd term}} + \mathcal{L}_{\text{nucleon CP-odd mass term}}$$

$$+ \mathcal{L}_{\text{EDM term}} + \mathcal{L}_{\text{CP-odd } \pi-\text{N coupling}} + (\text{CP} - \text{even terms}) , \qquad (1.8)$$

where the Goldstone boson CP-odd lagrangian will generate terms annihilating π^0 and η in the vacuum, or in other words, will produce meson condensates. The condensates will turn some of the CP-even terms (as we shall see, those proportional to quark masses) in the chiral lagrangian into CP-odd contributions. This will generate an additional CP-odd nucleon-mass term, neutron EDM term and CP-odd pion-nucleon coupling. Once this is done, one can rotate away the CP-odd nucleon mass term, generating further contributions to the neutron EDM terms and the CP-odd pion-nucleon coupling.

After taking into all these contributions, one can calculate the nEDM generated by certain four-quark operator, and at the meanwhile get the upper bound on its Wilson coefficients. The upper bounds of some four-quark operators are listed in Table 1.2.

Armed with the hadronic matrix elements, we follow an effective theory approach to calculate the nEDM in mLRSM. Our goal here is to derive a factorization formula for nEDM in this model, with QCD and other short-distance physics in the Wilson coefficients, and with long-distance physics in hadronic matrix elements ready for, for example, lattice QCD calculations. Using the state-of-the-art hadronic matrix elements, we derive the best constraints on the model parameters. In particular, we find the most stringent bound yet on the left-right symmetric scale

Operators	Upper bound of $|C_4|/(\text{GeV}^{-2})$
$\bar{u}i\gamma_5 u\bar{d}d$	5×10^{-12}
$\bar{u}u\bar{d}i\gamma_5 d$	4×10^{-12}
$\bar{u}i\gamma_5 u\bar{s}s$	6×10^{-12}
$\bar{d}i\gamma_5 d\bar{s}s$	6×10^{-12}
$\bar{u}i\gamma_5 u\bar{u}u$	8×10^{-12}
$\bar{d}i\gamma_5 d\bar{d}d$	5×10^{-12}
$\bar{u}i\gamma_5 \sigma^{\mu\nu}u\bar{d}\sigma_{\mu\nu}d$	2×10^{-11}
$\bar{u}i\gamma_5 t^a u\bar{d}t^a d$	4×10^{-10}
$\bar{u}t^a u\bar{d}i\gamma_5 t^a d$	4×10^{-11}
$\bar{u}i\gamma_5 t^a u\bar{u}t^a u$	3×10^{-11}
$\bar{d}i\gamma_5 t^a d\bar{d}t^a d$	2×10^{-11}
$\bar{u}i\gamma_5 \sigma^{\mu\nu}t^a u\bar{d}\sigma_{\mu\nu}t^a d$	3×10^{-11}

Table 1.2: Upper bound on the Wilson coefficients of P-odd, CP-odd four-quark operators, calculated using the experimental data and hadronic matrix elements in this work.

10 ± 3 TeV, which is beyond the detection capability of the Large Hadron Collider (LHC) [24].

1.4   Collider Constraints On Dark Matter

It now appears established that dark matter accounts for about one quarter of the energy density, Ω, of the universe and plays an essential role in the formation of large scale structure in it. The identity of dark matter, however, remains unknown since all the particles in the successful standard model can be ruled out as candidates. What the dark matter particles are, how they interact with visible matter and how their relic abundance originates, constitute some of the fundamental mysteries of particle physics and cosmology today. The most compelling vision of dark matter is that dark matter is a weakly interacting massive particle (WIMP), which offers the possibility to understand the relic abundance of dark matter as a natural consequence of the thermal evolution of the Universe through the so-called WIMP miracle, which indicates that the interaction between WIMP and ordinary particle can be directly detected by various detectors.

Many direct detection experiments have been carrying on in order to look for signals induced by the interaction between dark matter particles and nuclei. Among these direct detection experiments, CoGeNT collaboration reported their results from ultra low noise germanium detector with a very low-energy threshold of 0.4 keVee in the Sudan Underground Laboratory [25]. The observed excess could be explained by a WIMP signal with mass in the range 6~11 GeV, and a WIMP-

nucleon spin-independent (SI) cross section $10^{-41} \sim 10^{-40}$ cm^2. More recently, the CRESST-II group also reported their preliminary results whose target is made of CaWO$_4$ and 32 events have been observed which cannot be explained by known background and might be induced by collisions between nuclei and WIMPs with a mass around or less than 15 GeV, and the cross section about a few times of 10^{-41} cm^2 [26]. On the other hand, with considering the smearing effect of the detector, XENON100 could also probe the low WIMP mass region [27]. However, a tension exists between the CoGeNT and CRESST-II results and the null-result of XENON100, although an issue of the scintillation efficiency of nuclear recoils ($\mathcal{L}_{\mathrm{eff}}$) of xenon at low nuclear recoil region still remains. The upcoming new XENON100 result with detecting power increased by one order of magnitude will be published soon, and the parameter space of this region will be further probed.

The signals produced by WIMPs in the direct detection detectors are assumed to be induced by the interaction between WIMP and nuclei. Therefore, such a WIMP can be produced at hadron colliders like Tevatron and LHC, and the signal for WIMPs is missing transverse energy. However, Tevatron has not reported any anomalous results related to such kind of signal which cannot be explained by SM physics. This can be used to set constraints to on WIMP couplings to the quarks, which in turn can be translated to constraints on direct detection cross section.

1.5 The Organization of This Thesis

The organization of the thesis is in the following. In Chapter 2, we first give the definition and basic properties of nEDM, and then we discuss nEDM induced by various P-odd and CP-odd operators with concentration on four-quark operators. In Chapter 3, we try to calculate nEDM in the framework of mLRSM using the effective theory approach and give the most stringent bound to M_{W_R}. In Chapter 4, we discuss the constraints from collider physics on low mass dark matters.

Chapter 2

P-odd and CP-odd Four-Quark Operator Contribution to Neutron

Electric Dipole Moment

2.1   Introduction

2.1.1   Definition of Electric Dipole Moment

The EDM of a charged system with a charge density distribution $\rho(\vec{x})$ is defined as

$$\vec{d}_{\mathrm{e}} = \int d^3x \, \vec{x} \rho(\vec{x}) \ . \tag{2.1}$$

Under the external electric field, the potential energy of this charged system is defined as

$$H = -\vec{E} \cdot \vec{d}_{\mathrm{e}} \ , \tag{2.2}$$

where $\vec{E}$ is the electric field.

From the definition we can see that the EDM of a charged system is a vector, and depends on the internal structure of the system. For an elementary particle, the only intrinsic vector is the spin, so one can define the EDM of an elementary particle in the following relation.

$$\vec{d}_{\mathrm{e}} = d_{\mathrm{e}} \frac{\vec{s}}{|\vec{s}|} \ , \tag{2.3}$$

where $\vec{s}$ is the spin of the particle, and the number d_{e} is defined as the EDM of this particle. Therefore, the Hamiltonian of EDM interaction between an elementary particle and the external field can be written as

$$H = -d_{\mathrm{e}} \frac{\vec{s}}{|\vec{s}|} \cdot \vec{E} \ . \tag{2.4}$$

There is no doubt that the electric field is a vector field. On the other hand, however, the spin of an elementary particle is an axial-vector, just like angular momentum. Therefore, the product of them gives a pseudoscalar, which is odd under both parity transformation and CP transformation. As a result, the existence of a nonzero EDM of elementary particle means there are Parity violating and CP violating interactions in the system.

Since we are interested in spin-1/2 particle, so $|\vec{s}| = 1/2$, and the corresponding Lagrangian in quantum field theory can be written as

$$\mathcal{L} = -\frac{1}{2} d_{\mathrm{e}} \psi \sigma_{\mu\nu} i \gamma_5 \psi F^{\mu\nu} \ , \tag{2.5}$$

where $\sigma_{\mu\nu} = \frac{i}{2}[\gamma_\mu, \gamma_\nu]$ and $\gamma_5 = i\gamma^0\gamma^1\gamma^2\gamma^3$ in the standard Dirac representation, which is discussed in Appendix A, ψ is a Dirac spinor.

2.1.2   Classification of P-odd and CP-odd Operators

An efficient way to calculate the neutron EDM is to use the methodology of effective field theories (EFT). In this approach, one generates P-odd and CP-odd quark and gluon operators after integrating out the heavy particles (including heavy quarks, gauge bosons and new particles) and run these operators to a scale around 1

GeV where non-perturbative QCD physics becomes important. The effective degrees of freedom involves the light quarks (up, down and strange) and gluons. The CP-odd part of the lagrangian is generally written as a sum of CP-odd operators of different mechanical dimensions,

$$\mathcal{L}_{\text{CP-odd}} = \sum_{d=3}^{\infty} \sum_{i} C_{di}(\mu) \hat{O}_{di}(\mu) \ , \tag{2.6}$$

where $d = 3, 4, 5$, etc, is the mechanical dimension of the operators, μ is the renormalization scale (taken as $4\pi F_\pi$ in this paper) and i sums over operators of the same dimension.

The dim-3 operator is the usual CP-odd quark mass term $\bar{q}i\gamma_5 q$, and the dim-4 operator is the usual θ term $G\tilde{G}$. The Lagrangian containing dim-3 and dim-4 operators can be written as

$$\mathcal{L}_4 = \sum_q m_q \sin\theta_1 \bar{q}i\gamma_5 q - \frac{g^2 \theta_2}{32\pi^2} G^{\mu\nu} \tilde{G}_{\mu\nu} \ , \tag{2.7}$$

where m_q is the mass of quark q. Using the anomalous $U(1)_A$ transformation, θ_1 can be transferred to θ_2 and only the combination $\bar{\theta} = \theta_1 + \theta_2$ is related to physically observable quantities.

The Lagrangian containing dim-5 operators can be written as

$$\mathcal{L}_5 = \sum_q d_q^E(\mu) O_q^E(\mu) + \sum_q d_q^C(\mu) O_q^C(\mu) \ , \tag{2.8}$$

where $O_q^E = -\frac{1}{2}\bar{q}\sigma^{\mu\nu}i\gamma_5 q F_{\mu\nu}$ and $O_q^C = -\frac{1}{2}\bar{q}\sigma^{\mu\nu}i\gamma_5 t^a q G_{\mu\nu}^a$, and $F_{\mu\nu}$ and $G_{\mu\nu}^a$ are the electromagnetic and gluon field strengths, respectively, and t^a are generators of the $SU(3)$ color gauge group.

16

For dim-6 operators, the effective Lagrangian can be written as

$$\mathcal{L}_6 = \sum_i C_i(\mu) O_{4i}(\mu) + C_g(\mu) O_g(\mu) \ , \tag{2.9}$$

where the four-quark CP-odd operators can be divided into two groups. The first group includes operators with two different light flavors [18]

$$
\begin{aligned}
O_{11} &= (\bar{q} i \gamma_5 q)(\bar{q}' q') \ , \\[4pt]
O_{12} &= (\bar{q} q)(\bar{q}' i \gamma_5 q') \ , \\[4pt]
O_{21} &= (\bar{q} i \gamma_5 t^a q)(\bar{q}' t^a q') \ , \\[4pt]
O_{22} &= (\bar{q} t^a q)(\bar{q}' i \gamma_5 t^a q') \ , \\[4pt]
O_3 &= (\bar{q} i \gamma_5 \sigma^{\mu\nu} q)(\bar{q}' \sigma_{\mu\nu} q') \ , \\[4pt]
O_4 &= (\bar{q} i \gamma_5 \sigma^{\mu\nu} t^a q)(\bar{q}' \sigma_{\mu\nu} t^a q') \ ,
\end{aligned}
\tag{2.10}
$$

where $q, q' = u, d, s$ and $q \neq q'$. The second group includes operators with one quark flavor

$$
\begin{aligned}
O_1' &= (\bar{q} i \gamma_5 q)(\bar{q} q) \ , \\[4pt]
O_2' &= (\bar{q} i \gamma_5 t^a q)(\bar{q} t^a q) \ .
\end{aligned}
\tag{2.11}
$$

The Weinberg operator is defined as

$$O_g = -\frac{1}{6} f^{abc} \epsilon^{\mu\nu\alpha\beta} G^a_{\mu\rho} G^{b\rho}_\nu G^c_{\alpha\beta} \ , \tag{2.12}$$

where $\epsilon^{0123} = 1$.

The contribution from $\bar{\theta}$ and, to less extent, dim-5 operators and the Weinberg operator have been studied extensively in the literature [6, 7, 8, 9, 10, 11, 12, 13,

14, 15], which is discussed in Chapter 3 when we study mEDM in the framework of mLRSM. The uncertainty of the estimates are typically at the level of factor 2. The contributions of these operators have also been studied extensively in the context of various new physics models [16, 17]. However, the matrix elements of dim-6 operators have been a challenge to estimate. In some beyond-SM theories such as the LRSM, dim-6 four-quark operators dominate the contributions to nEDM. In the literature, the only serious approach that has been proposed to calculate their matrix elements is the naive factorization method: breaking the four-quark matrix elements into the product of two-quark matrix elements between the nucleon states and between pion and vacuum [18, 19, 20]. While the factorization involving mesons can be and has been tested using lattice QCD [21] and the results may be trustable to within a factor of 2, the same is not known for matrix elements involving the nucleon states. The goal of this chapter is to develop a chiral perturbation method combined with simple quark models to estimate the four-quark contribution to the nEDM with hopefully an improved accuracy.

2.1.3   The Strategy of The Calculation

The approach we are going to take is the standard chiral perturbation theory (χPT) (see, for example, Ref. [22, 23]) which has been used to calculate the contribution of θ-term to nEDM [8]. One of the successes of the chiral approach can be illustrated by the polarizabilities of the nucleon. The electric polarizabilities of the proton and neutron have been extracted from experimental data, $\alpha_p^{\text{exp}} =$

$(10.4 \pm 0.6) \times 10^{-4}\text{fm}^3$, $\alpha_n^{\exp} = (12.3 \pm 1.3) \times 10^{-4}\text{fm}^3$. The leading contribution in χPT comes from the pion-nucleon intermediate states,

$$\alpha_p = \alpha_n = \frac{5\alpha_{\text{em}}g_A^2}{96\pi F_\pi^2 m_\pi} \approx 11 \times 10^{-4}\text{fm}^3 \ , \tag{2.13}$$

which diverges linearly as $m_\pi \to 0$ and agrees well with the experimental data. One would expect then a similar pion dominance in the neutron EDM because the latter also involves the intermediate electric dipole excitations. Indeed a pioneering calculation by Crewther et al. found that the dominant contribution from the charged-pion chiral-loop diverges logarithmically as m_π goes to zero, and is proportional to the CP-odd pion-nucleon-nucleon coupling $\bar{g}_{\pi NN}$ [7]. In this paper, we take this contribution as dominating and consider the four-quark operator contribution to $\bar{g}_{\pi NN}$. Of course, there are chiral-regular contributions to the nEDM which are of the same order in chiral power counting and numerically competitive or even dominating in the real world [17]. We will consider these contributions as well, although the model-dependence becomes unavoidable.

χPT is a low energy effective theory of QCD, the effective theory shares the same symmetry as its UV completed theory. Since the masses of u, d and s quarks are small compared to the QCD scale, $SU(3)_L \times SU(3)_R$ can be seen as a global symmetry of QCD approximately, which is inherited by χPT. This approximation is good enough to our goal of accuracy. To use χPT to calculate nEDM, one needs also to get the corresponding P-odd and CP-odd operators in χPT. To do this, in the spirit of the Wigner-Echart Theorem, we first classify the four-quark operators by the irreducible representations of $SU(3)_L \times SU(3)_R$ symmetry group. Then,

we collect all the chiral operators in the corresponding representations. Then, by calculating some simple matrix elements we get the Wilson coefficients for those operators.

The effective chiral Lagrangian can be written in terms of meson and nucleon fields,

$$
\begin{aligned}
\mathcal{L} \; = \; & \mathcal{L}_{\text{Goldstone−boson CP−odd term}} + \mathcal{L}_{\text{nucleon CP−odd mass term}} \\
& +\mathcal{L}_{\text{EDM term}} + \mathcal{L}_{\text{CP−odd }\pi\text{−N coupling}} + (\text{CP} - \text{even terms})
\end{aligned}
\tag{2.14}
$$

where the Goldstone boson CP-odd lagrangian will generate terms annihilating π^0 and η in the vacuum, or in other words, will produce meson condensates. The condensates will turn some of the CP-even terms (as we shall see, those proportional to quark masses) in the chiral lagrangian into CP-odd contributions. This will generate an additional CP-odd nucleon-mass term, neutron EDM term and CP-odd pion-nucleon coupling. Once this is done, one can rotate away the CP-odd nucleon mass term, generating further contributions to the neutron EDM terms and the CP-odd pion-nucleon coupling.

The presentation of this chapter is organized as follows: In Sec. 2.2, we classify all flavor-neutral P-odd and CP-odd four-quark operators in chiral representations. We also present the leading-order QCD scale evolution of these operators. In Sec. 2.3, we match these operators to the corresponding Goldstone boson operators, baryon operators, and EDM operators in χPT. We also discuss in the case of Peccei-Quinn symmetry the size of the induced θ term in the presence of these four-quark operators. In Sec. 2.4, we calculate their contributions to the P-odd and CP-odd

nucleon-pion vertices and the CP-odd nucleon mass using factorization in the case of meson matrix elements and simple quark models for the nucleon ones. In Sec. 2.5, we study the four-quark contribution to the neutron EDM in the chiral approach supplemented with factorization and quark model estimates of counter terms, and the results are compared with other calculations in the literature. The comparison and analysis show that the hadronic physics uncertainties here can be quantified to within a factor of two for operators generating unsuppressed meson condensate contributions. We conclude this chapter in Sec. 2.6.

2.2 P-odd and CP-odd Four-quark operators: Classification, Running and Mixing

We consider three light quark flavors: up, down and strange. Flavor-neutral P-odd and CP-odd four-quark operators can be divided into two groups which are shown in Eqs. (2.10) and (2.11).

To match the above quark operators into the hadronic ones in χPT, we have to classify the former into irreducible representations of the chiral group $SU(3)_L \times SU(3)_R$. Take the operator $\bar{u}i\gamma_5 u \bar{d}d$ as an example, which can be decomposed as

$$\bar{u}i\gamma_5 u \bar{d}d = -i\bar{u}_R u_L \bar{d}_R d_L + i\bar{u}_L u_R \bar{d}_R d_L + \text{ h.c. },\qquad (2.15)$$

where $q_{L,R} = P_{L,R}q$ with $P_{L,R} = (1 \mp \gamma_5)/2$. The first term can be further decomposed

as

$$-i\bar{u}_R u_L \bar{d}_R d_L = -\frac{i}{2}(\bar{u}_R u_L \bar{d}_R d_L + \bar{d}_R u_L \bar{u}_R d_L)$$

$$-\frac{i}{2}(\bar{u}_R u_L \bar{d}_R d_L - \bar{d}_R u_L \bar{u}_R d_L)$$

$$= -\frac{i}{4}S^{ij}_{kl}\bar{q}_{Ri}q^k_L \bar{q}_{Rj}q^l_L - \frac{i}{4}\epsilon^{jkl}_{imn}A^i_j \bar{q}_{Rk}q^m_L \bar{q}_{Rl}q^n_L \;, \qquad (2.16)$$

where $\epsilon^{jkl}_{imn} \equiv \epsilon^{jkl}\epsilon^{imn}$, and

$$A = \begin{pmatrix} 0 & 0 & 0 \\ 0 & 0 & 0 \\ 0 & 0 & 1 \end{pmatrix}, \qquad (2.17)$$

and

$$S^{12}_{12} = S^{21}_{12} = S^{12}_{21} = S^{21}_{21} = 1, \qquad (2.18)$$

with other elements vanishing. The second term of Eq. (2.15) can be written as

$$i\bar{u}_L u_R \bar{d}_R d_L = iH^j_{1i}H^l_{2k}\bar{q}_{Lj}q^k_R \bar{q}_{Rl}q^i_L \;, \qquad (2.19)$$

where

$$H_1 = \begin{pmatrix} 0 & 1 & 0 \\ 0 & 0 & 0 \\ 0 & 0 & 0 \end{pmatrix}, \quad H_2 = \begin{pmatrix} 0 & 0 & 0 \\ 1 & 0 & 0 \\ 0 & 0 & 0 \end{pmatrix}. \qquad (2.20)$$

In this way the operator $\bar{u}i\gamma_5 u\bar{d}d$ is decomposed into $(\bar{3},3)$, $(6,\bar{6})$ and $(8,8)$ representations of $SU(3)_L \times SU(3)_R$, and A, S, H_1, and H_2 can be regarded as spurion fields in the sense that if they transform as $(3,\bar{3})$, $(\bar{6},6)$ and $(8,8)$ under chiral transformation, the corresponding terms in Eqs. (2.16) and (2.19) become invariant. These spurion fields will be used in χPT to construct the effective operators corresponding to the same four-quark operators. All spurion fields for four-quark operators with

22

different Dirac and color structures are shown in Table 2.2. [It is easy to see that there is no $(1, 1)$ operator because any such operator must be expressible in terms of products of chiral-even quark currents, which cannot yield CP-odd contributions.]

The four-quark operators usually emerge at a high energy scale where some heavy particles have been integrated out. To match them to hadronic operators in effective theories, one must run them down to a low energy scale where non-perturbative physics becomes important. We can choose this to be 1 GeV or the lattice cut-off $1/a$, where a is the lattice spacing. In this work, we take $\mu = 4\pi F_\pi$, with $F_\pi = 93$ MeV. These operators mix with each other when the energy scale changes. Although many of the mixings have been calculated in the literature before [see Ref. [28], for example], we recalculate them and present the complete result here for easy reference:

$$
\mu^2 \frac{d}{d\mu^2}
\begin{pmatrix}
O_{11} \\
O_{12} \\
O_{21} \\
O_{22} \\
O_3 \\
O_4
\end{pmatrix}
=
\frac{\alpha_S(\mu)}{4\pi}
\begin{pmatrix}
8 & 0 & 0 & 0 & 0 & 1 \\
0 & 8 & 0 & 0 & 0 & 1 \\
0 & 0 & -1 & 0 & \frac{2}{9} & \frac{5}{12} \\
0 & 0 & 0 & -1 & \frac{2}{9} & \frac{5}{12} \\
0 & 0 & 24 & 24 & -\frac{8}{3} & 0 \\
\frac{16}{3} & \frac{16}{3} & 10 & 10 & 0 & \frac{19}{3}
\end{pmatrix}
\begin{pmatrix}
O_{11} \\
O_{12} \\
O_{21} \\
O_{22} \\
O_3 \\
O_4
\end{pmatrix}
, \quad (2.21)
$$

$$
\mu^2 \frac{d}{d\mu^2}
\begin{pmatrix}
O_1' \\
O_2'
\end{pmatrix}
=
\frac{\alpha_S(\mu)}{4\pi}
\begin{pmatrix}
\frac{40}{9} & -\frac{4}{3} \\
-\frac{80}{27} & -\frac{46}{9}
\end{pmatrix}
\begin{pmatrix}
O_1' \\
O_2'
\end{pmatrix}
. \quad (2.22)
$$

Clearly operators with different quark flavor structures do not mix. Since $SU(3)_L \times SU(3)_R$ symmetry is broken only by quark masses, four-quark operators belonging to different chiral irreducible representations do not mix either. Therefore, we can

	$(\bar{3}, 3)$	$(6, \bar{6})$	$(8, 8)$	
$q = u$ $q' = d$	$\begin{pmatrix} 0 & 0 & 0 \\ 0 & 0 & 0 \\ 0 & 0 & 1 \end{pmatrix}$	$S^{12}_{12} = S^{12}_{21}$ $= S^{21}_{12} = S^{21}_{21} = 1$ others are zero	$\begin{pmatrix} 0 & 1 & 0 \\ 0 & 0 & 0 \\ 0 & 0 & 0 \end{pmatrix}$,	$\begin{pmatrix} 0 & 0 & 0 \\ 1 & 0 & 0 \\ 0 & 0 & 0 \end{pmatrix}$
$q = d$ $q' = u$	$\begin{pmatrix} 0 & 0 & 0 \\ 0 & 0 & 0 \\ 0 & 0 & 1 \end{pmatrix}$	$S^{12}_{12} = S^{12}_{21}$ $= S^{21}_{12} = S^{21}_{21} = 1$ others are zero	$\begin{pmatrix} 0 & 0 & 0 \\ 1 & 0 & 0 \\ 0 & 0 & 0 \end{pmatrix}$,	$\begin{pmatrix} 0 & 1 & 0 \\ 0 & 0 & 0 \\ 0 & 0 & 0 \end{pmatrix}$
$q = u$ $q' = s$	$\begin{pmatrix} 0 & 0 & 0 \\ 0 & 1 & 0 \\ 0 & 0 & 0 \end{pmatrix}$	$S^{13}_{13} = S^{13}_{31}$ $= S^{31}_{13} = S^{31}_{31} = 1$ others are zero	$\begin{pmatrix} 0 & 0 & 1 \\ 0 & 0 & 0 \\ 0 & 0 & 0 \end{pmatrix}$,	$\begin{pmatrix} 0 & 0 & 0 \\ 0 & 0 & 0 \\ 1 & 0 & 0 \end{pmatrix}$
$q = s$ $q' = u$	$\begin{pmatrix} 0 & 0 & 0 \\ 0 & 1 & 0 \\ 0 & 0 & 0 \end{pmatrix}$	$S^{13}_{13} = S^{13}_{31}$ $= S^{31}_{13} = S^{31}_{31} = 1$ others are zero	$\begin{pmatrix} 0 & 0 & 0 \\ 0 & 0 & 0 \\ 1 & 0 & 0 \end{pmatrix}$,	$\begin{pmatrix} 0 & 0 & 1 \\ 0 & 0 & 0 \\ 0 & 0 & 0 \end{pmatrix}$
$q = d$ $q' = s$	$\begin{pmatrix} 1 & 0 & 0 \\ 0 & 0 & 0 \\ 0 & 0 & 0 \end{pmatrix}$	$S^{23}_{23} = S^{23}_{32}$ $= S^{32}_{23} = S^{32}_{32} = 1$ others are zero	$\begin{pmatrix} 0 & 0 & 0 \\ 0 & 0 & 1 \\ 0 & 0 & 0 \end{pmatrix}$,	$\begin{pmatrix} 0 & 0 & 0 \\ 0 & 0 & 0 \\ 0 & 1 & 0 \end{pmatrix}$
$q = s$ $q' = d$	$\begin{pmatrix} 1 & 0 & 0 \\ 0 & 0 & 0 \\ 0 & 0 & 0 \end{pmatrix}$	$S^{23}_{23} = S^{23}_{32}$ $= S^{32}_{23} = S^{32}_{32} = 1$ others are zero	$\begin{pmatrix} 0 & 0 & 0 \\ 0 & 0 & 0 \\ 0 & 1 & 0 \end{pmatrix}$,	$\begin{pmatrix} 0 & 0 & 0 \\ 0 & 0 & 1 \\ 0 & 0 & 0 \end{pmatrix}$

Table 2.1: Spurions for CP-odd 4-quark operators. The first six together with three tensor structures yield 18 operators in Eq. (4) and the last three with two tensor structures yield six operators in Eq. (5).

	$(\bar{3},3)$	$(6,\bar{6})$	$(8,8)$
$q = u$ $q' = u$	0	$S^{11}_{11} = 4$ others are zero	$0, \quad 0$
$q = d$ $q' = d$	0	$S^{22}_{22} = 4$ others are zero	$0, \quad 0$
$q = s$ $q' = s$	0	$S^{33}_{33} = 4$ others are zero	$0, \quad 0$

Table 2.2: Spurions for CP-odd 4-quark operators. The first six together with three tensor structures yield 18 operators in Eq. (4) and the last three with two tensor structures yield six operators in Eq. (5).

further simplify Eq. (12),

$$\mu^2 \frac{d}{d\mu^2} \begin{pmatrix} O_1^{(3,6)} \\ O_2^{(3,6)} \\ O_3^{(3,6)} \\ O_4^{(3,6)} \end{pmatrix} = \frac{\alpha_S(\mu)}{4\pi} \begin{pmatrix} 8 & 0 & 0 & 1 \\ 0 & -1 & \frac{2}{9} & \frac{5}{12} \\ 0 & 48 & -\frac{8}{3} & 0 \\ \frac{32}{3} & 20 & 0 & \frac{19}{3} \end{pmatrix} \begin{pmatrix} O_1^{(3,6)} \\ O_2^{(3,6)} \\ O_3^{(3,6)} \\ O_4^{(3,6)} \end{pmatrix}, \quad (2.23)$$

$$\mu^2 \frac{d}{d\mu^2} \begin{pmatrix} O_1^{(8)} \\ O_2^{(8)} \end{pmatrix} = \frac{\alpha_S(\mu)}{4\pi} \begin{pmatrix} 8 & 0 \\ 0 & -1 \end{pmatrix} \begin{pmatrix} O_1^{(8)} \\ O_2^{(8)} \end{pmatrix}, \quad (2.24)$$

where $O_i^{(3,6,8)}$ means the projections of the operator O_i on the representations $(\bar{3},3)$, $(6,\bar{6})$ and $(8,8)$, respectively. It is easy to see that the $(\bar{3},3)$ and $(6,\bar{6})$ projections of O_{i1} and O_{i2} are the same with $i = 1, 2$, whereas their $(8,8)$ projections differ only by the sign. The tensor operators do not have $(8,8)$ components and therefore do

not participate in Eq. (2.24).

The four-quark operators may also mix with P-odd and CP-odd operators with dimension less or equal to 6. For mixing with lower-dimensional operators, either quark masses or power divergences will appear. The only other dimension-6 operator is the Weinberg operator [29]

$$O_W = -\frac{1}{6} f^{abc} \epsilon^{\mu\nu\alpha\beta} G^a_{\mu\rho} G^{b\rho}_{\nu} G^c_{\alpha\beta}, \qquad (2.25)$$

which is a singlet under chiral transformation. Since the four-quark operators contain no singlet component, the mixing between them and O_W vanishes. The evolution of the Weinberg operator can be found in Ref. [30].

The P-odd and CP-odd dimension-5 operators are the quark electric dipole moment operators (QEDM) and quark chromo-electric dipole moment operators (QCDM). In principle, they belong to $(\bar{3}, 3)$ of the chiral group. However, they can mix logarithmically with four-quark operators multiplied by the quark mass which transforms also like $(\bar{3}, 3)$ [31, 32].

Finally, the four-quark operators can have mixing with $m\bar{q}i\gamma_5 q$ with quadratically divergent coefficients. Usually, one defines the four-quark operators with quadratic divergences subtracted, as is natural in dimensional regularization where all quadratically divergent integrals vanish by definition. Equivalently, this can be achieved, for example, by demanding the CP-odd four-quark operators have vanishing contribution between QCD vacuum and CP-odd meson states in perturbation theory. However, as we shall see in the following section, they can have non-perturbative contributions. The exact physical implication of this non-perturbative

26

contribution will be discussed in Sec. 5.5.

2.3 Matching to Operators in Chiral Perturbation Theory

Generically, any P-odd, CP-odd quark-gluon operator contributes to all P-odd, CP-odd hadronic operators in χPT; the latter are constructed in terms of Goldstone-boson (pion, kaon, eta) fields and baryon fields. Here we consider just the contributions to the Goldstone-boson CP-odd interactions, nucleon CP-odd mass term, π-N CP-odd coupling, as well as the neutron EDM term,

$$\begin{aligned}
\mathcal{L} &= \mathcal{L}_{\text{Goldstone-boson CP-odd term}} + \mathcal{L}_{\text{nucleon CP-odd mass term}} \\
&\quad + \mathcal{L}_{\text{CP-odd } \pi\text{-N coupling}} + \mathcal{L}_{\text{EDM term}} \; .
\end{aligned} \tag{2.26}$$

Following the standard practice in the literature, we imbed the Goldstone-boson fields in the unitary matrix $U = \exp[2i\Sigma/F_\pi]$ with

$$\Sigma = \begin{pmatrix} \frac{1}{2}\pi^0 + \frac{1}{2\sqrt{3}}\eta & \frac{1}{\sqrt{2}}\pi^+ & \frac{1}{\sqrt{2}}K^+ \\ \frac{1}{\sqrt{2}}\pi^- & -\frac{1}{2}\pi^0 + \frac{1}{2\sqrt{3}}\eta & \frac{1}{\sqrt{2}}K^0 \\ \frac{1}{\sqrt{2}}K^- & \frac{1}{\sqrt{2}}\bar{K}^0 & -\frac{1}{\sqrt{3}}\eta \end{pmatrix} , \tag{2.27}$$

where F_π is the pion decay constant. Under chiral rotations, U transforms like $U \to LUR^\dagger$, where L and R are 3×3 unitary matrices belonging to $SU(3)_L$ and $SU(3)_R$ groups, respectively.

To include the baryon octet, we introduce

$$B = \begin{pmatrix} \frac{1}{\sqrt{2}}\Sigma^0 + \frac{1}{\sqrt{6}}\Lambda & \Sigma^+ & p \\ \Sigma^- & -\frac{1}{\sqrt{2}}\Sigma^0 + \frac{1}{\sqrt{6}}\Lambda & n \\ \Xi^- & \Xi^0 & -\frac{2}{\sqrt{6}}\Lambda \end{pmatrix} . \tag{2.28}$$

Again following the literature, we assume B transforms nonlinearly under chiral transformation,

$$B \to KBK^\dagger \qquad (2.29)$$

where K is a unitary matrix defined according to the transformation of $\xi = U^{1/2}$.

$$\xi \to L\xi K^\dagger, \quad \xi \to K\xi R^\dagger \qquad (2.30)$$

It is clear that K is a nonlinear function of the Goldstone-boson fields.

The quark-mass term breaks chiral symmetry and plays an important role in chiral expansion. To exhibit its physical effect, the usual practice is to introduce the spurion field χ, transforming as

$$\chi \to L\chi R^\dagger . \qquad (2.31)$$

However, to combine χ with the baryon field B, we introduce $\chi_\pm$

$$\chi_\pm = \xi^\dagger \chi \xi^\dagger \pm \xi \chi^\dagger \xi , \qquad (2.32)$$

which transform nonlinearly as $\chi_\pm \to K\chi_\pm K^\dagger$.

In the leading order, the chiral lagrangian for meson fields is

$$\mathcal{L} = \frac{1}{4}F_\pi^2 \mathrm{Tr}[\partial_\mu U^\dagger \partial^\mu U] + \frac{1}{2}F_\pi^2 B \mathrm{Tr}[M^\dagger U + U^\dagger M] , \qquad (2.33)$$

where $M = diag\{m_u, m_d, m_s\}$ is the mass matrix of light quarks. The leading-order chiral lagrangian for the baryon field is [23]

$$\mathcal{L} = \mathrm{Tr}\left\{ \bar{B}i\gamma^\mu D_\mu B - m_0 \bar{B}B + \frac{1}{2}D\bar{B}\gamma^\mu \gamma_5 u_\mu, B + \frac{1}{2}F\bar{B}\gamma_\mu \gamma_5 [u_\mu, B] \right\} , \qquad (2.34)$$

where $u_\mu = i(\xi^\dagger \partial_\mu \xi - \xi \partial_\mu \xi^\dagger)$ is an axial vector current, $D_\mu B = \partial_\mu B + [\Gamma_\mu, B]$ and $\Gamma_\mu = \{\xi^\dagger \partial_\mu \xi + \xi \partial_\mu \xi^\dagger\}/2$ is a vector current.

2.3.1   Matching to CP-Odd Goldstone-Boson Operators

Once there is a CP-odd term in the QCD lagrangian, it induces CP-odd terms in the effective Goldstone-boson lagrangian. These terms can annihilate odd-number (particularly, one) Goldstone bosons into the vacuum. Because of this CP-odd meson condensate, the original CP-even terms can now contribute to the CP-odd effects. Due to chiral symmetry, a meson condensate can generate physical effects only when the CP-even terms explicitly break the symmetry.

As discussed in the last section, P-odd and CP-odd four-quark operators can be decomposed into chiral $(\bar{3}, 3)$, $(6, \bar{6})$, $(8, 8)$ and their hermitian conjugate representations. They in turn can be matched to the corresponding chiral operators in the same representations. The leading ones without derivatives are unique and are shown in Table 2.3.

Rep.	$(\bar{3}, 3)$	$(6, \bar{6})$	$(8, 8)$
Operator	$O_3^m = i\mathrm{Tr}[AU^\dagger]$	$O_6^m = iS_{kl}^{ij}U_i^kU_j^l$	$O_8^m = i\mathrm{Tr}[H_1UH_2U^\dagger]$

Table 2.3: Leading meson operators in individual irreducible chiral representations where A, S, H_1 and H_2 are spurion fields in Table 2.2. The appearance of i in front of each operator indicates that these operators generate P-odd and CP-odd vertices in the meson lagrangian; their Wilson coefficients in the lagrangian are defined to be real.

We illustrate the matching process using $O_{11}^{ud} = \bar{u}i\gamma_5 u\bar{d}d$ as an example. As discussed in the last section, this quark operator can be decomposed into irreducible

29

representations of the chiral group using the spurion fields

$$O_{11}^{ud} = O_{11}^{ud,(\bar{3},3)} + O_{11}^{ud,(6,\bar{6})} + O_{11}^{ud,(8,8)} + \text{h.c.} \qquad (2.35)$$

Then, we can match each of the operators to the corresponding one in the meson sector through the non-perturbative Wilson coefficients $C's$

$$O_{11}^{ud,(\bar{3},3)} \sim C^{(\bar{3},3)} O_3 \;, \;\; O_{11}^{ud,(6,\bar{6})} \sim C^{(6,\bar{6})} O_6 \;, \;\; O_{11}^{ud,(8,8)} \sim C^{(8,8)} O_8 \;. \qquad (2.36)$$

The Wilson coefficients can be obtained by matching the simplest matrix elements: $\langle 0|O|\pi^0 \rangle$ and $\langle 0|O|\eta \rangle$, which can be calculated using non-perturbative methods such as lattice QCD.

In this paper, we use factorization approximation to estimate these non-perturbative matrix elements. Lattice QCD calculations demonstrate that the matrix elements of four-quark operators can be factorized typically to within a factor of 2. Again take the operator O_{11}^{ud} as an example, which can annihilate π^0 and η to the vacuum. [In principle, it also annihilates η', but this contribution is suppressed by the mass of η'. A brief discussion of the contribution from η' condensate can be found in Appendix C.] The annihilation amplitude can be estimated using vacuum saturation,

$$\langle 0|\bar{u}i\gamma_5 u\bar{d}d|\pi^0 \rangle \approx \langle 0|\bar{d}d|0 \rangle \langle 0|\bar{u}i\gamma_5 u|\pi^0 \rangle. \qquad (2.37)$$

Using chiral symmetry, one can get $\langle 0|\bar{u}i\gamma_5 u|\pi^0 \rangle = \frac{1}{F_\pi}\langle 0|\bar{u}u|0 \rangle \equiv -F_\pi B_0$, and $\langle 0|\bar{u}i\gamma_5 u|\eta \rangle = -F_\pi B_0/\sqrt{3}$. (This is consistent with the definition of the chiral rotation of U defined below Eq. (2.27).) Therefore, a term $C_4 O_{11}^{ud}$ in the QCD

lagrangian can be matched to the linear terms in π^0 and η in the chiral lagrangian

$$\mathcal{L} = C_4 B_0^2 F_\pi^3 \pi^0 + \frac{1}{\sqrt{3}} C_4 B_0^2 F_\pi^3 \eta + ... , \qquad (2.38)$$

where ... represents higher-power meson fields. Then the leading terms in the potential of π^0 and η can be written as

$$
\begin{aligned}
V &= \frac{1}{2} B_0 \left[(m_u + m_d)(\pi^0)^2 + \frac{1}{3}(m_u + m_d + 4m_s)\eta^2 \right] \\
&\quad + \frac{B_0}{\sqrt{3}}(m_u - m_d)\pi^0 \eta - C_4 B_0^2 F_\pi^3 \left(\pi^0 + \frac{1}{\sqrt{3}}\eta \right) ,
\end{aligned}
\qquad (2.39)
$$

which can be minimized to yield a condensate $\langle \pi^0 \rangle$ and $\langle \eta \rangle$.

The above discussion can be easily generalized to an arbitrary four-quark operator, for which Eq. (2.38) can be written as

$$\mathcal{L} = g_\pi C_4 B_0^2 F_\pi^3 \pi^0 + g_\eta C_4 B_0^2 F_\pi^3 \eta + ... , \qquad (2.40)$$

where g_π and g_η are numerical factors generated through the vacuum saturation approximation. Then, the vevs of meson fields can be written as

$$
\begin{aligned}
\langle \pi^0 \rangle &= \frac{B_0 F_\pi^3 C_4 \left[g_\pi(m_u + m_d + 4m_s) - \sqrt{3} g_\eta(m_u - m_d) \right]}{4(m_u m_d + m_d m_s + m_s m_u)} , \\
\langle \eta \rangle &= \frac{B_0 F_\pi^3 C_4 \left[-\sqrt{3} g_\pi(m_u - m_d) + 3 g_\eta(m_u + m_d) \right]}{4(m_u m_d + m_d m_s + m_s m_u)} ,
\end{aligned}
\qquad (2.41)
$$

which is inversely proportional to quark masses! The vev of U can be written as

$$
\langle U \rangle = \exp \left[i \begin{pmatrix} \langle \pi^0 \rangle + \frac{1}{\sqrt{3}} \langle \eta \rangle & 0 & 0 \\ 0 & -\langle \pi^0 \rangle + \frac{1}{\sqrt{3}} \langle \eta \rangle & 0 \\ 0 & 0 & -\frac{2}{\sqrt{3}} \langle \eta \rangle \end{pmatrix} / F_\pi \right] . \qquad (2.42)
$$

This defines the vacuum state of Goldstone-boson fields.

31

Therefore, we can redefine the meson fields in the following way:

$$U = \langle U \rangle U' \ , \tag{2.43}$$

where U' collects the physical meson excitations. Through this redefinition, the meson lagrangian no longer contains terms annihilating the physical Goldstone bosons. Correspondingly, we redefine the baryon fields,

$$\xi B \xi = \langle U \rangle \xi' B' \xi' \ , \tag{2.44}$$

through a chiral transformation with $L = \langle U \rangle$ and $R = 1$.

The above redefinition can change P-even and CP-even terms with explicit chiral symmetry breaking to P-odd and CP-odd terms. This is particularly true for the CP-even baryon lagrangian with linear dependence on quark masses,

$$\mathcal{L}_c = c_1 \text{Tr}[\bar{B}B]\text{Tr}[MU^\dagger] + c_2 \text{Tr}[M\xi^\dagger \bar{B}B\xi^\dagger] + c_3 \text{Tr}[\bar{B}\xi^\dagger M\xi^\dagger B] \ + \ \text{h.c.} \tag{2.45}$$

and

$$\mathcal{L}_d = d_1 \text{Tr}[\bar{B}\gamma_5 B]\text{Tr}[MU^\dagger] + d_2 \text{Tr}[M\xi^\dagger \bar{B}\gamma_5 B\xi^\dagger] + d_3 \text{Tr}[\bar{B}\gamma_5 \xi^\dagger M\xi^\dagger B] \ + \ \text{h.c.} \tag{2.46}$$

Substituting $\langle U \rangle$ to the above equation, we get CP-odd pion-nucleon couplings through

$$c_1 \text{Tr}[\bar{B}'B']\text{Tr}[\langle U \rangle^\dagger MU'^\dagger] + c_2 \text{Tr}[\langle U \rangle^\dagger M\xi'^\dagger \bar{B}'B'\xi'^\dagger] + c_3 \text{Tr}[\bar{B}'\xi'^\dagger \langle U \rangle^\dagger M\xi'^\dagger B'] + \text{h.c.}$$

$$\tag{2.47}$$

and the CP-odd masses of baryons

$$d_1 \text{Tr}[\bar{B}'\gamma_5 B']\text{Tr}[\langle U \rangle^\dagger MU'^\dagger] + d_2 \text{Tr}[\langle U \rangle^\dagger M\xi'^\dagger \bar{B}'\gamma_5 B'\xi'^\dagger] + d_3 \text{Tr}[\bar{B}'\gamma_5 \xi'^\dagger \langle U \rangle^\dagger M\xi'^\dagger B'] + \text{h.c.}$$

$$\tag{2.48}$$

which is part of the CP-odd mass generated by the four-quark operator. Note that since $\langle U \rangle$ is inversely proportional to the quark mass, the above contribution is not suppressed in the chiral limit.

One can also get a CP-odd dipole moment by considering a photo-pion production term off the nucleon. When the pion is condensed through CP-odd effects, one generates a new contribution to the CP-odd moment, which is beyond the scope of this paper.

2.3.2 Matching to CP-Odd Baryon Operators

In this subsection, we construct the leading P-odd and CP-odd baryon operators induced by the CP-odd four-quark operators. These include all the operators with one baryon and one conjugate baryon fields, and without any quark masses or derivatives. All the independent operators are listed in Table 2.4. A brief proof of the completeness and independence of these operators is shown in Appendix B.

There are two types of operators in Table 2.4, those with and without tilde. For the first group without tilde, the expansion of the pion field generates the P-odd and CP-odd nucleon-pion vertices

$$\mathcal{L}_{NN\pi}^{\text{CP-odd}} = (h_c \bar{p} n \pi^+ + \text{h.c.}) + h_n \bar{n} n \pi^0 + h_p \bar{p} p \pi^0 \ . \tag{2.49}$$

For the second group, the leading order expansion is a bilinear-baryon term with a CP-odd mass structure,

$$\mathcal{L}_{\text{mass}}^{\text{CP-odd}} \sim -m_\star \bar{n} i \gamma_5 n. \tag{2.50}$$

This term contributes to the CP-odd baryon wave function.

33

Rept.	Operators
$(\bar{3}, 3)$	$O_3^{(1)} = i\text{Tr}[\bar{B}B]\text{Tr}[AU^\dagger], O_3^{(2)} = i\text{Tr}[A\xi^\dagger \bar{B}B\xi^\dagger], O_3^{(3)} = i\text{Tr}[\bar{B}\xi^\dagger A\xi^\dagger B],$ $\tilde{O}_3^{(1)} = i\text{Tr}[\bar{B}\gamma_5 B]\text{Tr}[AU^\dagger], \tilde{O}_3^{(2)} = i\text{Tr}[A\xi^\dagger \bar{B}\gamma_5 B\xi^\dagger], \tilde{O}_3^{(3)} = i\text{Tr}[\bar{B}\gamma_5\xi^\dagger A\xi^\dagger B],$
$(6, \bar{6})$	$O_6^{(1)} = iS_{kl}^{ij}(\xi\bar{B}\xi)_i^k(\xi B\xi)_j^l,\ O_6^{(2)} = iS_{kl}^{ij}(\xi\bar{B}B\xi)_i^k U_j^l,$ $O_6^{(3)} = iS_{kl}^{ij}(\bar{B}\xi)_i^m(\xi B)_m^k U_j^l,\ O_6^{(4)} = i\text{Tr}[\bar{B}B]S_{kl}^{ij}U_i^k U_j^l.$ $\tilde{O}_6^{(1)} = iS_{kl}^{ij}(\xi\bar{B}\gamma_5\xi)_i^k(\xi B\xi)_j^l,\ \tilde{O}_6^{(2)} = iS_{kl}^{ij}(\xi\bar{B}\gamma_5 B\xi)_i^k U_j^l,$ $\tilde{O}_6^{(3)} = iS_{kl}^{ij}(\bar{B}\gamma_5\xi)_i^m(\xi B)_m^k U_j^l,\ \tilde{O}_6^{(4)} = i\text{Tr}[\bar{B}\gamma_5 B]S_{kl}^{ij}U_i^k U_j^l$
$(8, 8)$	$O_8^{(1)} = i\text{Tr}[\bar{B}\xi^\dagger H_1 U H_2\xi^\dagger B],\ O_8^{(2)} = i\text{Tr}[\xi^\dagger \bar{B}B\xi^\dagger H_1 U H_2],$ $O_8^{(3)} = i\text{Tr}[\xi\bar{B}B\xi H_2 U^\dagger H_1],\ O_8^{(4)} = i\text{Tr}[\bar{B}\xi H_2 U^\dagger H_1\xi B],$ $O_8^{(5)} = i\text{Tr}[\xi\bar{B}\xi^\dagger H_1]\text{Tr}[\xi^\dagger B\xi H_2],\ O_8^{(6)} = i\text{Tr}[\xi^\dagger \bar{B}\xi H_2]\text{Tr}[\xi B\xi^\dagger H_1],$ $O_8^{(7)} = i\text{Tr}[\xi\bar{B}\xi H_2\xi^\dagger B\xi^\dagger H_1],\ O_8^{(8)} = i\text{Tr}[\xi^\dagger \bar{B}\xi^\dagger H_1\xi B\xi H_2].$ $\tilde{O}_8^{(1)} = i\text{Tr}[\bar{B}\gamma_5\xi^\dagger H_1 U H_2\xi^\dagger B],\ \tilde{O}_8^{(2)} = i\text{Tr}[\xi^\dagger \bar{B}\gamma_5 B\xi^\dagger H_1 U H_2],$ $\tilde{O}_8^{(3)} = i\text{Tr}[\xi\bar{B}\gamma_5 B\xi H_2 U^\dagger H_1],\ \tilde{O}_8^{(4)} = i\text{Tr}[\bar{B}\gamma_5\xi H_2 U^\dagger H_1\xi B],$ $\tilde{O}_8^{(5)} = i\text{Tr}[\xi\bar{B}\gamma_5\xi^\dagger H_1]\text{Tr}[\xi^\dagger B\xi H_2],\ \tilde{O}_8^{(6)} = i\text{Tr}[\xi^\dagger \bar{B}\gamma_5\xi H_2]\text{Tr}[\xi B\xi^\dagger H_1],$ $\tilde{O}_8^{(7)} = i\text{Tr}[\xi\bar{B}\gamma_5\xi H_2\xi^\dagger B\xi^\dagger H_1],\ \tilde{O}_8^{(8)} = i\text{Tr}[\xi^\dagger \bar{B}\gamma_5\xi^\dagger H_1\xi B\xi H_2]$

Table 2.4: Hadronic operators that have the same quantum numbers as four-quark operators in different irreducible representations.

Traditionally, P-odd and CP-odd pion-nucleon couplings are defined in terms of isospin 0, 1, and 2 of the operators, which can be written as [17]

$$\mathcal{L}_{\pi NN} = \bar{g}_{\pi NN}^{(0)} \bar{N} \tau^a N \pi^a + \bar{g}_{\pi NN}^{(1)} \bar{N} N \phi^0 + \bar{g}_{\pi NN}^{(2)} (\bar{N} \tau^a N \pi^a - 3\bar{N} \tau^3 N \pi^0) \ , \qquad (2.51)$$

where $\bar{g}_{\pi NN}^{(i)}$ is the coupling of the isospin-i term and τ^i are the Pauli matrices. Then, in terms of $\bar{g}_{\pi NN}^{(i)}$, h_c, h_n, and h_p can be written as

$$h_c = \sqrt{2}(\bar{g}_{\pi NN}^{(0)} + \bar{g}_{\pi NN}^{(2)}), \quad h_n = (-\bar{g}_{\pi NN}^{(0)} + \bar{g}_{\pi NN}^{(1)} + 2\bar{g}_{\pi NN}^{(2)}), \quad h_p = (\bar{g}_{\pi NN}^{(0)} + \bar{g}_{\pi NN}^{(1)} - 2\bar{g}_{\pi NN}^{(2)}) \ ,$$

$$(2.52)$$

where h_p does not contribute to nEDM.

To match the P-odd and CP-odd four-quark operators to the above baryon operators, one must find ways to calculate the corresponding non-perturbative Wilson coefficients. This can be done by considering the matrix elements of the quark operators in simple states. Take $O_{11}^{ud} = \bar{u} i \gamma_5 u \bar{d} d$ as an example. As shown in the last section, it can be decomposed into irreducible representations of the chiral group,

$$O_{11}^{ud} = O_{11}^{ud,(\bar{3},3)} + O_{11}^{ud,(6,\bar{6})} + O_{11}^{ud,(8,8)} + \text{h.c.} \qquad (2.53)$$

The spurions related to this operator are given in Eqs. (2.17), (2.18) and (2.20). $O_{11}^{ud,(\bar{3},3)}$, $O_{11}^{ud,(6,\bar{6})}$ and $O_{11}^{ud,(8,8)}$ must be matched to the hadronic operators in the same irreducible representations and with the same spurions. Take the un-tilded

hadronic operators as an example:

$$
\begin{aligned}
O_{11}^{ud,(\bar{3},3)} &= \sum_{i=1}^{3} C_3^{(i)} O_3^{(i)} + ... \,, \\
O_{11}^{ud,(6,\bar{6})} &= \sum_{i=1}^{4} C_6^{(i)} O_6^{(i)} + ... \,, \\
O_{11}^{ud,(8,8)} &= \sum_{i=1}^{8} C_8^{(i)} O_8^{(i)} + ... \,,
\end{aligned}
\tag{2.54}
$$

where "..." represents higher order operators.

Note that, an operator can be separated into hermitian part and anti-hermitian part. Since the QCD Lagrangian is hermitian, the hermitian part and the anti-hermitian part must have the same Wilson coefficient in the effective theory. Take the operator $\bar{q}_L q_R$ as an example, it is a $(\bar{3}, 3)$ operator, so it can be matched to $CU^\dagger$ in the chiral perturbation theory, while its hermitian conjugation $\bar{q}_R q_L$ is matched to CU with exactly the same Wilson coefficient since the QCD Lagrangian is invariant under the hermitian conjugate transformation. Therefore, the hermitian part of $\bar{q}_L q_R$ can be matched to $C(U^\dagger + U)/2$ whereas the anti-hermitian part can be matched to $C(U^\dagger - U)/2$. As a result, one can use either the hermitian part or the anti-hermitian part of the operators to get their Wilson coefficients depending on which way is easier. For the operators without tilde listed in Table 2.4, the anti-hermitian parts contain terms having only one baryon field and one anti-baryon field which is easy to do the matching, while for the operators with tilde, the hermitian part is easier. Therefore, we choose to match the anti-hermitian part of the operators without a tilde whereas match the hermitian part of the operators with a tilde to get the Wilson coefficients of them. One can show that this matching procedure

works when current algebra is valid such as in non-relativistic quark model.

The leading-order expansion of the hadronic operators are, for $(\bar{3}, 3)$ operators,

$$
\begin{aligned}
O_3^{(1)} &\simeq i\bar{p}p + i\bar{n}n + i\bar{\Lambda}\Lambda + i\bar{\Sigma}^0\Sigma^0 + i\bar{\Sigma}^+\Sigma^+ + i\bar{\Sigma}^-\Sigma^- + i\bar{\Xi}^0\Xi^0 + i\bar{\Xi}^-\Xi^- \; , \\
O_3^{(2)} &\simeq i\bar{p}p + i\bar{n}n + \frac{2i}{3}\bar{\Lambda}\Lambda \; , \\
O_3^{(3)} &\simeq \frac{2i}{3}\bar{\Lambda}\Lambda + i\bar{\Xi}^0\Xi^0 + i\bar{\Xi}^-\Xi^- \; .
\end{aligned}
\tag{2.55}
$$

Therefore, we can determine the Wilson coefficients with four physical matrix elements,

$$
\begin{aligned}
C_3^{(1)} + C_3^{(2)} &= (-i)\langle p|O_{11}^{ud,(\bar{3},3)}|p\rangle \; , \\
C_3^{(1)} &= (-i)\langle \Sigma^0|O_{11}^{ud,(\bar{3},3)}|\Sigma^0\rangle \; , \\
C_3^{(1)} + \frac{2}{3}C_3^{(2)} &= (-i)\langle \Lambda|O_{11}^{ud,(\bar{3},3)}|\Lambda\rangle \; , \\
C_3^{(1)} + C_3^{(3)} &= (-i)\langle \Xi^0|O_{11}^{ud,(\bar{3},3)}|\Xi^0\rangle \; ,
\end{aligned}
\tag{2.56}
$$

where we have chosen the normalization condition

$$
\langle \vec{P}|\vec{P}'\rangle = (2\pi)^3\delta^3(\vec{P} - \vec{P}') \; ,
\tag{2.57}
$$

where $\vec{P}$ and $\vec{P}'$ are the momenta of the states.

Since the number of equations is larger than the number of variables, to get a solution the following condition must be satisfied,

$$
\det
\begin{pmatrix}
1 & 1 & 0 & \langle p|O_{11}^{ud,(\bar{3},3)}|p\rangle \\
1 & 0 & 0 & \langle \Sigma^0|O_{11}^{ud,(\bar{3},3)}|\Sigma^0\rangle \\
1 & \frac{2}{3} & 0 & \langle \Lambda|O_{11}^{ud,(\bar{3},3)}|\Lambda\rangle \\
1 & 0 & 1 & \langle \Xi^0|O_{11}^{ud,(\bar{3},3)}|\Xi^0\rangle
\end{pmatrix}
= 0 \; ,
\tag{2.58}
$$

37

which gives a nontrivial relation among these matrix elements;

$$-\frac{2}{3}\langle p|O^{ud,(\bar{3},3)}|p\rangle - \frac{1}{3}\langle\Sigma^0|O_{11}^{ud,(\bar{3},3)}|\Sigma^0\rangle + \langle\Lambda|O_{11}^{ud,(\bar{3},3)}|\Lambda\rangle = 0 \ . \qquad (2.59)$$

This relation must be satisfied in the chiral limit, so it is a test for direct calculations of the matrix elements. Similarly, a simple inspection of Eq. (2.55) can give us some more relations among matrix elements

$$\langle p|O_{11}^{ud,(\bar{3},3)}|p\rangle \ = \ \langle n|O_{11}^{ud,(\bar{3},3)}|n\rangle \ ,$$

$$\langle\Sigma^0|O_{11}^{ud,(\bar{3},3)}|\Sigma^0\rangle \ = \ \langle\Sigma^+|O_{11}^{ud,(\bar{3},3)}|\Sigma^+\rangle \ = \ \langle\Sigma^-|O_{11}^{ud,(\bar{3},3)}|\Sigma^-\rangle \ ,$$

$$\langle\Xi^0|O_{11}^{ud,(\bar{3},3)}|\Xi^0\rangle \ = \ \langle\Xi^-|O_{11}^{ud,(\bar{3},3)}|\Xi^-\rangle \ . \qquad (2.60)$$

Generalizing the above discussion to $(6,\bar{6})$ and $(8,8)$ operators, we write down the leading expansion of the hadronic operators,

$$O_6^{(1)} \ \simeq \ \frac{i}{3}\bar{\Lambda}\Lambda - i\bar{\Sigma}^0\Sigma^0 + i\bar{\Sigma}^+\Sigma^+ + i\bar{\Sigma}^-\Sigma^- \ ,$$

$$O_6^{(2)} \ \simeq \ i\bar{p}p + i\bar{n}n + \frac{i}{3}\bar{\Lambda}\Lambda + i\bar{\Sigma}^0\Sigma^0 + i\bar{\Sigma}^+\Sigma^+ + i\bar{\Sigma}^-\Sigma^- \ ,$$

$$O_6^{(3)} \ \simeq \ \frac{i}{3}\bar{\Lambda}\Lambda + i\bar{\Xi}^0\Xi^0 + i\bar{\Xi}^-\Xi^- + i\bar{\Sigma}^0\Sigma^0 + i\bar{\Sigma}^+\Sigma^+ + i\bar{\Sigma}^-\Sigma^- \ ,$$

$$O_6^{(4)} \ \simeq \ 2i\left(\bar{p}p + \bar{n}n + \bar{\Lambda}\Lambda + i\bar{\Xi}^0\Xi^0 + \bar{\Xi}^-\Xi^- + \bar{\Sigma}^0\Sigma^0 + \bar{\Sigma}^+\Sigma^+ + \bar{\Sigma}^-\Sigma^-\right) \ (2.61)$$

$$
\begin{aligned}
O_8^{(1)} &\simeq i\left(\bar{p}p + \frac{1}{6}\bar{\Lambda}\Lambda + \frac{1}{2\sqrt{3}}\bar{\Lambda}\Sigma^0 + \frac{1}{2\sqrt{3}}\bar{\Sigma}^0\Lambda + \frac{1}{2}\bar{\Sigma}^0\Sigma^0 + \bar{\Sigma}^+\Sigma^+\right) \;, \\
O_8^{(2)} &\simeq i\left(\frac{1}{6}\bar{\Lambda}\Lambda + \bar{\Xi}^-\Xi^- + \frac{1}{2\sqrt{3}}\bar{\Lambda}\Sigma^0 + \frac{1}{2\sqrt{3}}\bar{\Sigma}^0\lambda + \frac{1}{2}\bar{\Sigma}^0\Sigma^0 + \bar{\Sigma}^-\Sigma^-\right) \;, \\
O_8^{(3)} &\simeq i\left(\frac{1}{6}\bar{\Lambda}\Lambda + \bar{\Xi}^0\Xi^0 - \frac{1}{2\sqrt{3}}\bar{\Lambda}\Sigma^0 - \frac{1}{2\sqrt{3}}\bar{\Sigma}^0\lambda + \frac{1}{2}\bar{\Sigma}^0\Sigma^0 + \bar{\Sigma}^+\Sigma^+\right) \;, \\
O_8^{(4)} &\simeq i\left(\bar{n}n + \frac{1}{6}\bar{\Lambda}\Lambda - \frac{1}{2\sqrt{3}}\bar{\Lambda}\Sigma^0 - \frac{1}{2\sqrt{3}}\bar{\Sigma}^0\Lambda + \frac{1}{2}\bar{\Sigma}^0\Sigma^0 + \bar{\Sigma}^-\Sigma^-\right) \\
O_8^{(5)} &\simeq i\bar{\Sigma}^+\Sigma^+ \;, \\[4pt]
O_8^{(6)} &\simeq i\bar{\Sigma}^-\Sigma^- \;, \\[4pt]
O_8^{(7)} &\simeq i\left(\frac{1}{6}\bar{\Lambda}\Lambda + \frac{1}{2\sqrt{3}}\bar{\Lambda}\Sigma^0 - \bar{\Sigma}^0\Lambda - \frac{1}{2}\bar{\Sigma}^0\Sigma^0\right) \;, \\
O_8^{(8)} &\simeq i\left(\frac{1}{6}\bar{\Lambda}\Lambda - \frac{1}{2\sqrt{3}}\bar{\Lambda}\Sigma^0 + \bar{\Sigma}^0\Lambda - \frac{1}{2}\bar{\Sigma}^0\Sigma^0\right) \;, \quad\quad\quad (2.62)
\end{aligned}
$$

from which we can get similar relations among matrix elements just like in the $(\bar{3}, 3)$ case shown in Table 2.5. The other four-quark operators with the same flavor structures have the same relations among hadronic matrix elements as in this case.

One can either build models or do lattice QCD calculations to get these simplest four-quark matrix elements. Once known, one can get the Wilson coefficients by solving Eq. (2.56) and similar equations for $(6, \bar{6})$ and $(8, 8)$ operators. Then one can expand these hadronic operators to the first order with one meson field in each term to get the P-odd and CP-odd pion-nucleon vertices. A similar method works for baryon operators with tilde. We will consider these matrix elements in the next section.

Rep.	Relations
$(\bar{3},3)$	$\langle p\|O_{11}^{ud,(\bar{3},3)}\|p\rangle = \langle n\|O_{11}^{ud,(\bar{3},3)}\|n\rangle, \langle\Xi^0\|O_{11}^{ud,(\bar{3},3)}\|\Xi^0\rangle = \langle\Xi^-\|O_{11}^{ud,(\bar{3},3)}\|\Xi^-\rangle,$ $\langle\Sigma^0\|O_{11}^{ud,(\bar{3},3)}\|\Sigma^0\rangle = \langle\Sigma^+\|O_{11}^{ud,(\bar{3},3)}\|\Sigma^+\rangle = \langle\Sigma^-\|O_{11}^{ud,(\bar{3},3)}\|\Sigma^-\rangle,$ $-\frac{2}{3}\langle p\|O_{11}^{ud,(\bar{3},3)}\|p\rangle - \frac{1}{3}\langle\Sigma^0\|O_{11}^{ud,(\bar{3},3)}\|\Sigma^0\rangle + \langle\Lambda\|O_{11}^{ud,(\bar{3},3)}\|\Lambda\rangle = 0$
$(6,\bar{6})$	$\langle p\|O_{11}^{ud,(6,\bar{6})}\|p\rangle = \langle n\|O_{11}^{ud,(6,\bar{6})}\|n\rangle$ $\langle\Xi^+\|O_{11}^{ud,(6,\bar{6})}\|\Xi^+\rangle = \langle\Xi^-\|O_{11}^{ud,(6,\bar{6})}\|\Xi^-\rangle$ $2\langle p\|O_{11}^{ud,6,\bar{6}}\|p\rangle - \langle\Sigma^0\|O_{11}^{ud,(6,\bar{6}))}\|\Sigma^0\rangle - 3\langle\Lambda\|O_{11}^{ud,(6,\bar{6})}\|\Lambda\rangle + 2\langle\Xi^0\|O_{11}^{ud,(6,\bar{6})}\|\Xi^0\rangle = 0$
$(8,8)$	$\langle p\|O_{11}^{ud,(8,8)}\|p\rangle + \langle n\|O_{11}^{ud,(8,8)}\|n\rangle + \langle\Sigma^0\|O_{11}^{ud,(8,8)}\|\Sigma^0\rangle - 3\langle\Lambda\|O_{11}^{ud,(8,8)}\|\Lambda\rangle$ $+\langle\Xi^0\|O_{11}^{ud,(8,8)}\|\Xi^0\rangle + \langle\Xi^-\|O_{11}^{ud,(8,8)}\|\Xi^-\rangle = 0$ $\langle p\|O_{11}^{ud,(8,8)}\|p\rangle - \langle n\|O_{11}^{ud,(8,8)}\|n\rangle - \langle\Xi^0\|O_{11}^{ud,(8,8)}\|\Xi^0\rangle + \langle\Xi^-\|O_{11}^{ud,(8,8)}\|\Xi^-\rangle$ $-\sqrt{3}\langle\Lambda\|O_{11}^{ud,(8,8)}\|\Sigma^0\rangle - \sqrt{3}\langle\Sigma^0\|O_{11}^{ud,(8,8)}\|\Lambda\rangle = 0$

Table 2.5: Relations among hadronic matrix elements of the four-quark operators in different chiral representations.

2.3.3 Matching to EDM-Type Operators

In χPT, any CP-odd quark-gluon operator will generate directly an EDM contribution to the neutron, analytical in the chiral limit. To write down such a contribution, introduce vector and axial vector octet potential v_μ and a_μ, which transform under local chiral rotations (with space-time dependent chiral transformation) as

$$r_\mu \equiv v_\mu + a_\mu \longrightarrow v'_\mu + a'_\mu = R(v_\mu + a_\mu)R^\dagger + iR\partial_\mu R^\dagger ,$$

$$l_\mu \equiv v_\mu - a_\mu \longrightarrow v'_\mu - a'_\mu = L(v_\mu - a_\mu)L^\dagger + iL\partial_\mu L^\dagger . \quad (2.63)$$

The corresponding gauge fields are defined as

$$f^R_{\mu\nu} = \partial_\mu r_\nu - \partial_\nu r_\mu - i[r_\mu, r_\nu] ,$$

$$f^L_{\mu\nu} = \partial_\mu l_\nu - \partial_\nu l_\mu - i[l_\mu, l_\nu] . \quad (2.64)$$

The gauge fields with definite parity are defined as

$$f^\pm_{\mu\nu} = \xi^\dagger f^R_{\mu\nu}\xi \pm \xi f^L_{\mu\nu}\xi^\dagger, \quad (2.65)$$

which transform under chiral transformation as

$$f^\pm_{\mu\nu} \to K f^\pm_{\mu\nu} K^\dagger . \quad (2.66)$$

When reducing to the electromagnetic field, $a_\mu = 0$, $f^\pm_{\mu\nu} = (\xi^\dagger Q\xi \pm \xi Q\xi^\dagger)F_{\mu\nu}$, where $Q = \mathrm{diag}(2/3, -1/3, -1/3)$ and $F_{\mu\nu}$ is the electromagnetic ffield [23].

One can write down a number of EDM type of operators which contain $\bar{B}$ and B, $f^\pm_{\mu\nu}$, and the spurion fields A, H, and S. These contributions are direct matching contributions to the neutron EDM, and cannot be calculated in χPT. These chiral constants can in principle be calculated in lattice QCD. However, we will present quark-model estimates in Sec. V.

41

2.3.4 Peccei-Quinn Symmetry and Induced θ-Term

The experimental upper bound on the neutron EDM gives a strong constraint on the P-odd and CP-odd θ-term, $\theta G\tilde{G}$, in the QCD lagrangian [7, 14, 6]. A brief discussion of θ-term contribution to nEDM can be found in Appendix C. Using the current experimental limit [33],

$$d_n < 2.9 \times 10^{-26} e \text{ cm} , \tag{2.67}$$

one can get the upper bound,

$$\theta < 10^{-10} . \tag{2.68}$$

On the other hand, it is unnatural for a parameter of the fundamental theory to be so small without fine tuning. There are generally two ways to solve this strong CP problem in the literature. The first is by introducing the spontaneous breaking of parity. Since the θ-term also breaks parity, if at some high energy scale parity is conserved, then the θ-term at low energy scale can only be generated by loop effects and will be suppressed naturally [34].

The other way is to introduce the Peccei-Quinn symmetry, $U(1)_A$ [35]. After the spontaneous breaking of the symmetry, there emerges a pseudo-goldstone boson, a, which is called the axion [36, 37, 38]. The effective Lagrangian for the axion field can be written as

$$\mathcal{L}_a = \frac{1}{2}\partial_\mu a \partial^\mu a + \frac{a}{f_a}\frac{\alpha_s}{8\pi}G^a_{\mu\nu}\tilde{G}^{a\mu\nu}, \tag{2.69}$$

which includes an effective interaction with $G\tilde{G}$. The axion field gets a small mass

through the non-vanishing correlation function

$$K = i \left\{ \int d^4x e^{ik \cdot x} \left\langle 0 \left| T \left(\frac{\alpha_s}{8\pi} G\tilde{G}(x), \frac{\alpha_s}{8\pi} G\tilde{G}(0) \right) \right| 0 \right\rangle \right\}_{k=0}, \quad (2.70)$$

after taking into account the non-perturbative QCD effect [37, 38].

When there is an additional neutral P-odd, CP-odd quark operator, $O_{\text{CP}-\text{odd}}$, in the lagrangian, the correlation function

$$K_1 = i \left\{ \int d^4x e^{ik \cdot x} \left\langle 0 \left| T \left(\frac{\alpha_s}{8\pi} G\tilde{G}(x), O_{\text{CP}-\text{odd}}(0) \right) \right| 0 \right\rangle \right\}_{k=0} \quad (2.71)$$

will be generally nonzero. Therefore, the vev of a, which cancels precisely the θ-term in the original lagrangian, will now be shifted by a small amount proportional to K_1. A non-vanishing effective θ-term is induced as [39]

$$\theta_{\text{ind}} = -\frac{K_1}{K}, \quad (2.72)$$

which can contribute to the neutron EDM.

Following Ref. [39], we take the operator $\bar{u}i\gamma_5 u \bar{d}d$ as an example to calculate the contribution to neutron EDM through the induced θ-term. Then, K_1 can then be written as

$$K_1 = i \left\{ \int d^4x e^{ik \cdot x} \left\langle 0 \left| T \left(\frac{\alpha_s}{8\pi} G\tilde{G}(x), C_4 \bar{u}i\gamma_5 u \bar{d}d(0) \right) \right| 0 \right\rangle \right\}_{k=0}. \quad (2.73)$$

Using the chiral anomaly [40], one can get

$$\frac{\alpha_s}{4\pi} G\tilde{G} = \partial_\mu J_5^\mu - 2m_*(\bar{u}i\gamma_5 u + \bar{d}i\gamma_5 d + \bar{s}i\gamma_5 s), \quad (2.74)$$

where

$$J_5^\mu \equiv \left(\frac{m_*}{m_u} \bar{u}\gamma^\mu\gamma_5 u + \frac{m_*}{m_d} \bar{d}\gamma^\mu\gamma_5 d + \frac{m_*}{m_s} \bar{s}\gamma^\mu\gamma_5 s \right). \quad (2.75)$$

43

Then one can get

$$
\begin{aligned}
K_1 &= \frac{i}{2} \int d^4 x \, e^{ik \cdot x} \left\langle 0 \left| T \left(\partial_\mu J_5^\mu(x), C_4 \bar{u} i \gamma_5 u \bar{d} d(0) \right) \right| 0 \right\rangle_{k=0} \\
&\quad - \frac{i}{2} \int d^4 x \, e^{ik \cdot x} \left\langle 0 \left| T \left(2 m_* (\bar{u} i \gamma_5 u + \bar{d} i \gamma_5 d + \bar{s} i \gamma_5 s)(x), C_4 \bar{u} i \gamma_5 u \bar{d} d(0) \right) \right| 0 \right\rangle_{k=0}
\end{aligned}
\tag{2.76}
$$

The second term on the right-hand side of the above equation is negligible compared to the first term because it is explicitly proportional to the reduced quark mass m_* and the operator $\bar{u} i \gamma_5 u + \bar{d} i \gamma_5 d + \bar{s} i \gamma_5 s$ cannot annihilate light mesons. Therefore K_1 can be calculated as

$$
\begin{aligned}
K_1 &\approx \frac{i}{2} \int d^4 x \, e^{ik \cdot x} \langle 0 | T(\partial_\mu J_5^\mu(x), C_4 \bar{u} i \gamma_5 u \bar{d} d(0)) | 0 \rangle_{k=0} \\
&= -\frac{i}{2} C_4 \langle 0 | [Q_5(0), \bar{u} i \gamma_5 u \bar{d} d(0)] | 0 \rangle,
\end{aligned}
\tag{2.77}
$$

where Q_5 is the charge related to the current J_5^μ defined in Eq. (2.75). In the spirit of large N_C [41, 42] expansion one can assume that

$$
\langle 0 | \bar{u} i \gamma_5 u \bar{d} i \gamma_5 d | 0 \rangle \ll \langle 0 | \bar{u} u \bar{d} d | 0 \rangle \approx \langle 0 | \bar{u} u | 0 \rangle \langle 0 | \bar{d} d | 0 \rangle.
\tag{2.78}
$$

Therefore, we can get

$$
\begin{aligned}
K_1 &\simeq -\frac{i}{2} C_4 \langle 0 | [Q_5(0), \bar{u} i \gamma_5 u(0)] | 0 \rangle \langle 0 | \bar{d} d | 0 \rangle = -C_4 \frac{m_*}{m_u} \langle 0 | \bar{u} u | 0 \rangle \langle 0 | \bar{d} d | 0 \rangle \\
&= -\frac{m_*}{m_u} C_4 B_0^2 F_\pi^4 \ .
\end{aligned}
\tag{2.79}
$$

Using the previously known result [38]

$$
K = -m_* F_\pi^2 B_0 \ ,
\tag{2.80}
$$

one can get the θ angle induced by the operator $\bar{u} i \gamma_5 u \bar{d} d$,

$$
\theta_{\text{ind}} = -\frac{K_1}{K} = -\frac{C_4 B_0 F_\pi^2}{m_u} \ .
\tag{2.81}
$$

44

A similar result can be obtained for any other CP-odd four-quark operator.

Using the standard chiral result in the literature [8], we write down the effective chiral lagrangian corresponding to this induced θ term;

$$\mathcal{L}_\theta = \frac{4\theta m_*}{F_\pi} \left(c_2 \text{Tr}[\Sigma \bar{B} B] + c_3 \text{Tr}[\bar{B} \Sigma B] \right) + 2m_*\theta(3d_1 + d_2 + d_3)\text{Tr}[\bar{B} i\gamma_5 B] \ . \quad (2.82)$$

From the above, we read off the CP-odd pion-nucleon coupling and the CP-odd mass of the neutron;

$$h_c = -\frac{2\sqrt{2}C_4 B_0 F_\pi m_*}{m_u} \quad h_n = \frac{2C_4 B_0 F_\pi m_*}{m_u} \ ,$$
$$M_\star = \frac{2C_4 B_0 F_\pi^2 m_*}{m_u}(3d_1 + d_2 + d_3) \ . \quad (2.83)$$

Comparing this with the meson condensates contribution in Eq. (2.85), one finds that they are in the same order. If the Peccei-Quinn symmetry exists, one should add this contribution to the neutron EDM. However, since it is not known if the axion mechanism is in operation, we will not include this contribution to the nEDM in the remainder of the paper.

2.4 P-odd and CP-odd nucleon-pion vertices and CP-odd Nucleon Mass

In this section, we study the induced physical P-odd and CP-odd nucleon-pion vertices as well as the CP-odd nucleon mass from four-quark operators. There are a number of contributions to consider: First, the CP-odd meson lagrangian will generate meson condensates which can convert a CP-even vertex into a CP-odd one. Second, the baryon wave function contains the CP-odd part due to the CP-odd

nucleon mass, which can also rotate a CP-even coupling into a CP-odd one. Finally, there is the contribution from the direct matching operators (without a tilde) in TABLE II. We will consider all of these in this section.

2.4.1 Meson Condensates Contribution

We use the vacuum saturation approximation to calculate the meson effective lagrangian; the vevs of π^0 and η can be obtained from Eq. (2.41), where g_π and g_η for all the four-quark operators built with color-singlet and octet scalar currents are listed in Table 2.6. Those induced by tensor operators vanish in this approximation.

In the large N_c QCD [41] (also see Ref. [42] for a good review), the leading contributions for operators constructed from two color-octet currents and two tensor currents are shown as diagrams (a) and (b) in Fig. 2.1, respectively. Detailed analysis shows that the diagrams (a) and (b) suffer from $1/N_c^2$ suppressions compared with (c), which stands for the operator constructed from two scalar color-singlet currents.

Terms contributing to the P-odd, CP-odd nucleon-pion vertices through the condensates of neutral mesons are shown in Eq. (2.47). At tree level, one can relate the coefficients c_1, c_2, and c_3 to the mass differences of the baryons and the πN σ-term, and their values can be found in the literature [23];

$$c_1 = 2B_0 b_0 \ , \ \ c_2 = 2B_0(b_d - b_f) \ , \ \ c_3 = 2B_0(b_d + b_f) \ , \tag{2.84}$$

where $b_0 = -0.517 \ \text{GeV}^{-1}$, $b_d = 0.066 \ \text{GeV}^{-1}$ and $b_f = -0.213 \ \text{GeV}^{-1}$.

The vertices we are interested in have two nucleons and one pion because of

Operator	g_π	g_η	Operator	g_π	g_η
$\bar{u}i\gamma_5 u\bar{d}d$	1	$1/\sqrt{3}$	$\bar{u}i\gamma_5 t^a u\bar{d}t^a d$	0	0
$\bar{d}i\gamma_5 d\bar{u}u$	-1	$1/\sqrt{3}$	$\bar{d}i\gamma_5 t^a d\bar{u}t^a u$	0	0
$\bar{u}i\gamma_5 u\bar{s}s$	1	$1/\sqrt{3}$	$\bar{u}i\gamma_5 t^a u\bar{s}t^a s$	0	0
$\bar{s}i\gamma_5 s\bar{u}u$	0	$-2/\sqrt{3}$	$\bar{s}i\gamma_5 t^a s\bar{u}t^a u$	0	0
$\bar{d}i\gamma_5 d\bar{s}s$	-1	$1/\sqrt{3}$	$\bar{d}i\gamma_5 t^a d\bar{s}t^a s$	0	0
$\bar{s}i\gamma_5 s\bar{d}d$	0	$-2/\sqrt{3}$	$\bar{s}i\gamma_5 t^a s\bar{d}t^a d$	0	0
$\bar{u}i\gamma_5 u\bar{u}u$	$5/6$	$5/(6\sqrt{3})$	$\bar{u}i\gamma_5 t^a u\bar{u}t^a u$	$-2/9$	$-2/(9\sqrt{3})$
$\bar{d}i\gamma_5 d\bar{d}d$	$-5/6$	$5/(6\sqrt{3})$	$\bar{d}i\gamma_5 t^a d\bar{d}t^a d$	$2/9$	$-2/(9\sqrt{3})$
$\bar{s}i\gamma_5 s\bar{s}s$	0	$-5/(3\sqrt{3})$	$\bar{s}i\gamma_5 t^a s\bar{s}t^a s$	0	$4/(9\sqrt{3})$

Table 2.6: g_π and g_η induced by four-quark operators constructed by scalar currents. Those induced by products of tensor currents are zero.

	Meson condensates contribution		Factorization	
Operator	h_c ($C_4 B_0^2$)	h_n ($C_4 B_0^2$)	h_c ($C_4 B_0^2$)	h_n ($C_4 B_0^2$)
$\bar{u} i \gamma_5 u \bar{d} d$	-0.0117	0.225	0.0063	-0.24
$\bar{d} i \gamma_5 d \bar{u} u$	0.0130	-0.227	0.0063	0.19
$\bar{u} i \gamma_5 u \bar{s} s$	-0.0117	0.225	0	-0.088
$\bar{s} i \gamma_5 s \bar{u} u$	-0.00122	0.000864	0	0
$\bar{d} i \gamma_5 d \bar{s} s$	0.0130	-0.227	0	0.087
$\bar{s} i \gamma_5 s \bar{d} d$	-0.00122	0.000864	0	0
$\bar{u} i \gamma_5 u \bar{u} u$	-0.00976	0.188	0	-0.16
$\bar{d} i \gamma_5 d \bar{d} d$	0.0108	-0.189	0	0.20
$\bar{s} i \gamma_5 s \bar{s} s$	-0.00102	0.000722	0	0
$\bar{u} i \gamma_5 \sigma^{\mu\nu} u \bar{d} \sigma_{\mu\nu} d$	0	0	0.076	0
$\bar{u} i \gamma_5 \sigma^{\mu\nu} u \bar{s} \sigma_{\mu\nu} s$	0	0	0	0
$\bar{d} i \gamma_5 \sigma^{\mu\nu} d \bar{s} \sigma_{\mu\nu} s$	0	0	0	0

Table 2.7: CP-odd pion-nucleon couplings induced by meson condensates. C_4 is the Wilson coefficient of the corresponding four-quark operator. The two columns on the right side shows the P-odd and CP-odd pion-nucleon vertices calculated using factorization which will be discussed in Sec. V.

Operator	Meson condensates contribution		Factorization	
	h_c $(C_4 B_0^2)$	h_n $(C_4 B_0^2)$	h_c $(C_4 B_0^2)$	h_n $(C_4 B_0^2)$
$\bar{u}i\gamma_5 t^a u \bar{d} t^a d$	0	0	0.0085	0
$\bar{d}i\gamma_5 t^a d \bar{u} t^a u$	0	0	0.0085	0
$\bar{u}i\gamma_5 t^a u \bar{s} t^a s$	0	0	0	0
$\bar{s}i\gamma_5 t^a s \bar{u} t^a u$	0	0	0	0
$\bar{d}i\gamma_5 t^a d \bar{s} t^a s$	0	0	0	0
$\bar{s}i\gamma_5 t^a s \bar{d} t^a d$	0	0	0	0
$\bar{u}i\gamma_5 t^a u \bar{u} t^a u$	0.00261	-0.0501	0	0.042
$\bar{d}i\gamma_5 t^a d \bar{d} t^a d$	-0.00288	0.0503	0	-0.054
$\bar{s}i\gamma_5 t^a s \bar{s} t^a s$	0.000272	-0.000192	0	0
$\bar{u}i\gamma_5 \sigma^{\mu\nu} t^a u \bar{d} \sigma_{\mu\nu} t^a d$	0	0	0.101	0
$\bar{u}i\gamma_5 \sigma^{\mu\nu} t^a u \bar{s} \sigma_{\mu\nu} t^a s$	0	0	0	0
$\bar{d}i\gamma_5 \sigma^{\mu\nu} t^a d \bar{s} \sigma_{\mu\nu} t^a s$	0	0	0	0

Table 2.8: CP-odd pion-nucleon couplings induced by meson condensates. C_4 is the Wilson coefficient of the corresponding four-quark operator. The two columns on the right side shows the P-odd and CP-odd pion-nucleon vertices calculated using factorization which will be discussed in Sec. V.
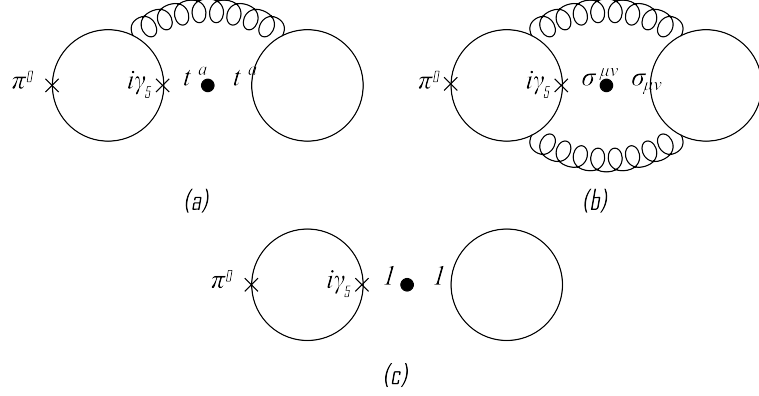
Figure 2.1: Annihilation of pion by four-quark operators: (a) operator constructed from two color-octet current, like $\bar{u}i\gamma_5 t^a u \bar{d} t^a d$; (b) operator from two tensor currents, like $\bar{u}\sigma^{\mu\nu}i\gamma_5 u \bar{d}\sigma_{\mu\nu}d$; (c) operator from two scalar currents, like $\bar{u}i\gamma_5 u \bar{d}d$.

the infrared enhancement in the pion loop [7]. From Eq. (2.47) we can read off the relevant terms,

$$
\begin{aligned}
&-\frac{1}{3F_\pi^2}\left\{c_3[3\sqrt{2}\langle\pi^0\rangle(m_u - m_d) + \sqrt{6}\langle\eta\rangle(m_u + m_d)]\right\}(\bar{n}p\pi^- + \bar{p}n\pi^+)\\
&-\frac{2}{3F_\pi^2}\left\{c_3 m_d(3\langle\pi^0\rangle - \sqrt{3}\langle\eta\rangle) + c_1[3(m_u + m_d)\langle\pi^0\rangle + \sqrt{3}\langle\eta\rangle(m_u - m_d)]\right\}\bar{n}n\pi^0 ,
\end{aligned}
$$

(2.85)

in which $\langle\pi^0\rangle$ and $\langle\eta\rangle$ are given in Eq. (2.41). It is customary to define the P-odd, CP-odd nucleon-pion couplings

$$
\mathcal{L}_{CPV} = h_c(\bar{p}n\pi^+ + \bar{n}p\pi^-) + h_n\bar{n}n\pi^0,
$$

(2.86)

where h_c and h_n induced by meson condensates are listed in Tables 2.7 and 2.8. Typical values of h_c are one order of magnitude smaller than the value of h_n because $\sqrt{2}c_3(m_d - m_u) \ll 4c_1(m_u + m_d)$. For h_c or h_n generated by a certain four-quark operator, if the contribution from $\langle\pi^0\rangle$ is non-vanishing, the contribution from $\langle\eta\rangle$

50

can be neglected since $\langle \pi^0 \rangle / \langle \eta \rangle \simeq m_s / \hat{m} \simeq 30$. This also explains the contributions from operators with the $\bar{s} i \gamma_5 s$ factor are much smaller than those without. Finally, the contributions from operators made of color-octet currents are smaller than those from operators made of color-singlet currents because a Fierz transformation is needed for color-octet operators to annihilate the mesons, introducing a suppressing factor of 1/4.

In Tables 2.7 and 2.8 one can see that the P-odd and CP-odd pion-nucleon couplings are proportional to B_0^2, which is related to the quark condensates. The value of B_0 can be extracted from the pion mass

$$m_\pi^2 = B_0(m_u + m_d) \ . \tag{2.87}$$

The natural scale for χPT is $4\pi F_\pi$ [43], and for simplicity we use the same scale to define the quark masses to get B_0. The quark masses we use are $m_u = 2.4$ MeV and $m_d = 4.75$ MeV in $\overline{\text{MS}}$ at 2 GeV. Using the one-loop renormalization group to run them down to $\mu = 4\pi F_\pi$, we have

$$B_0 = 2.2 \text{ GeV} \ . \tag{2.88}$$

Here we have used one-loop $\Lambda_{\text{QCD}} = 250$ MeV.

2.4.2 Direct Contribution from Matching

To get the P-odd and CP-odd meson-nucleon coupling through direct matching, one needs to calculate the matrix elements listed in Table 2.5. Lattice QCD is perhaps the ultimate choice for calculating hadronic matrix elements. However, it is

still quite difficult to directly calculate the matrix elements of four-quark operators between baryons. Therefore, we resort to quark models to get an estimate. In the remainder of this subsection we will use two different quark models to calculate these hadronic matrix elements: the simple non-relativistic quark model [44, 45, 46, 47, 48] and the MIT bag model [49, 50, 51, 52, 48]. We also discuss the significance of the model calculations from the viewpoint of naive factorization.

2.4.2.1 Non-relativistic Quark Model

Here we consider the simplest version of the non-relativistic quark model with harmonic oscillator interacting potentials,

$$H = -\sum_{i=1}^{3} \frac{1}{2m}\nabla_i^2 + \frac{1}{2}\frac{m_c}{3}\omega^2 \left[(\vec{r}_1 - \vec{r}_2)^2 + (\vec{r}_2 - \vec{r}_3)^2 + (\vec{r}_3 - \vec{r}_1)^2\right] \; , \qquad (2.89)$$

where $\vec{r}_1$, $\vec{r}_2$, and $\vec{r}_3$ are positions of the three quarks inside the baryon, m_c is the mass of the constituent quarks and ω is the angular frequency. One can isolate the center of mass by introducing the Jacobi coordinates,

$$\begin{aligned}
\vec{R} &= \frac{1}{\sqrt{3}}(\vec{r}_1 + \vec{r}_2 + \vec{r}_3) \; , \\
\vec{\rho} &= \frac{1}{\sqrt{2}}(\vec{r}_1 - \vec{r}_2) \; , \\
\vec{\lambda} &= \frac{1}{\sqrt{6}}(\vec{r}_1 + \vec{r}_2 - 2\vec{r}_3) \; .
\end{aligned} \qquad (2.90)$$

Then the spatial wave function of the nucleon can be written as

$$f(\vec{r}_1, \vec{r}_2, \vec{r}_3; \vec{k}) = (3\sqrt{3})^{-1/2}\exp(i\vec{P}\cdot\vec{R}/\sqrt{3})\psi(\vec{\rho}, \vec{\lambda}) \; , \qquad (2.91)$$

where $\psi(\vec{\rho}, \vec{\lambda}) = (\alpha^3/\pi^{3/2})\exp\left[-\alpha^2(\rho^2 + \lambda^2)/2\right]$ in which $\alpha = (m\omega)^{1/2} \approx 0.41$ GeV [47] is the oscillator parameter, and $\vec{P}$ is the nucleon momentum. It is easy to check

that the wave function is normalized to $(2\pi)^3\delta^3(\vec{P}-\vec{P'})$. The internal part of the wave function is assumed to have $SU(6)$ spin-flavor symmetry. For example, the spin-up proton state has the following wave function,

$$
\begin{aligned}
|p_\uparrow\rangle \;=\; & \frac{1}{\sqrt{18}}\int d^3r_1 d^3r_2 d^3r_3 f(\vec{r}_1,\vec{r}_2,\vec{r}_3)\epsilon^{abc} \\
& \left[u_\downarrow^{a\dagger}(\vec{r}_1)d_\uparrow^{b\dagger}(\vec{r}_2)-u_\uparrow^{a\dagger}(\vec{r}_1)d_\downarrow^{b\dagger}(\vec{r}_2)\right]u_\uparrow^{c\dagger}(\vec{r}_3)|0\rangle\;,
\end{aligned}
\tag{2.92}
$$

where a, b, and c are color indices and the anti-commutation relation of the non-relativistic quark creation and annihilation operators is defined as $\{u_\alpha^{a\dagger}(\vec{x}),u_\beta^b(\vec{y})\}=\delta_{ab}\delta_{\alpha\beta}\delta^3(\vec{x}-\vec{y})$ with α and β as spin indices. The spatial part of the wave functions is common for all members of the baryon octet. The SU(6) internal wave functions are listed in Table 2.9 for easy reference.

$$|p_\uparrow\rangle \sim \tfrac{1}{\sqrt{18}}\epsilon^{abc}[u_\downarrow^{a\dagger}d_\uparrow^{b\dagger}-u_\uparrow^{a\dagger}d_\downarrow^{b\dagger}]u_\uparrow^{c\dagger}|0\rangle;$$

$$|n_\uparrow\rangle \sim \tfrac{1}{\sqrt{18}}\epsilon^{abc}[d_\uparrow^{a\dagger}u_\downarrow^{b\dagger}-d_\downarrow^{a\dagger}u_\uparrow^{b\dagger}]d_\uparrow^{c\dagger}|0\rangle;$$

$$|\Lambda_\uparrow\rangle \sim \tfrac{1}{\sqrt{12}}\epsilon^{abc}[u_\uparrow^{a\dagger}d_\downarrow^{b\dagger}-u_\downarrow^{a\dagger}d_\uparrow^{b\dagger}]s_\uparrow^{c\dagger}|0\rangle;$$

$$|\Sigma_\uparrow^+\rangle \sim \tfrac{1}{\sqrt{18}}\epsilon^{abc}[s_\downarrow^{a\dagger}u_\uparrow^{b\dagger}-s_\uparrow^{a\dagger}u_\downarrow^{b\dagger}]u_\uparrow^{c\dagger}|0\rangle;$$

$$|\Sigma_\uparrow^0\rangle \sim \tfrac{1}{6}\epsilon^{abc}[s_\uparrow^{a\dagger}d_\downarrow^{b\dagger}u_\uparrow^{c\dagger}+s_\uparrow^{a\dagger}d_\uparrow^{b\dagger}u_\downarrow^{c\dagger}-2s_\downarrow^{a\dagger}d_\uparrow^{b\dagger}u_\uparrow^{c\dagger}]|0\rangle;$$

$$|\Sigma_\uparrow^-\rangle \sim \tfrac{1}{\sqrt{18}}\epsilon^{abc}[s_\uparrow^{a\dagger}d_\downarrow^{b\dagger}-s_\downarrow^{a\dagger}d_\uparrow^{b\dagger}]d_\uparrow^{c\dagger}|0\rangle;$$

$$|\Xi_\uparrow^0\rangle \sim \tfrac{1}{\sqrt{18}}\epsilon^{abc}[s_\downarrow^{a\dagger}u_\uparrow^{b\dagger}-s_\uparrow^{a\dagger}u_\downarrow^{b\dagger}]s_\uparrow^{c\dagger}|0\rangle;$$

$$|\Xi_\uparrow^-\rangle \sim \tfrac{1}{\sqrt{18}}\epsilon^{abc}[s_\uparrow^{a\dagger}d_\downarrow^{b\dagger}-s_\downarrow^{a\dagger}d_\uparrow^{b\dagger}]s_\uparrow^{c\dagger}|0\rangle.$$

Table 2.9: SU(6) wave functions of baryon spin-1/2 octet.

Using Eqs. (2.15)-(2.20), one can project operator $\bar{u}i\gamma_5 u\bar{d}d$ into different irreducible representations of the chiral group, $O_{11}^{ud,(\bar{3},3)}$, $O_{11}^{ud,(6,\bar{6})}$, and $O_{11}^{ud,(8,8)}$ as in Eq.

(D.12). Restricting to the non-relativistic case, these operators become

$$O_{11}^{ud,(\bar{3},3)}(x) \simeq -\frac{i}{8} : \left(u_\alpha^{a\dagger}(x)u_\alpha^a(x)d_\beta^{b\dagger}(x)d_\beta^b(x) - d_\alpha^{a\dagger}(x)u_\alpha^a(x)u_\beta^{b\dagger}(x)d_\beta^b(x) \right) :$$

$$O_{11}^{ud,(6,\bar{6})}(x) \simeq -\frac{i}{8} : \left(u_\alpha^{a\dagger}(x)u_\alpha^a(x)d_\beta^{b\dagger}(x)d_\beta^b(x) + d_\alpha^{a\dagger}(x)u_\alpha^a(x)u_\beta^{b\dagger}(x)d_\beta^b(x) \right) :$$

$$O_{11}^{ud,(8,8)}(x) \simeq \frac{i}{4} : u_\alpha^{a\dagger}(x)u_\alpha^a(x)d_\beta^{b\dagger}(x)d_\beta^b(x) : . \tag{2.93}$$

where u and d are non-relativistic two-component quark annihilation operators, a and b label the color, α and β label the spin, and the ": :" means that the products of the constituent quark fields are normal-ordered.

Considering the $(6, \bar{6})$ component as an example, the simple quark model gives the following matrix elements:

$$\langle p_\uparrow(P)|O_{11}^{ud,(6,\bar{6})}|p_\uparrow(P)\rangle = \langle n_\uparrow(P)|O_{11}^{ud,(6,\bar{6})}|n_\uparrow(P)\rangle = -\frac{i}{8}a \ ,$$

$$\langle \Sigma_\uparrow^+(P)|O_{11}^{ud,(6,\bar{6})}|\Sigma_\uparrow^+(P)\rangle = \langle \Sigma_\uparrow^-(P)|O_{11}^{ud,(6,\bar{6})}|\Sigma_\uparrow^-(P)\rangle = 0 \ ,$$

$$\langle \Sigma_\uparrow^0(P)|O_{11}^{ud,(6,\bar{6})}|\Sigma_\uparrow^0(P)\rangle = -\frac{i}{4}a \ ,$$

$$\langle \Lambda_\uparrow(P)|O_{11}^{ud,(6,\bar{6})}|\Lambda_\uparrow(P)\rangle = 0 \ ,$$

$$\langle \Xi_\uparrow^0(P)|O_{11}^{ud,(6,\bar{6})}|\Xi_\uparrow^0(P)\rangle = \langle \Xi_\uparrow^-(P)|O_{11}^{ud,(6,\bar{6})}|\Xi_\uparrow^-(P)\rangle = 0 \ , \tag{2.94}$$

where $a = \int d^3r f^*(\vec{P}; \vec{x}, \vec{x}, \vec{r}) f(\vec{P}; \vec{x}, \vec{x}, \vec{r})$ is independent of $\vec{x}$. It is easy to check that these matrix elements satisfy the symmetry conditions listed in Table 2.5. Using Eq. (2.61), one can get the Wilson coefficients for $(6, \bar{6})$ hadronic operators defined in Eq. (2.54);

$$C_6^{(1)} = -C_6^{(2)} = \frac{1}{8}\frac{\alpha^3}{(2\pi)^{3/2}};$$

$$C_6^{(3)} = C_4^{(4)} = 0 \ . \tag{2.95}$$

54

Expanding the hadronic operators to the first order, one can get the P-odd, CP-odd three-point nucleon-pion couplings, h_c and h_n. The result induced by $O_{11}^{ud,(6,\bar{6})}$ is

$$h_c = C_{11}^{ud}\alpha^3/(8\pi^{3/2}F_\pi) \simeq 0.022 C_{11}^{ud}\alpha^3/F_\pi \ , \quad h_n = 0 \ . \tag{2.96}$$

In the same way one can calculate h_c and h_n induced by the $(\bar{3},3)$ and $(8,8)$ components of $\bar{u}i\gamma_5 u\bar{d}d$. Taking into account the hermitian conjugate part of each component, the contribution for h_c and h_n is doubled.

2.4.2.2 MIT Bag Model

The basic idea of the bag model is that valence quarks are confined in a bag where the vacuum is in a phase different from the true QCD vacuum. The inside has a constant energy-momentum density generating a negative pressure, B, which is balanced by the positive pressure of the quarks. The bag is usually taken as a sphere of radius R_0. The quarks inside the bag move freely with the following wave functions,

$$\psi_{n,-1,1/2,m}(\vec{r},t) \ = \ \frac{N}{\sqrt{4\pi}}\begin{pmatrix} ij_0(\omega_{n,-1}r/R_0)\chi_m \\ \\ -j_1(\omega_{n,-1}r/R_0)\vec{\sigma}\cdot\hat{r}\chi_m \end{pmatrix} . \tag{2.97}$$

The normalization factor of the above is

$$N(\omega_{n\kappa}) = \left(\frac{\omega_{n\kappa}^3}{2R_0^3(\omega_{n\kappa}+\kappa)\sin^2\omega_{n\kappa}}\right)^{1/2} . \tag{2.98}$$

The boundary condition gives the energy eigenvalue equation,

$$\tan\omega_{n\kappa} = \frac{\omega_{n\kappa}}{\omega_{n\kappa}+\kappa} \ , \tag{2.99}$$

and numerical calculation gives $\omega_0 = 2.043$. The ground state of quarks is $\kappa = -1$, $n = 0$ state. For the baryon octet, all the quarks are in this state. Keeping only this, the quark operator can be written as

$$q(x) = \psi_{0,-1,1/2,m}(\vec{x})e^{-i\omega_{0,-1}t/R_0}b_{0,-1,1/2,m} + (\text{anti-quark creation}) . \qquad (2.100)$$

The physical meaning of the operator $b_m(0)$ is that it annihilates a quark with quantum number described by the wave function $\psi_{0,-1,1/2,m}$. Due to the assumption that inside the bag the interaction between quarks and gluons is negligible, flavor and spin automatically become good quantum numbers.

We again take the $(6,\bar{6})$ component of $\bar{u}i\gamma_5 u\bar{d}d$ as an example, which can be written as

$$
\begin{aligned}
O_{11}^{ud(6,\bar{6})} \quad \sim \quad &-\frac{i}{2}\bar{\psi}_\lambda(\vec{x})\mathbb{P}_L\psi_\sigma(\vec{x})\bar{\psi}_\rho(\vec{x})\mathbb{P}_L\psi_\tau(\vec{x}) \\
&\times \left[u_\lambda^{a\dagger}u_\sigma^a d_\rho^{b\dagger}d_\tau^b + d_\lambda^{a\dagger}u_\sigma^a u_\rho^{b\dagger}d_\tau^b \right] ,
\end{aligned}
\qquad (2.101)
$$

where a and b are indices of color, λ, σ, ρ, τ labeling the spin. The creation and annihilation operators here are just like $b_{0,-1,1/2,m}$ in Eq. (2.100). Using

$$
\begin{aligned}
&\bar{\psi}_\lambda(x)\mathbb{P}_L\psi_\sigma(x) \\
= \quad &\frac{N^2}{8\pi} \left\{ \left[j_0^2(\omega_0 r/R_0) - j_1^2(\omega_0 r/R_0) \right] \delta_{\lambda\sigma} \right. \\
&\left. -2ij_0(\omega r/R_0)j_0(\omega r/R)\chi_\lambda^\dagger \vec{\sigma}\cdot\hat{r}\chi_\sigma \right\} ,
\end{aligned}
\qquad (2.102)
$$

and only keeping the terms which give non-vanishing contributions after integrating

Operators	NR quark model		MIT bag model	
	$h_c/(\alpha^3/F_\pi)$	$h_n/(\alpha^3/F_\pi)$	$h_c/(1/(R_0^3 F_\pi))$	$h_n/(1/(R_0^3 F_\pi))$
$\bar{u}i\gamma_5 u\bar{d}d$	0.045	0.13	0.029	-0.024
$\bar{d}i\gamma_5 d\bar{u}u$	0.045	-0.13	0.029	0.024
$\bar{u}i\gamma_5 u\bar{s}s$	0	0	0	0
$\bar{s}i\gamma_5 s\bar{u}u$	0	0	0	0
$\bar{d}i\gamma_5 d\bar{s}s$	0	0	0	0
$\bar{s}i\gamma_5 s\bar{d}d$	0	0	0	0
$\bar{u}i\gamma_5 u\bar{u}u$	0.045	0	0.029	0
$\bar{d}i\gamma_5 d\bar{d}d$	0.045	-0.13	0.029	-0.083
$\bar{s}i\gamma_5 s\bar{s}s$	0	0	0	0
$\bar{u}i\gamma_5\sigma^{\mu\nu}u\bar{d}\sigma_{\mu\nu}d$	0.18	0	0.12	0
$\bar{d}i\gamma_5\sigma^{\mu\nu}d\bar{u}\sigma_{\mu\nu}u$	0.18	0	0.12	0
$\bar{u}i\gamma_5\sigma^{\mu\nu}u\bar{s}\sigma_{\mu\nu}s$	0	0	0	0
$\bar{s}i\gamma_5\sigma^{\mu\nu}s\bar{u}\sigma_{\mu\nu}u$	0	0	0	0
$\bar{d}i\gamma_5\sigma^{\mu\nu}d\bar{s}\sigma_{\mu\nu}s$	0	0	0	0
$\bar{s}i\gamma_5\sigma^{\mu\nu}s\bar{d}\sigma_{\mu\nu}d$	0	0	0	0

Table 2.10: P-odd, CP-odd three-point pion-nucleon vertices generated by P-odd, CP-odd four-quark operators. The couplings induced by operators constructed by two color-octet currents are equal to the couplings induced by corresponding color-singlet operators multiplying by $-2/3$.

over a spherical region, we have

$$\bar{\psi}_\lambda(x)\mathbb{P}_L\psi_\sigma(x)\bar{\psi}_\rho(x)\mathbb{P}_L\psi_\tau(x)$$

$$\simeq \frac{N^4}{64\pi^2}\left\{\left[j_0^2(\omega_o r/R_0) - j_1^2(\omega_0 r/R_0)\right]^2 \delta_{\lambda\sigma}\delta_{\rho\tau}\right.$$

$$\left. - 4j_0^2(\omega_0 r/R_0)j_1^2(\omega_0 r/R_0)(\chi_\lambda^\dagger\vec{\sigma}\cdot\hat{r}\chi_\sigma)(\chi_\rho^\dagger\vec{\sigma}\cdot\hat{r}\chi_\tau)\right\} \;,$$

where we neglect the term proportional to $\vec{\sigma}\cdot\hat{r}$. In a proton state normalized to our convention before, the expectation value of the operator can be written as

$$\langle p_\uparrow|O_{11}^{ud(6,\bar{6})}|p_\uparrow\rangle = -\frac{i}{2}N(w_0)^4\frac{1}{64\pi^2}\int d^3x$$

$$\times\left\{\left[j_0^2(\omega_o r/R_0) - j_1^2(\omega_o r/R_0)\right]^2\langle p_\uparrow|A|p_\uparrow\rangle - 4j_0^2(\omega_0 r/R_0)j_1^2(\omega_0 r/R_0)\langle p_\uparrow|B|p_\uparrow\rangle\right\} \;,$$

$$(2.103)$$

where

$$A = \; : u_\lambda^{a\dagger}u_\lambda^a d_\rho^{b\dagger}d_\rho^b : + : d_\lambda^{a\dagger}u_\lambda^a u_\rho^{b\dagger}d_\rho^b :$$

$$B = \; : u_\lambda^{a\dagger}(\chi_\lambda^\dagger\vec{\sigma}\cdot\hat{r}\chi_\sigma)u_\sigma^a d_\rho^{b\dagger}(\chi_\rho^\dagger\vec{\sigma}\cdot\hat{r}\chi_\tau)d_\tau^b :$$

$$+ : d^{a\dagger}(\chi_\lambda^\dagger\vec{\sigma}\cdot\hat{r}\chi_\sigma)u_\sigma^a u_\rho^{b\dagger}(\chi_\rho^\dagger\vec{\sigma}\cdot\hat{r}\chi_\tau)d_\tau^b : \;. \qquad (2.104)$$

A straightforward calculation gives

$$\langle p_\uparrow|A|p_\uparrow\rangle = \langle n_\uparrow|A|n_\uparrow\rangle = 1$$

$$\langle\Sigma_\uparrow^+|A|\Sigma_\uparrow^+\rangle = \langle\Sigma_\uparrow^-|A|\Sigma_\uparrow^-\rangle = 0$$

$$\langle\Sigma_\uparrow^0|A|\Sigma_\uparrow^0\rangle = 2$$

$$\langle\Lambda_\uparrow|A|\Lambda_\uparrow\rangle = 0$$

$$\langle\Xi_\uparrow^0|A|\Xi_\uparrow^0\rangle = \langle\Xi_\uparrow^-|A|\Xi_\uparrow^-\rangle = 0 \;, \qquad (2.105)$$

and

$$\langle p_\uparrow | B | p_\uparrow \rangle \;=\; \langle n_\uparrow | B | n_\uparrow \rangle \;=\; 1/3$$

$$\langle \Sigma_\uparrow^+ | B | \Sigma_\uparrow^+ \rangle \;=\; \langle \Sigma_\uparrow^- | B | \Sigma_\uparrow^- \rangle \;=\; 0$$

$$\langle \Sigma_\uparrow^0 | B | \Sigma_\uparrow^0 \rangle \;=\; 2/3$$

$$\langle \Lambda_\uparrow | B | \Lambda_\uparrow \rangle \;=\; 0$$

$$\langle \Xi_\uparrow^0 | B | \Xi_\uparrow^0 \rangle \;=\; \langle \Xi_\uparrow^- | B | \Xi_\uparrow^- \rangle \;=\; 0 \; . \tag{2.106}$$

Therefore we can get in the MIT bag model

$$\langle p_\uparrow | O_{11}^{ud(6,\bar{6})}(x) | p_\uparrow \rangle \;=\; i\mathbb{A} + \frac{i}{3}\mathbb{B} \; , \tag{2.107}$$

where

$$\mathbb{A} \;=\; -\frac{1}{2} N(\omega_0)^4 \frac{1}{16\pi} R_0^3 \int_0^1 \left(\frac{r}{R_0}\right)^2 d\left(\frac{r}{R_0}\right) \left[j_0^2(\omega_0 r/R_0) - j_1^2(\omega_0 r/R_0) \right]^2 \; ,$$

$$\mathbb{B} \;=\; \frac{1}{2} N(\omega_0)^4 \frac{1}{4\pi} R_0^3 \int_0^1 \left(\frac{r}{R_0}\right)^2 d\left(\frac{r}{R_0}\right) j_0^2(\omega_0 r/R_0) j_1^2(\omega_0 r/R_0) \; , \tag{2.108}$$

and similarly for other matrix elements.

Then, using the method we used in the non-relativistic quark model, we can get h_c and h_n induced by $O_{11}^{ud(6,\bar{6})}$,

$$h_c = \frac{0.015 C_{11}^{ud}}{R_0^3 F_\pi} \; , \quad h_n = 0 \; . \tag{2.109}$$

One can compare this with the result from the non-relativistic quark model in Eq. (2.96), where h_c is proportional to α^3. From the definition of ψ below Eq. (2.91), $1/\alpha$ can also be seen as the radius of the baryon. It is well known that $1/\alpha = 0.5$ fm gives a too small value for the proton's charge radius and the pion cloud is usually

	NR quark model		MIT bag model	
Operators	h_c	h_n	h_c	h_n
$\bar{u}i\gamma_5 u\bar{d}d$	0.0883	0.374	0.0560	-0.0690
$\bar{d}i\gamma_5 d\bar{u}u$	0.0883	-0.374	0.0560	0.0690
$\bar{u}i\gamma_5 t^a u\bar{d}t^a d$	-0.0343	-0.0759	-0.0222	0.0140
$\bar{d}i\gamma_5 t^a d\bar{u}t^a u$	-0.0343	0.0759	-0.0222	-0.0140
$\bar{u}i\gamma_5 u\bar{u}u$	0.0883	0	0.0569	0
$\bar{d}i\gamma_5 d\bar{d}d$	0.0883	-0.255	0.0569	-0.163
$\bar{u}i\gamma_5 t^a u\bar{u}t^a u$	-0.0343	0	-0.0221	0
$\bar{d}i\gamma_5 t^a d\bar{d}t^a d$	-0.0343	0.0991	-0.0221	0.0633
$\bar{u}i\gamma_5\sigma^{\mu\nu}u\bar{d}\sigma_{\mu\nu}d$	-0.0397	0	-0.0230	0
$\bar{u}i\gamma_5\sigma^{\mu\nu}t^a u\bar{d}\sigma_{\mu\nu}t^a d$	-0.268	0	-0.180	0

Table 2.11: Same as Table 2.10, except the matrix elements are quoted here at the scale $\mu = 4\pi F_\pi$ assuming the quark model scale of 400 MeV. The units of h_c and h_n in NR quark model and MIT bag model are $C_4\alpha^3/F_\pi$ and $C_4/(R_0^3 F_\pi)$, respectively.

invoked to gap it. On the other hand, the bag radius is usually taken to be 1.0 fm, which will give a considerably smaller h_c. In any case, it is reasonable to consider $R_0 \sim 1/\alpha$ and take the non-relativistic quark model result as the representative.

The couplings h_c and h_n induced by color-singlet four-quark operators are listed in Table 2.10 and those by color-octet operators are equal to the above multiplying by $-2/3$. In Table 2.10, many four-quark operators yield zero h_c and h_n because we neglect the "sea quark" contribution. By making the four-quark operators normal ordered in Eq. (2.93) and (2.104), one cannot get any contribution to h_c and h_n from four-quark operators containing strange quarks.

Model calculations do not have explicit QCD scale dependence. To match the results with QCD matrix elements, we have to assume a model scale and using perturbative QCD (pQCD) evolution to run them to appropriate perturbative scale, for which we choose to be $\mu = 4\pi F_\pi$. In this work, we assume the model scale to be at 400 MeV and $\Lambda_{\mathrm{QCD}} = 250$ MeV and take into account the pQCD effect using one-loop renormalization group equation to run the operators down to the energy scale of the model. At this low energy regime the strong coupling is large and the one-loop pQCD evolution is by no means accurate, but it may still serve as an estimate of the pQCD effect. The matrix elements at scale μ are shown in Table 2.11.
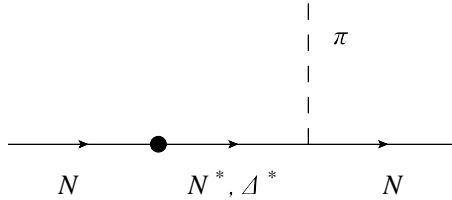
Figure 2.2: P-odd and CP-odd pion-nucleon coupling generated by the four-quark operators through parity-odd resonances, where the black dot is the CP-odd, four-quark operator, N^* and Δ^* are the CP-odd excited states.

2.4.2.3 Contribution from odd-parity resonances

The P-odd and CP-odd quark operators can also generate a CP-odd pion-nucleon interaction through the parity-odd excited resonances which is shown in Fig. 2.2. The P-odd and CP-odd quark operators can generate mixings between nucleons and parity-odd excited resonances which can be calculated using quark models [53]. Take the operator $O_{11}^{(ud)} = \bar{u}i\gamma_5 u \bar{d}d$ and the intermediate state N(1535) as an example, using the harmonic oscillator non-relativistic quark model the mass mixing between neutron and $N(1535)$ resonance can be estimated as $\delta = m_c \omega^2/(8\sqrt{3}\pi^{3/2})$, where $m_c \approx \omega \approx 300$ MeV are the constituent quark mass and the frequency of the harmonic oscillator, respectively. The resonance can decay into a nucleon plus a pion, the partial decay width is about 50 MeV [54]. The effective Lagrangian for this process can be written as

$$\mathcal{L}_{N^*} = g_{N^*}\bar{N}N^*\pi + h.c. \ , \tag{2.110}$$

where as an order-of-magnitude estimate we discard the isospin quantum number. Then, from the partial decay width one can get $g_{N^*} \sim \mathcal{O}(1)$. The P-odd and CP-odd

pion-nucleon coupling induced by this mixing can be written as

$$h_{mix} = \frac{C_4 g_{N^*} \delta}{M_{N^*} - m_n} \approx 6 \times 10^{-4} C_4 \text{GeV}^2 \ , \tag{2.111}$$

where C_4 is the Wilson coefficient of the four-quark operator. Compared with the direct matching contribution listed in Table 2.10, one can see that h_{mix} is about two orders of magnitude smaller and therefore its contribution to nEDM is negligible.

The contribution from Fig. 2.2 can be seen as a one-loop contribution since the intermediate resonances may also be described as scattering states of pion and nucleon. Therefore, this contribution is suppressed by a loop factor.

2.4.3 Tree-Level CP-Odd Mass of Neutron

The nucleon CP-odd observables receive contributions from its CP-odd mass term $m' \bar\psi i \gamma_5 \psi$. In χPT, there are also two sources of CP-odd mass: that induced by the condensates of meson fields, namely $\langle \pi^0 \rangle$ and $\langle \eta \rangle$, and that from the direct matching contribution of the four-quark operators.

2.4.3.1 Meson Condensates

The relevant terms contributing to the CP-odd mass of neutron can be read from expanding Eq. (2.48), which gives

$$\bar{n} i \gamma_5 n \frac{1}{F_\pi} \left\{ -d_1 [(m_u - m_d)\langle \pi^0 \rangle + \frac{1}{\sqrt{3}}(m_u + m_d)\langle \eta \rangle - \frac{2}{\sqrt{3}} m_s \langle \eta \rangle] \right.$$
$$\left. + d_2 \frac{2}{\sqrt{3}} m_s \langle \eta \rangle + d_3 m_d (\langle \pi^0 \rangle - \frac{1}{\sqrt{3}} \langle \eta \rangle) \right\} \ , \tag{2.112}$$

where d_1, d_2 and d_3 can be related to the discrepancy of the Goldberger-Treiman relation, and the values d_2 and d_3 have been determined in the literature [55].

$$d_2 = -2B_0 m_0 (D_{19} - F_{19}) \ , \quad d_3 = -2B_0 m_0 (D_{19} + F_{19}) \ , \qquad (2.113)$$

where m_0 is the common octet mass in the chiral limit, and

$$m_0 F_{19} \approx -0.2 \ , \quad m_0 D_{19} \approx -0.4 \ . \qquad (2.114)$$

Note that the signs of the F_{19} and D_{19} here are different from those in Ref. [55]. Since d_1 has not been determined from isospin-violation effect, we will set it to be zero in the following calculation. One should note that disregarding d_1 leads to some errors because $m_s \langle \eta \rangle$ might be the same order as $m_d \langle \pi^0 \rangle$.

2.4.3.2 Direct Contribution

The leading-order expansion of the tilded hadronic operators listed in Table 2.4 are hermitian. Take $\tilde{O}_6^{(2)}$ as an example. It can be written as

$$\tilde{O}_6^{(2)} \simeq \bar{p} i \gamma_5 p + \bar{n} i \gamma_5 n + \frac{1}{3} \bar{\Lambda} i \gamma_5 \Lambda + \bar{\Sigma}^0 i \gamma_5 \Sigma^0 + \bar{\Sigma}^+ i \gamma_5 \Sigma^+ + \bar{\Sigma}^- i \gamma_5 \Sigma^- \ , \qquad (2.115)$$

which gives a CP-odd mass of neutron. To calculate the matching coefficients, we can see from above that the leading-order expansion is parity-odd, and we need to calculate a parity-odd quantity. The simplest is $\Delta \vec{s} \cdot \Delta \vec{p}$, where $\Delta \vec{s}$ is the spin difference between the initial and final states and $\Delta \vec{p}$ is the momentum difference between the initial and final states.

In the non-relativistic quark model, take the $(6, \bar{6})$ components of $\bar{u} i \gamma_5 u \bar{d} d$, as an example, to calculate the matrix elements proportional to $\Delta \vec{s} \cdot \Delta \vec{p}$; the relevant

Operators	$m'_n/(10^{-3}C_4 B_0^2 \text{ GeV})$	Operators	$m'_n/(10^{-3}C_4 B_0^2 \text{ GeV})$
$\bar{u}i\gamma_5 u\bar{d}d$	-8.8	$\bar{u}t^a i\gamma_5 u\bar{d}t^a d$	0
$\bar{d}i\gamma_5 d\bar{u}u$	5.7	$\bar{d}t^a i\gamma_5 d\bar{u}t^a u$	0
$\bar{u}i\gamma_5 d\bar{s}s$	-8.8	$\bar{u}t^a i\gamma_5 u\bar{s}t^a s$	0
$\bar{s}i\gamma_5 s\bar{u}u$	3.2	$\bar{s}t^a i\gamma_5 s\bar{u}t^a u$	0
$\bar{d}i\gamma_5 d\bar{s}s$	5.7	$\bar{d}t^a i\gamma_5 d\bar{s}t^a s$	0
$\bar{s}i\gamma_5 s\bar{d}d$	3.2	$\bar{s}t^a i\gamma_5 s\bar{d}t^a d$	0
$\bar{u}i\gamma_5 u\bar{u}u$	-7.4	$\bar{u}t^a i\gamma_5 u\bar{u}t^a u$	2.0
$\bar{d}i\gamma_5 d\bar{d}d$	4.7	$\bar{d}t^a i\gamma_5 d\bar{d}t^a d$	-1.3
$\bar{s}i\gamma_5 s\bar{s}s$	2.6	$\bar{s}t^a i\gamma_5 s\bar{s}t^a s$	0.7

Table 2.12: CP-odd mass of the neutron induced by meson condensates. Contributions from operators made of tensor currents are neglected due to the large-N_C suppression.

Operators	CP-odd mass/$(\alpha^3 C_4)$	Operators	CP-odd mass /$(\alpha^3 C_4)$
$\bar{u} i \gamma_5 u \bar{d} d$	0.0635	$\bar{u} i \gamma_5 \sigma^{\mu\nu} u \bar{d} \sigma_{\mu\nu} d$	-0.127
$\bar{d} i \gamma_5 d \bar{u} u$	-0.127	–	–
$\bar{u} i \gamma_5 u \bar{s} s$	0	$\bar{u} i \gamma_5 \sigma^{\mu\nu} u \bar{s} \sigma_{\mu\nu} s$	0
$\bar{s} i \gamma_5 s \bar{u} u$	0	–	–
$\bar{d} i \gamma_5 d \bar{s} s$	0	$\bar{d} i \gamma_5 \sigma^{\mu\nu} d \bar{s} \sigma_{\mu\nu} s$	0
$\bar{s} i \gamma_5 s \bar{d} d$	0	–	–
$\bar{u} i \gamma_5 u \bar{u} u$	0	–	–
$\bar{d} i \gamma_5 d \bar{d} d$	-0.127	–	–
$\bar{s} i \gamma_5 s \bar{s} s$	0	–	–

Table 2.13: CP-odd mass of neutron induced directly by color-singlet four-quark operators. The CP-odd mass induced by color-octet four-quark operators are equal to the one induced by corresponding color-singlet operators multiplied by $-2/3$.

Operators	CP-odd mass/$(\alpha^3 C_4)$	Operators	CP-odd mass /$(\alpha^3 C_4)$
$\bar{u}i\gamma_5 u\bar{d}d$	0.212	$\bar{u}i\gamma_5\sigma^{\mu\nu}u\bar{d}\sigma_{\mu\nu}d$	0.0280
$\bar{d}i\gamma_5 d\bar{u}u$	-0.336	$\bar{u}i\gamma_5\sigma^{\mu\nu}t^a u\bar{d}\sigma_{\mu\nu}t^a d$	0.189
$\bar{u}i\gamma_5 t^a u\bar{d}t^a d$	-0.0314	$-$	$-$
$\bar{d}i\gamma_5 t^a d\bar{u}t^a u$	0.0799	$-$	$-$
$\bar{u}i\gamma_5 u\bar{u}u$	0	$\bar{u}i\gamma_5 t^a u\bar{u}t^a u$	0
$\bar{d}i\gamma_5 d\bar{d}d$	-0.249	$\bar{d}i\gamma_5 t^a d\bar{d}t^a d$	0.0968

Table 2.14: Same as Fig. 2.13. The matrix elements are now evolved to the scale where $\mu = 4\pi F_\pi$.

part of the four-quark operator can be written as

$$
\begin{aligned}
O_{11}^{ud,(6,\bar{6})} \quad \sim \quad &-\frac{i}{8}\left\{ \frac{i}{2m_C} : [\nabla \cdot (u^\dagger \vec{\sigma}u)](d^\dagger d) : + \frac{i}{2m_C} : (u^\dagger u)[\nabla \cdot (d^\dagger \vec{\sigma}d)] : \right. \\
&\left. -\frac{i}{2m_C} : [\nabla \cdot (d^\dagger \vec{\sigma}u)](u^\dagger d) : -\frac{i}{2m_C} : (d^\dagger u)[\nabla \cdot (u^\dagger \vec{\sigma}d)] : \right\} \quad (2.116)
\end{aligned}
$$

where u and d are two-component quark operators, m_C is the mass of the constituent quark which is set to be one-third of the nucleon mass. The wave functions of baryons in the non-relativistic quark model are listed in Eq. (2.92) and Table 2.9. Then using the same method as described in the last section one can get the CP-odd mass of the neutron directly induced by the tilded operators, and the results are listed in Table 2.13. After the leading-order QCD evolution to the scale where $\mu = 4\pi F_\pi$, the result is shown in Table 2.14.

2.4.3.3 Contribution to CP-Odd Meson-Nucleon Coupling

If rotating away the CP-odd nucleon mass through $U_A(1)$ transformation, one can generate new contributions to the CP-odd meson-nucleon coupling from CP-even chiral operators. However, this contribution is of higher order in chiral power counting because all the CP-even meson-nucleon interactions are suppressed in the chiral limit, whereas the CP-odd coupling we considered in the previous subsections are not.

2.5 Four-Quark Contribution to nEDM in χPT

In this section, we study the CP-odd four-quark contributions to the neutron EDM in χPT. The approach here is completely general and is applicable to any CP-odd quark-gluon operators. Some results presented can be found in the literature; however, to our knowledge, this is the most systematic and thorough discussion in the context of the CP-odd four-quark operators. In the last subsection, we make a comparison of the four-quark contributions in different approximations of non-perturbative QCD physics.

In χPT, the leading contributions come from many different sources. Since the CP-violating pion-nucleon couplings are $\mathcal{O}(1)$, the pion loop contribution to the neutron EDM is $\mathcal{O}(1)$, apart from possible enhancement by chiral logarithms. On the other hand, the direct matching contribution is also $\mathcal{O}(1)$, along with the pion condensate contribution through photo-production amplitudes. Finally, the CP-odd mass terms contribute through the nucleon magnetic moment after chiral

rotation. This contribution is again $\mathcal{O}(1)$ in chiral power counting. We will consider all these leading contributions in the following subsections. We ignore the subleading contribution in this work.

2.5.1 Direct Matching from Quark Model

We have first considered the direct matching contribution from the four-quark operators to the neutron EDM in Sec. IV. When any CP-odd quark-gluon operator is matched in χPT, there appear many tree-level neutron EDM-like operators in the chiral Lagrangian [8]. We do not have much to say about the size of the Wilson coefficients other than they are $\mathcal{O}(1)$ in chiral power counting. Since they also serve as the counter terms for ultraviolet-divergent chiral-loop calculations, they depend on the regularization scheme and subtraction scale. In this work, we choose to estimate this contribution using nucleon models with dipole excitations into odd-parity resonances, such as S_{11}, following the work in [53].
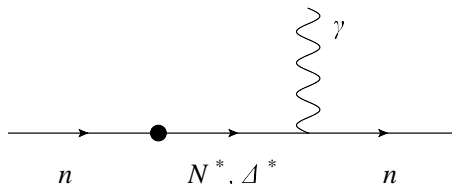
Figure 2.3: Direct calculation of the neutron EDM in quark models. The neutron makes a transition to a CP-odd excited state and goes back via electromagnetic interaction, where the black dot is the CP-odd, four-quark operator, N^* and Δ^* are the CP-odd excited states.

We use the non-relativistic quark model with harmonic oscillator potentials to

estimate the contribution from the first CP-odd excited states, which is shown in Fig. 2.3. The wave functions of the lowest CP-odd excited states can be written as

$$
\begin{aligned}
|N_\uparrow^*\rangle &= N_1 \epsilon^{abc} \int d^3r_1 d^3r_2 d^3r_3 \exp\left(\frac{i\vec{P}\cdot\vec{R}}{\sqrt{3}} - \frac{\alpha^2}{2}(\rho^2 + \lambda^2)\right) \\
&\quad \left\{ (\lambda_x + i\lambda_y)[u_\downarrow^{a\dagger}(r_1)d_\uparrow^{b\dagger}(r_2)d_\downarrow^{c\dagger}(r_3) - u_\uparrow^{a\dagger}(r_1)d_\downarrow^{b\dagger}(r_2)d_\downarrow^{c\dagger}(r_3)]|0\rangle \right. \\
&\quad \left. -\lambda_z[u_\uparrow^{a\dagger}(r_1)d_\downarrow^{b\dagger}(r_2)d_\uparrow^{c\dagger}(r_3) - u_\downarrow^{a\dagger}(r_1)d_\uparrow^{b\dagger}(r_2)d_\uparrow^{c\dagger}(r_3)]|0\rangle \right\} ; \\
|\Delta_\uparrow^*\rangle &= N_2 \epsilon^{abc} \int d^3r_1 d^3r_2 d^3r_3 \exp\left(\frac{i\vec{P}\cdot\vec{R}}{\sqrt{3}} - \frac{\alpha^2}{2}(\rho^2 + \lambda^2)\right) \\
&\quad \left\{ (\lambda_x + i\lambda_y)[2u_\downarrow^{a\dagger}(r_1)d_\downarrow^{b\dagger}(r_2)d_\uparrow^{c\dagger}(r_3) + d_\downarrow^{a\dagger}(r_1)d_\downarrow^{b\dagger}(r_2)u_\uparrow^{c\dagger}(r_3)]|0\rangle \right. \\
&\quad \left. -\lambda_z[2u_\uparrow^{a\dagger}(r_1)d_\uparrow^{b\dagger}(r_2)d_\downarrow^{c\dagger}(r_3) + d_\uparrow^{a\dagger}(r_1)d_\uparrow^{b\dagger}(r_2)u_\downarrow^{c\dagger}(r_3)]|0\rangle \right\} .
\end{aligned}
\tag{2.117}
$$

In the above formulas λ_x, λ_y and λ_z are the x, y and z components of λ, respectively. N_1 and N_2 are normalization factors of the states with $N_1 = 2^{1/2}\alpha^4/(3^{9/4}\pi^{3/2})$, $N_2 = \alpha^4/(2^{1/2}3^{9/4}\pi^{3/2})$.

The results are shown in Table 2.15, which agree with the results extracted from Ref. [53]. We also need to take into account the evolution of the operators between $4\pi F_\pi$ and the energy scale of the quark model. The results are shown in Table 2.16 with $\alpha = 0.41$ GeV.

2.5.2 Meson Condensate Contribution through Photo-Pion Production

In photon-pion production, there are CP-even electric-dipole couplings between the baryon-octet and electromagnetic fields through using $f_\pm^{\mu\nu}$ [8]. Some of these couplings can generate the neutron EDM if they violate the chiral symmetry

Operators	nEDM/$(e\alpha C_4)$	Operators	nEDM/$(e\alpha C_4)$
$\bar{u}i\gamma_5 u\bar{d}d$	$-\frac{1}{6\sqrt{2}\pi^{3/2}}$	$\bar{u}i\gamma_5 t^a u\bar{d}t^a d$	$\frac{1}{9\sqrt{2}\pi^{3/2}}$
$\bar{d}i\gamma_5 d\bar{u}u$	$-\frac{1}{3\sqrt{2}\pi^{3/2}}$	$\bar{d}i\gamma_5 t^a d\bar{u}t^a u$	$\frac{\sqrt{2}}{9\pi^{3/2}}$
$\bar{u}i\gamma_5\sigma^{\mu\nu}u\bar{d}\sigma_{\mu\nu}d$	$\frac{1}{\sqrt{2}\pi^{3/2}}$	$\bar{u}i\gamma_5\sigma^{\mu\nu}t^a u\bar{d}\sigma_{\mu\nu}t^a d$	$-\frac{\sqrt{2}}{3\pi^{3/2}}$
$\bar{u}i\gamma_5 u\bar{u}u$	0	$\bar{u}i\gamma_5 t^a u\bar{u}t^a u$	0
$\bar{d}i\gamma_5 d\bar{d}d$	0	$\bar{d}i\gamma_5 t^a d\bar{d}t^a d$	0

Table 2.15: nEDM contributed from first excited CP-odd states in the non-relativistic quark model, where C_4 is the Wilson coefficients of the quark models, α is defined below Eq. (2.91). The unit of nEDM used here is $e\cdot\mathrm{GeV}^{-1}$, which is different from the traditional one $e\cdot$cm due to that the Wilson coefficients of the four-quark operators are unknown which are always in the unit of GeV^{-2}. The translation between the two units is $e\cdot\mathrm{GeV}^{-1}\simeq 2\times 10^{-14}e\cdot$cm.

Operators	nEDM/$(10^{-3}eC_4\mathrm{GeV})$	Operators	nEDM/$(10^{-3}eC_4\mathrm{GeV})$
$\bar{u}i\gamma_5 u\bar{d}d$	-37.6	$\bar{u}i\gamma_5 t^a u\bar{d}t^a d$	3.80
$\bar{d}i\gamma_5 d\bar{u}u$	-62.6	$\bar{d}i\gamma_5 t^a d\bar{u}t^a u$	8.87
$\bar{u}i\gamma_5\sigma^{\mu\nu}u\bar{d}\sigma_{\mu\nu}d$	77.5	$\bar{u}i\gamma_5\sigma^{\mu\nu}t^a u\bar{d}\sigma_{\mu\nu}t^a d$	-103
$\bar{u}i\gamma_5 u\bar{u}u$	0	$\bar{u}i\gamma_5 t^a u\bar{u}t^a u$	0
$\bar{d}i\gamma_5 d\bar{d}d$	0	$\bar{d}i\gamma_5 t^a d\bar{d}t^a d$	0

Table 2.16: Same as Table XIII, except the renormalization scale is now at $4\pi F_\pi$.

through the quark masses and at the same time the meson fields acquire vacuum condensates through the CP-odd four-quark operators. In more physical language, the contact terms for the pion-photoproduction processes give rise to the neutron EDM through the diagram in Fig. 2.4. Although the electromagnetic field also

Figure 2.4: Pion-photoproduction diagram with the pion field annihilated by the four-quark operator into the vacuum, where the cross is a four-quark operator.

violates chiral symmetry, it cannot generate an EDM through meson condensates by itself—a quark mass factor is essential.

The terms of interest are made of linear products of baryon fields $\bar{B}$ and B, χ_- and f_+ [8],

$$\mathcal{L}_{\pi\gamma}^C = \frac{1}{16\pi^2 F_\pi^2} \left[\delta_1 \text{Tr}[\bar{B}\sigma_{\mu\nu}\gamma_5\{\chi_-, f_+^{\mu\nu}\}B] + \delta_2 \text{Tr}[\bar{B}\sigma_{\mu\nu}\gamma_5 f_+^{\mu\nu}B]\text{Tr}[\chi_-] + ... \right] \ ,$$

(2.118)

where we have shown two of the ten possible terms. It is difficult, however, to extract the Wilson coefficients δ_i directly from experimental data. Some of the coefficients have been estimated by calculating the contribution from the excited baryon states in the context of the two-flavor scenario [56]. In the two-flavor scenario, neglecting the isospin violation generated by the difference between the up and down quark masses, the terms relevant to nEDM can be written as

$$\mathcal{L}_{\pi\gamma}^{2-flavor} = \bar{N}\gamma_5\sigma_{\mu\nu}[(a_1^p - a_1^n)f_+^{\mu\nu} + a_1^n\text{Tr}(f_+^{\mu\nu})]\chi_- N \ , \qquad (2.119)$$

Operators	$d_{\pi\gamma}/(10^{-3}eC_4B_0^2 \text{ GeV}^{-1})$	Operators	$d_{\pi\gamma}/(10^{-3}eC_4B_0^2 \text{ GeV}^{-1})$
$\bar{u}i\gamma_5 u\bar{d}d$	10.6	$\bar{u}t^a i\gamma_5 u\bar{d}t^a d$	0
$\bar{d}i\gamma_5 d\bar{u}u$	-10.5	$\bar{d}t^a i\gamma_5 d\bar{u}t^a u$	0
$\bar{u}i\gamma_5 d\bar{s}s$	10.6	$\bar{u}t^a i\gamma_5 u\bar{s}t^a s$	0
$\bar{s}i\gamma_5 s\bar{u}u$	-0.12	$\bar{s}t^a i\gamma_5 s\bar{u}t^a u$	0
$\bar{d}i\gamma_5 d\bar{s}s$	-10.5	$\bar{d}t^a i\gamma_5 d\bar{s}t^a s$	0
$\bar{s}i\gamma_5 s\bar{d}d$	-0.12	$\bar{s}t^a i\gamma_5 s\bar{d}t^a d$	0
$\bar{u}i\gamma_5 u\bar{u}u$	8.87	$\bar{u}t^a i\gamma_5 u\bar{u}t^a u$	-2.37
$\bar{d}i\gamma_5 d\bar{d}d$	-8.77	$\bar{d}t^a i\gamma_5 d\bar{d}t^a d$	2.34
$\bar{s}i\gamma_5 s\bar{s}s$	-0.10	$\bar{s}t^a i\gamma_5 s\bar{s}t^a s$	0.03

Table 2.17: nEDM induced by meson condensates through pion-photoproduction. Contribution from operators constructed by tensor operators are neglected due to the large-N_C suppression.

where $N = \begin{pmatrix} p \\ n \end{pmatrix}$, and in the two-flavor case, $f_+^{\mu\nu} \equiv e(\xi^\dagger Q\xi + \xi Q\xi^\dagger)F^{\mu\nu}$, in which $Q = (1 + \tau^3)/2$. Expanding $f_+^{\mu\nu}$ and χ_-, we can get the nEDM induced by the condensate of π^0;

$$d_{\pi\gamma} = -\frac{8ea_1^n B_0(m_u + m_d)\langle\pi^0\rangle}{F_\pi} \ . \tag{2.120}$$

From Ref. [56], one can get the contribution to a_1 from Δ and ρ internal states, which is

$$a_1 = -0.156\text{GeV}^{-3} \ . \tag{2.121}$$

Using this, one can estimate the nEDM induced by the pion condensate, as shown in Table 2.17.

2.5.3 CP-Odd Baryon Mass Contribution

The CP-odd baryon-mass terms considered in the previous section generate a CP-odd part of the baryon wave function. This part can transform a magnetic moment term into an EDM contribution. The physics of this is shown in Fig. 2.5.
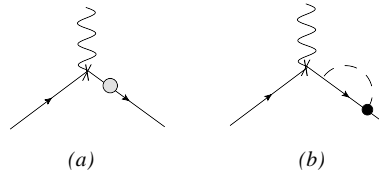
Figure 2.5: The CP-odd mass of neutron turns the tree level magnetic moment into an EDM. The cross is the tree level magnetic moment, the gray dot is the CP-odd mass of the neutron and the black dot is the CP-odd pion-nucleon coupling.

The mass terms of the neutron can be written as

$$\mathcal{L}_{mass} = -m_n \bar{n}n - m'_n \bar{n}i\gamma_5 n \; . \tag{2.122}$$

Note that the neutron field n here is already redefined using the transformation in Eq. (2.44) after taking into account the meson condensate effect as discussed in the previous section. Redefining the neutron field again through a chiral rotation,

$$n = \exp(-i\frac{m'_n}{2m_n})\gamma_5 n' \; , \tag{2.123}$$

the mass term becomes the standard one,

$$\mathcal{L}_{mass} = -m_n \bar{n}'n' \; . \tag{2.124}$$

On the other hand, the tree level anomalous magnetic moment of the neutron can be written as

$$\mathcal{L}_{mag.mom.} = -\frac{1}{4}\frac{\kappa_n}{m_n}\bar{n}\sigma^{\mu\nu}nF_{\mu\nu} \; . \tag{2.125}$$

The redefinition in Eq. (2.123) generates a neutron EDM,

$$d_{CP-oddmass}^{EDM} = -\frac{\kappa_n m'_n}{2m_n^2} \; . \tag{2.126}$$

The experimental values of the anomalous magnetic dipole moments of the nucleons are $\kappa_p = 1.7928$, $\kappa_n = -1.9131$. The numerical values of this contribution have been shown in Tables 2.18 and 2.19. For the tensor operator $\bar{u}i\gamma_5\sigma^{\mu\nu}u\bar{d}\sigma_{\mu\nu}d$, the contribution from the CP-odd mass of the nucleon is particularly large. The CP-odd mass also gets a quantum correction shown in diagram (b) of Fig. 2.5. It is easy to see that this term does not have any chiral enhancement and is of a higher-order effect.

2.5.4   Leading Chiral Loop Contribution

The contribution we have considered so far has a smooth chiral limit, i.e., regular as the quark masses go to zero. The leading contribution in the chiral limit, however, involves the pion loop with an infrared divergence. This contribution was first calculated by Crewther et al [7], and has been studied thoroughly in the literature (see Fig. 2.6). Diagrams (a) and (b) in Fig. 2.6 contain an infrared divergence which is regularized by the mass of pion and an analytical part. The constant part is canceled by diagrams (c) and (d). Diagrams (e) and (f) cancel with each other [8]. Therefore, up to terms of order (m_π/m_n), the neutron EDM
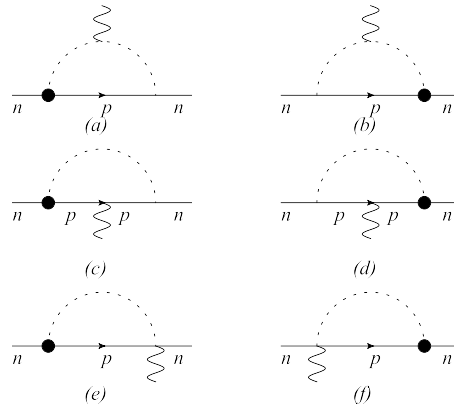
Figure 2.6: Charged-pion loop contribution to neutron EDM (without the anomalous magnetic moment), where the black dots represent the CP-odd vertices.

generated by the charged pion loop can be written as [8]

$$d_{\pi^+}^{\mathrm{n}} = -\frac{e\sqrt{2}}{16\pi^2 F_\pi} h_c (D+F) \ln\left(m_\pi^2/m_n^2\right), \qquad (2.127)$$

where $D + F = -g_A = -1.26$ is the CP-even pion-nucleon coupling (the signs of D and F is different from that in Ref. [23] because we are using a different definition of

76
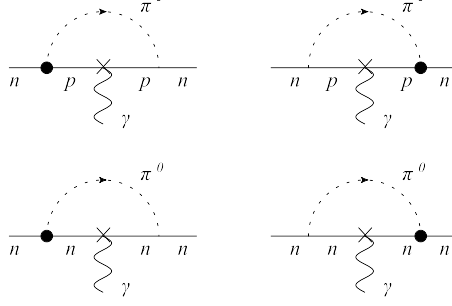
Figure 2.7: Contribution from the tree level anomalous magnetic moments of proton and neutron, where the crosses are anomalous magnetic moments of nucleons and the dots are CP-odd vertices.

the chiral transformation of U), and h_c is the CP-odd pion-nucleon coupling defined in Eq. (2.86). Note that, in Fig. 2.6, the contribution from the proton's anomalous magnetic moment has not been included. To include this contribution, we consider all these diagrams in Fig. 2.7 where the neutral pion loop is also present, and the result is Ref. [20].

$$ d^n_{\pi_0+\kappa} = \frac{e}{16\pi^2} \frac{D+F}{F_\pi} \left(-\sqrt{2}h_c\kappa_p + h_n\kappa_n \right) F_n \left(\frac{m_\pi^2}{m_n^2} \right) , \qquad (2.128) $$

where κ_n and κ_n are tree-level anomalous magnetic moments of protons and neutrons, respectively, and

$$ F_n(s) = \frac{3}{2} - s - \frac{3s - s^2}{2} \ln s + \frac{s(5s - s^2) - 4s}{2\sqrt{s - s^2/4}} \arctan \frac{\sqrt{s - s^2/4}}{s/2}. \qquad (2.129) $$

We can see that there is no chiral enhancement in $F_n(s)$.

Using the above, we estimate the pion-loop and the CP-odd mass contributions to neutron EDM due to the P-odd and CP-odd four-quark operators. The results are listed in Tables 2.18 and 2.19. Although the charged pion-loop (Fig. 2.6) dominates

operators	contact term	meson photo-production	π-N coupling direct Fig. 2.6	Fig. 2.7	π-N coupling, $\langle\pi^0\rangle$, $\langle\eta\rangle$ Fig. 2.6	Fig. 2.7	CP-odd mass direct	CP-odd mass $\langle\pi^0\rangle$, $\langle\eta\rangle$	total
$\bar{u}i\gamma_5u\bar{d}d$	-37.6	52.9	-30.9	71.3	27.2	202.1	15.8	-47.6	253.2
$\bar{u}u\bar{d}i\gamma_5d$	-62.6	-52.3	-30.9	-37.3	-30.2	-202.3	-25.1	30.6	-410.2
$\bar{u}i\gamma_5u\bar{s}s$	0	52.9	0	0	27.2	202.1	0	-47.6	234.6
$\bar{u}u\bar{s}i\gamma_5s$	0	-0.6	0	0	2.8	-0.7	0	17.1	18.5
$\bar{d}i\gamma_5d\bar{s}s$	0	-52.3	0	0	-30.2	-202.3	0	30.6	-254.3
$\bar{d}d\bar{s}i\gamma_5s$	0	-0.6	0	0	2.8	-0.7	0	17.1	18.5
$\bar{u}i\gamma_5u\bar{u}u$	0	44.1	-30.9	17.0	22.7	168.9	0	-39.7	182.1
$\bar{d}i\gamma_5d\bar{d}d$	0	-43.6	-30.9	-20.0	-25.1	-168.5	-18.6	25.5	-281.2
$\bar{s}i\gamma_5s\bar{s}s$	0	-0.5	0	0	2.4	-0.6	0	14.2	15.5
O^T_{ud}	0	0	13.9	-7.7	0	0	2.1	0	85.8
O^T_{us}	0	0	0	0	0	0	0	0	0
O^T_{ds}	0	0	0	0	0	0	0	0	0

nEDM from different contributions / $(10^{-3}eC_4$ GeV$)$

Table 2.18: nEDM from the P-odd and CP-odd four-quark operators composed of color-singlet currents. Different contributions are shown. In the table, $O^T_{ud} \equiv \bar{u}i\gamma_5\sigma^{\mu\nu}u\bar{d}\sigma_{\mu\nu}d$, $O^T_{us} \equiv \bar{u}i\gamma_5\sigma^{\mu\nu}u\bar{s}\sigma_{\mu\nu}s$, $O^T_{ds} \equiv \bar{d}i\gamma_5\sigma^{\mu\nu}d\bar{s}\sigma_{\mu\nu}s$.

operators	contact term	meson photo-production	π-N coupling direct Fig. 2.6	Fig. 2.7	π-N coupling, $\langle\pi^0\rangle$, $\langle\eta\rangle$ Fig. 2.6	Fig. 2.7	CP-odd mass direct	CP-odd mass $\langle\pi^0\rangle$, $\langle\eta\rangle$	total
$\bar{u}i\gamma_5 t^a u\bar{d}t^a d$	3.8	0	12.0	-17.6	0	0	-2.34	0	-4.2
$\bar{u}t^a u\bar{d}i\gamma_5 t^a d$	8.9	0	12.0	4.42	0	0	6.0	0	31.2
$\bar{u}i\gamma_5 t^a u\bar{s}t^a s$	0	0	0	0	0	0	0	0	0
$\bar{u}t^a u\bar{s}i\gamma_5 t^a s$	0	0	0	0	0	0	0	0	0
$\bar{d}i\gamma_5 t^a d\bar{s}t^a s$	0	0	0	0	0	0	0	0	0
$\bar{d}t^a d\bar{s}i\gamma_5 t^a s$	0	0	0	0	0	0	0	0	0
$\bar{u}i\gamma_5 t^a u\bar{u}t^a u$	0	-11.8	12.0	-6.6	-6.1	-45.0	0	10.6	-46.8
$\bar{d}i\gamma_5 t^a d\bar{d}t^a d$	0	11.6	12.0	7.8	6.7	44.8	7.2	-6.8	83.4
$\bar{s}i\gamma_5 t^a s\bar{s}t^a s$	0	0.1	0	0	-0.6	0.2	0	-3.8	-4.1
O_{ud}^{Tc}	-103.1	0	93.8	-51.6	0	0	14.1	0	-46.9
O_{us}^{Tc}	0	0	0	0	0	0	0	0	0
O_{ds}^{Tc}	0	0	0	0	0	0	0	0	0

nEDM from different contributions / ($10^{-3}eC_4$ GeV)

Table 2.19: Neutron EDM generated by P-odd and CP-odd four-quark operators composed of color-octet currents. The labels have the same meaning as in Table 2.18. $O_{us}^{Tc} \equiv \bar{u}i\gamma_5\sigma^{\mu\nu}t^a u\bar{s}\sigma_{\mu\nu}t^a s$, $O_{us}^{Tc} \equiv \bar{u}i\gamma_5\sigma^{\mu\nu}t^a u\bar{s}\sigma_{\mu\nu}t^a s$, $O_{ds}^{Tc} \equiv \bar{d}i\gamma_5\sigma^{\mu\nu}t^a d\bar{s}\sigma_{\mu\nu}t^a s$.

in the chiral limit, its numerical value is actually about an order of magnitude smaller than the analytical chiral-loop contribution (Fig. 2.7). This is due to the enhancement of h_n relative to h_c in the large N_c limit.

The P-odd and CP-odd four-quark operators can also lead to nonvanishing P-odd and CP-odd interaction like $n \to K\Sigma$ and $n \to \Lambda\eta$. These interactions can generate nEDM through kaon- or eta-loop diagrams. However, there is no reason to believe that the kaon- or eta-loop contribution should be more important than the pion-loop contribution so that it would not change the order-of-magnitude estimate of nEDM generated by those four-quark operators without the strange quark. For those operators containing strange quark the estimation may not be reliable and the kaon- or eta-loop contributions should be included.

2.5.5   Comparison with Other Calculations and the Error-bars of this Calculation

The P-odd and CP-odd four-quark contributions to neutron EDM have been studied using different approximation methods in the literature [18, 19, 20]. The problem is that it is difficult to get an estimate on the errors in any of these methods. This is the strong motivation for the alternative study presented here. By using a completely different approach, we hope to get a better idea how well one actually estimates these hadronic matrix elements.

In Ref. [18], the authors used the external field method, factorization and QCD sum rules to make a direct calculation of the neutron EDM. Their result is

supposed to be the total contribution, although it is unclear how the chiral physics would be included in this approach. Their numbers are listed in Tables 2.20 and 2.21 as "factorization and QCD sum rule." The result is, in general, comparable to the charged pion-loop contribution, although the contribution to the tensor operator is particularly large.

In Ref. [19], the authors also calculated the contributions of the pion-loop as we do in this paper. They used entirely the factorization method to calculate the CP-odd pion-nucleon couplings, including the effects that the CP-odd operators can annihilate the neutral pion in the vacuum. Taking the operator $\bar{u}i\gamma_5 u \bar{d}d$ as an example, their factorization works like this:

$$
\begin{aligned}
\langle n\pi^0|\bar{u}i\gamma_5 u\bar{d}d|n\rangle &= \langle n|\bar{d}d|n\rangle\langle \pi^0|\bar{u}i\gamma_5 u|0\rangle \\
&+ \langle 0|\bar{d}d|0\rangle \left(\langle n\pi^0|\bar{u}i\gamma_5 u|n\rangle - \frac{1}{m_\pi^2}\langle n\pi^0|\mathcal{L}_{QCD}^m|n\pi^0\rangle\langle \pi^0|\bar{u}i\gamma_5 u|0\rangle \right) ,
\end{aligned}
\tag{2.130}
$$

where $\mathcal{L}_{QCD}$ is the usual QCD Lagrangian. The terms inside the bracket on the second line of the above formula cancel each other. The reason is that $\bar{u}i\gamma_5 u$ is just a CP-odd mass of the up-quark which can be rotated away through chiral transformation, except for a possible $U_A(1)$ contribution. Thus these two contributions should cancel with each other exactly. This is first noticed in Ref. [57] in the spirit of the Feinberg-Weinberg-Kabir theorem [58]. Using this method, one can get the CP-odd vertices, h_c and h_n as shown in Tables 2.7 and 2.8. For the charged coupling h_c, one needs to do a Fierz transformation, from which one can get a suppression factor of 1/12, where 1/3 is from the color factor and the other 1/4 is from the spin.

81

Therefore, h_c is one order of magnitude smaller than h_n. The corresponding nEDM calculated using this method is included in Tables 2.20 and 2.21 as well.

From Tables 2.20 and 2.21, taking the operator $\bar{u}i\gamma_5 u \bar{d}d$ as an example, one can see that the magnitude of our result is comparable with what obtained using naïve factorization method but with a different sign; also the our result is about one order of magnitude larger than the result estimated using QCD sum rules. In our calculation, we separate the contribution into the meson condensate contribution and the direct matching contribution. The vacuum saturation method is used to calculate the meson condensate contribution to h_c and h_n. This vacuum saturation method using to calculate the meson matrix elements is accurate in the large-N_C limit, which means the calculation for this contribution is accurate up to $1/N_C$ [42]. From Table 2.18, one can see that the meson condensate contributions dominate over the direct matching contributions. Therefore, for operators generating unsuppressed meson condensates (see Sec IV for detailed discussions), a conservative uncertainty can be set to be a factor of two.

In Ref. [19], the authors also used the vacuum saturation approach to get the factorization result as shown in Eq. (2.130). However, in the case of baryon matrix element, the non-factorized contribution is not suppressed in the large-N_C limit [42], therefore the missed non-factorized contribution should be of the same order as the factorized contribution shown in Eq. (2.130). The calculation using QCD sum rules in Ref. [18] did not include the meson condensate contribution, therefore, their calculation might miss an important contribution.

The factor of two uncertainty can also be seen from the Feinberg-Weinberg-

Operators	Our results	Naive factorization	Factorization & QCD sum rules
$\bar{u}i\gamma_5 u\bar{d}d$	253	-248	17.5
$\bar{d}i\gamma_5 d\bar{u}u$	-410	177	-17.5
$\bar{u}i\gamma_5 d\bar{s}s$	235	-85.8	$-$
$\bar{s}i\gamma_5 s\bar{u}u$	18.5	0	$-$
$\bar{d}i\gamma_5 d\bar{s}s$	-254	85.8	$-$
$\bar{s}i\gamma_5 s\bar{d}d$	18.5	0	$-$
$\bar{u}i\gamma_5 u\bar{u}u$	182	-154	-17.7
$\bar{d}i\gamma_5 d\bar{d}d$	-281	203	15.2
$\bar{s}i\gamma_5 s\bar{s}s$	15.5	0	$-$
$\bar{u}i\gamma_5\sigma^{\mu\nu}u\bar{d}\sigma_{\mu\nu}d$	85.8	-79.4	-127.5
$\bar{u}i\gamma_5\sigma^{\mu\nu}u\bar{s}\sigma_{\mu\nu}s$	0	0	$-$
$\bar{d}i\gamma_5\sigma^{\mu\nu}d\bar{s}\sigma_{\mu\nu}s$	0	0	$-$

Table 2.20: Comparison of different methods, nEDM calculated by factorization in Ref. [19, 20] are shown as "naive factorization". The column on the right side shows nEDM calculated using factorization and QCD sum rules [18]. The unit of the numbers is $10^{-3}eC_4\mathrm{GeV}$.

Operators	Our results	Naive factorization	Factorization & QCD sum rules
$\bar{u}t^a i\gamma_5 u\bar{d}t^a d$	-4.2	-8.88	-3.18
$\bar{d}t^a i\gamma_5 d\bar{u}t^a u$	31.3	-8.88	3.18
$\bar{u}t^a i\gamma_5 u\bar{s}t^a s$	0	0	$-$
$\bar{s}t^a i\gamma_5 s\bar{u}t^a u$	0	0	$-$
$\bar{d}t^a i\gamma_5 d\bar{s}t^a s$	0	0	$-$
$\bar{s}t^a i\gamma_5 s\bar{d}t^a d$	0	0	$-$
$\bar{u}t^a i\gamma_5 u\bar{u}t^a u$	-46.8	39.5	-23.5
$\bar{d}t^a i\gamma_5 d\bar{d}t^a d$	83.4	-51.1	9.3
$\bar{s}t^a i\gamma_5 s\bar{s}t^a s$	-4.12	0	$-$
$\bar{u}t^a i\gamma_5 \sigma^{\mu\nu} u\bar{d}t^a \sigma_{\mu\nu}d$	-46.9	-106	14.3
$\bar{u}t^a i\gamma_5 \sigma^{\mu\nu} u\bar{s}t^a \sigma_{\mu\nu}s$	0	0	$-$
$\bar{d}t^a i\gamma_5 \sigma^{\mu\nu} d\bar{s}t^a \sigma_{\mu\nu}s$	0	0	$-$

Table 2.21: Comparison of different methods, nEDM calculated by factorization in Ref. [19, 20] are shown as "naive factorization". The column on the right side shows nEDM calculated using factorization and QCD sum rules [18]. The unit of the numbers is $10^{-3}eC_4$GeV.

Kabir theorem [58]. Applying to this context, the theorem dictates that CP-odd $(3, \bar{3})$ two-quark operators give no contribution to CP-odd processes. A brief discussion of this theorem can be found in Appendix D. However, since we are using a hybrid method, this theorem may not be satisfied. Therefore, the amount of violation of this theorem can be seen as an estimate of the error of this calculation. Take the operator $\bar{u}i\gamma_5 u - \bar{d}i\gamma_5 d$ as an example, following the prescription in Secs. III and IV, one can get meson-condensate contribution to the neutral CP-odd pion-nucleon coupling which can be written as

$$h_n^{mc} = \frac{2C_3(2c_1 + c_3)}{F_\pi} \approx -\frac{10C_3}{F_\pi} \ , \tag{2.131}$$

where $m_u = m_d = \bar{m}$ is assumed for the sake of simplicity, C_3 is the Wilson coefficient of the two-quark operator and the definitions of c_1 and c_3 can be found in Eq. (2.84). If the σ-term is also employed to do the direct matching, one can easily show that the direct matching contribution cancels the meson condensate contribution exactly. Instead, in order to get the uncertainty of our calculation we need to do the direct matching using the quark model. Since the operator includes only products of two quark fields, the calculation using the quark model is straightforward, which gives

$$h_n^{dir} = R\frac{3C_3}{F_\pi} \approx \frac{5C_3}{F_\pi} \ , \tag{2.132}$$

where the factor of 3 is due to that in the quark model the nucleon contains three constituent quarks. $R \approx 1.7$ comes from the perturbative QCD effect as discussed in Sec. V. The anomalous dimensions of the operator discussing here is as the same as the anomalous dimensions of the quark mass. The relative sign between the direct contribution and the meson condensate contribution is as desired. However,

the magnitude of the direct contribution is about two times smaller than the meson condensate contribution. The mismatch between the two contributions is due to that quark model does not differentiate $\langle N|\bar{q}q|N\rangle$ and $\langle N|q^\dagger q|N\rangle$. From this mismatch one can see that the inaccuracy of the direct contribution calculated using quark model might be a factor of two. Therefore, conservatively, the total inaccuracy for those operators having unsuppressed vacuum condensate contributions can be seen as a factor of two.

2.6   Summary

In this chapter, we studied the four-quark contributions to the neutron EDM, which dominate over other QCD operators in some new physics models. Our approach was based on chiral expansion and simple quark models. It is well known in the literature that the leading chiral contribution comes from one-pion loop which dominates in the chiral limit $m_\pi \to 0$, just like in the case of the nucleon electric polarizability. Therefore, one needs to calculate the four-quark contribution to the CP-odd pion nucleon couplings. We studied these couplings in simple quark models, as an alternate to large-N_c factorization. We also considered $\mathcal{O}(1)$ contribution from direct matching and pion-condensation to the dipole moment, as well as the CP-odd nucleon mass contribution through the magnetic moment. The resulting nEDM can be compared with those from the naive factorization and QCD sum rules. The comparison provides us some idea on the hadronic physics uncertainty in the neutron EDM calculation. Our approach also provides a formalism for lattice

QCD calculations of the nucleon matrix elements of the four-quark operators.

Using the matrix elements thus obtained, we obtain new-physics-independent upper bounds on the Wilson coefficients of four-quark operators from the experimental data. The current experimental upper bound on neutron EDM is $2.9 \times 10^{-26} e$ cm [33]. If we assume that there is no significant cancelations among the contributions from these operators, we can use the experiment limit to give upper bounds to the Wilson coefficients of individual operators. In our calculation, the strange quark effects were ignored, and we considered only operators composed of up and down quarks. The final results are shown in Table 1.2.

It is interesting to note that the chiral-enhanced contribution is actually large-N_c suppressed. In fact, the non-singular part of the chiral-loop contribution numerically dominates over the singular one. This suggests a large-N_c analysis of the neutron EDM, including the delta resonance contribution. However, this might be discussed in future works.

Chapter 3

Systematic Calculation of Neutron EDM in Minimal LRSM

3.1 General CP-Violating Effective Lagrangian

In this section, we lay out a general approach to calculating the nEDM using the effective Lagrangian method, independent of new physics. In this approach, one integrates out all heavy particles including SM gauge bosons and heavy-quarks. The resulting flavor neutral CP-violating effective Lagrangian has an expansion in terms of operators consisting of light-quark fields, u, d, and s and the gluon field $G^{\mu\nu}$, with increasing dimensions, the general P-odd and CP-odd Lagrangian is given in Eq. (2.6), and the operators contained in it are listed in Eqs. (2.8), (2.9), (2.10), (2.11) and (2.12).

As discussed in Chapter 2. To calculate nEDM systematically we need to crank down the energy scale to the hadronic scale. Therefore, the anomalous dimensions of the operators are needed.

At dimension-five level, the one-loop evolution equations are [31]

$$\mu^2 \frac{d}{d\mu^2} O_q^C(\mu) = -\left(\frac{2}{3} - \frac{b_f}{2}\right) \frac{\alpha_S(\mu)}{4\pi} O_q^C(\mu) , \qquad (3.1)$$

$$\mu^2 \frac{d}{d\mu^2} O_q^E(\mu) = -\frac{4}{3} \frac{\alpha_S(\mu)}{4\pi} O_q^E(\mu) , \qquad (3.2)$$

where $b_f = 11 - 2n_f/3$, n_f is the number of quark flavors. It is easy to see that

the dependence of the evolution of the quark CDM on n_f is the same as that of the strong coupling, since they are both derived from wave function renormalization of the gluon field.

For dimension-six operators, the leading-order QCD evolution equations for dimension-six operator are listed in Eq. 2.21 in Chapter 2. The anomalous dimension of the Weinberg, γ_{gg}, has been calculated in the literature [30], $\gamma_{gg} = -C_A/2 - n_f$, where $C_A = 3$. The dimension-six operators mix with the dimension-five operators when scale evolves, however at the energy scale where only the light quarks exist, the mixing can be neglected because the dimension-five quark EDM and CDM are chirality flipping and thus proportional to the quark mass. At higher energies, the mixing is important and we will discuss it in the following sections.

There is no mixing between the Weinberg operator and the four-quark operators listed in Eqs. (2.10) and (2.11). To see this, we can decompose the four-quark operators into irreducible representations of the $SU(3)_L \times SU(3)_R$ chiral group and only $(3, \bar{3})$, $(6, \bar{6})$, $(8, 8)$ and their conjugate representations are found as discussed in Chapter 2. On the other hand, the three-gluon operator is a chiral singlet. QCD evolution maintains the chiral structure of operators.

When scale changes, the pure quark-gluon CP-odd operators generate perturbative contributions to quark EDM through the following T-product

$$\int d^4x \ \mathrm{T} \left(eA_\mu(x) j^\mu_{em}(x) \sum_i{}' O_i(0) \right) , \qquad (3.3)$$

where the summation neglects the quark EDM operator itself. The contributions are divergent so they induce additional running of the CP-odd operators. The

contributions from the dimension-six operators are proportional to the mass of light quarks and can be neglected. The only large contribution is from the quark CDM operator, whose running has an effective inhomogenous term, [31]

$$\mu^2 \frac{d}{d\mu^2} O_q^C = \frac{\alpha_S(\mu)}{4\pi} \left(-\left(\frac{2}{3} - \frac{b_f}{2}\right) O_q^C - \frac{16}{3} \frac{e}{g_S(\mu)} Q_q O_q^E \right) , \qquad (3.4)$$

where Q_q is the electric charge of the quarks and g_S is the coupling of strong interaction. Inversely, the quark EDM operators can also generate quark CDM operators through the electromagnetic interaction which is, however, proportional to the electromagnetic fine-structure constant.

Therefore, omitting the θ-contribution, one can define the following electric dipole form factor

$$-F_n^E(q^2)\bar{U}_n(\vec{k}_2)\sigma^{\mu\nu}\gamma_5 q_\mu U_n(\vec{k}_1)\epsilon_\nu(q)$$

$$= \langle N(\vec{k}_2)| \sum_q d_q^E(\mu)O_q^E(0;\mu)$$

$$+i \int d^4x \, \mathrm{T} \left[eA_\mu(x)j_{em}^\mu(x) \left(\sum_q d_q^C(\mu)O_q^C(0;\mu) \right. \right.$$

$$\left. \left. + \sum_i C_i(\mu)O_{4i}(0;\mu) + C_g(\mu)O_g(0;\mu) \right) \right] |\gamma(q)N(\vec{k}_1)\rangle , \qquad (3.5)$$

where $q^\mu = k_2^\mu - k_1^\mu$ and U_n is the wavefunction of neutron and ϵ^ν is the polarization of the incoming photon. The static nEDM is just the zero-momentum limit of the form factor $d_n^E = F_n^E(0)$.

3.2   Wilson Coefficients in LRSM

Following the previous section, we make calculation of nEDM in the mLRSM by first evaluating the Wilson coefficients of the effective quark-gluon operators at

90

the electroweak scale, and subsequently running them to hadronic scale. The detail of the model can be found in Ref. [3], in which the spontaneous CP-violation is controlled by a phase angle α in the Higgs sector, and additional parameters of the model include, among others, the masses of the right-handed gauge boson and the new Higgs bosons. In the following subsections, we study the Wilson coefficients of various CP-violating operators separately. We will ignore the contribution of the θ-term as it will usually generate a much too large nEDM: We assume certain mechanisms such as Peccei-Quinn symmetry [35] is in operation to suppress it.

3.2.1 CP-Odd Four-Quark Operators

To leading order, diagrams in Fig. 3.1 generate the CP-odd four-quark operators induced by the exchange of gauge bosons and Higgs bosons. The operators are listed in Eq. (2.10) and (2.11). The corresponding Wilson coefficients can be easily

read through the diagrams,

$$C_{11}^{ab} = \frac{\sqrt{8}G_F}{6}\sin 2\zeta \mathrm{Im}(e^{-i\alpha}V_L^{ab}V_R^{ab*}) + \frac{\sqrt{8}G_F}{M_{H_0}^2}\mathrm{Im}(C^{aa}D^{bb})$$

$$+\frac{\sqrt{8}G_F}{6M_{H_2}^2}(m_a^2-m_b^2)\xi \mathrm{\ Im}(e^{-i\alpha}V_L^{ab}V_R^{ab*}) \ ,$$

$$C_{12}^{ab} = -\frac{\sqrt{8}G_F}{6}\sin 2\zeta \mathrm{Im}(e^{-i\alpha}V_L^{ab}V_R^{ab*}) + \frac{\sqrt{8}G_F}{M_{H_0}^2}\mathrm{Im}(C^{aa}D^{bb})$$

$$+\frac{\sqrt{8}G_F}{6M_{H_2}^2}(m_a^2-m_b^2)\xi \mathrm{\ Im}(e^{-i\alpha}V_L^{ab}V_R^{ab*}) \ ,$$

$$C_{21}^{ab} = \sqrt{8}G_F \sin 2\zeta \mathrm{Im}(e^{-i\alpha}V_L^{ab}V_R^{ab*})$$

$$+\frac{\sqrt{8}G_F}{M_{H_2}^2}(m_a^2-m_b^2)\xi \mathrm{\ Im}(e^{-i\alpha}V_L^{\alpha\beta}V_R^{\alpha\beta*}) \ ,$$

$$C_{22}^{ab} = -\sqrt{8}G_F \sin 2\zeta \mathrm{Im}(e^{-i\alpha}V_L^{ab}V_R^{ab*})$$

$$+\frac{\sqrt{8}G_F}{M_{H_2}^2}(m_a^2-m_b^2)\xi \mathrm{\ Im}(e^{-i\alpha}V_L^{\alpha\beta}V_R^{\alpha\beta*}) \ , \tag{3.6}$$

$$C_3^{ab} = \frac{\sqrt{8}G_F}{6M_{H_2}^2}(m_a^2-m_b^2)\xi \mathrm{\ Im}(e^{-i\alpha}V_L^{\alpha\beta}V_R^{\alpha\beta*}) \ ,$$

$$C_4^{ab} = \frac{\sqrt{8}G_F}{M_{H_2}^2}(m_a^2-m_b^2)\xi \mathrm{\ Im}(e^{-i\alpha}V_L^{\alpha\beta}V_R^{\alpha\beta*}) \ ,$$

$$C_{11}^{aa'} = \frac{2\sqrt{8}G_F}{M_{H_0}^2}\mathrm{Im}(C^{aa}C^{a'a'*}) \ ,$$

$$C_{12}^{aa'} = -\frac{2\sqrt{8}G_F}{M_{H_0}^2}\mathrm{Im}(C^{aa}C^{a'a'*}) \ ,$$

$$C_{11}^{bb'} = \frac{2\sqrt{8}G_F}{M_{H_0}^2}\mathrm{Im}(D^{aa}D^{a'a'*}) \ ,$$

$$C_{12}^{bb'} = -\frac{2\sqrt{8}G_F}{M_{H_0}^2}\mathrm{Im}(D^{aa}D^{a'a'*}) \ , \tag{3.7}$$

where $a, a' \in u, c, t, \ a \neq a'$ and $b, b' \in d, s, b, \ b \neq b'$, $C = V_L\hat{M}_D V_R^\dagger - 2\xi e^{i\alpha}\hat{M}_U$,

$D = V_L^\dagger \hat{M}_U V_R - 2\xi e^{-i\alpha}\hat{M}_D$, M_{H_0} is the mass of the flavor changing neutral Higgs

(FCNH) and M_{H_2} is the mass of H_2^+ which is a charged Higgs in mLRSM [3]. $\hat{M}_U$

and $\hat{M}_D$ are diagonalized quark mass matrices. ζ is the mixing angle between the

lefthanded and righthanded W-bosons that

$$\sin 2\zeta \simeq -r\frac{4m_b}{m_t}\left(\frac{M_1}{M_2}\right)^2 \ , \tag{3.8}$$

where $r \equiv (m_t/m_b)\xi$ and ξ is the ratio between the two vevs of the Higgs bidoublet in mLRSM [3]. The contributions due to the Higgs exchanges are always proportional to quark masses. Since we are only interested in operators with at least two of the quarks being light, the Wilson coefficients are always proportional to at least one light quark mass, or they are proportional to heavy quark masses but must be suppressed by the non-diagonal CKM matrix elements. Furthermore, the mass of FCNH is strongly constrained to very large value by the mass differences and the CP-violating decay properties of the neutral K-bosons and B-bosons [3, 59], and detailed calculation shows H_2^+ is as heavy as FCNH. If we are interested in the case of a few TeV right-handed W-boson mass, we can safely neglect the Higgs exchange contributions. Then at the electroweak scale the Wilson coefficients of the CP-odd four-quark operators can be simplified to

$$
\begin{aligned}
C_{11}^{ab} &= -C_{12}^{ab} = \frac{\sqrt{8}G_F}{6}\sin 2\zeta \ \mathrm{Im}(e^{-i\alpha}V_L^{ab}V_R^{ab*}) \ , \\
C_{21}^{ab} &= -C_{22}^{ab} = \sqrt{8}G_F \sin 2\zeta \ \mathrm{Im}(e^{-i\alpha}V_L^{ab}V_R^{ab*}) \ .
\end{aligned}
\tag{3.9}
$$

We will take this simple limit in the following discussion.

3.2.2 Quark EDM and CDM Operators

The one-loop contributions to the quark EDM from the gauge interactions are shown in Fig. 3.2, where the internal wavy lines represent the light charged

gauge-boson W_1 which is dominated by W_L, but has a small admixture of W_R. The dashed lines represent the charged-Goldstone boson present in Feynman gauge, and the external wavy line is the static electric field or photon. Diagrams a) and b) have the photon interacting with the quarks directly, and these from c) to f) have the photon interacting with charged bosons. For the quark CDM case we have the first two diagrams only with the external wavy line representing a gluon.

These diagrams have been calculated in the literature long ago [12], our result is somewhat different from theirs in the infrared part. The CP-odd part of the diagrams in Fig. 3.2 can be expressed in terms of the coefficients of the EDM and CDM operators. For the up quark, we have $d_u^E O_u^E + d_u^C O_u^C$ with,

$$
\begin{aligned}
d_u^E &= \frac{1}{16\pi^2} \sum_{i=d,s,b} m_{di} e \sqrt{8} G_F \sin 2\zeta \, \mathrm{Im}(e^{-i\alpha} V_L^{1i} V_R^{1i*}) \\
&\times \frac{1}{(1-r_i)^3} \left(\frac{4}{3} - 4r_i + 3r_i^2 - \frac{1}{3}r_i^3 + \frac{1}{2}r_i \ln r_i - \frac{3}{2}r_i^2 \ln r_i \right) , \\
d_u^C &= \frac{1}{16\pi^2} \sum_{i=d,s,b} m_{di} g_s \sqrt{8} G_F \sin 2\zeta \, \mathrm{Im}(e^{-i\alpha} V_L^{1i} V_R^{1i*}) \\
&\times \frac{1}{(1-r_i)^3} \left(1 - \frac{3}{4}r_i - \frac{1}{4}r_i^3 + \frac{3}{2}r_i \ln r_i \right) .
\end{aligned}
\tag{3.10}
$$

And for the down quark, the contribution is $d_d^E O_d^E + d_d^C O_d^C$ with

$$
\begin{aligned}
d_d^E &= \frac{1}{16\pi^2} \sum_{i=u,c,t} m_{ui} e \sqrt{8} G_F \sin 2\zeta \, \mathrm{Im}(e^{-i\alpha} V_L^{1i} V_R^{1i*}) \\
&\times \frac{1}{(1-r_i')^3} \left(\frac{5}{3} - \frac{17}{4}r_i' + 3r_i'^2 - \frac{5}{12}r_i'^3 + r_i' \ln r_i' - \frac{3}{2}r_i'^2 \ln r_i' \right) , \\
d_d^C &= -\frac{1}{16\pi^2} \sum_{i=u,c,t} m_{ui} g_s \sqrt{8} G_F \sin 2\zeta \, \mathrm{Im}(e^{-i\alpha} V_L^{i1} V_R^{i1*}) \\
&\times \frac{1}{(1-r_i')^3} \left(1 - \frac{3}{4}r_i' - \frac{1}{4}r_i'^3 + \frac{3}{2}r_i' \ln r_i' \right) .
\end{aligned}
\tag{3.11}
$$

It is easy to see that this mixing angle is suppressed by the mass ratio of bottom

and top quarks and by the ratio of the left and right handed W-boson masses. m_{ui} are the masses of up-type intermediate quarks, $r_i = m_{di}^2/M_W^2$, $r_i' = m_{ui}^2/M_W^2$, V_L and V_R are the left and right-handed CKM mixing matrices, respetively, α is the spontaneous CP phase mentioned earlier.

In mLRSM, H_2^+ also gives contribution to the quark EDM and CDM. The relevant diagrams are shown in Fig. 3.3, and the result is

$$
\begin{aligned}
d_u^E &= -\sum_{a\in\{d,s,b\}} \frac{1}{16\pi^2}\sqrt{8}G_F \frac{2m_a(m_u^2-m_a^2)}{M_{H_2}^2}\xi\,\mathrm{Im}(e^{-i\alpha}V_L^{1a}V_R^{1a*}) \\
&\qquad \left[e_d\frac{3-4r_j+r_j^2+2\ln r_j}{2(-1+r_j)^3} - e\frac{-1+r_j^2-2r_j\ln r_j}{2(-1+r_j)^3}\right], \\
d_u^C &= \sum_{a\in\{d,s,b\}}\frac{g_s}{16\pi^2}\sqrt{8}G_F\frac{2m_a(m_u^2-m_a^2)}{M_{H_2}^2}\,\mathrm{Im}(e^{-i\alpha}V_L^{1a}V_R^{1a*})\frac{3-4r_j+r_j^2+2\ln r_j}{2(-1+r_j)^3},
\end{aligned}
\tag{3.12}
$$

$$
\begin{aligned}
d_d^E &= -\sum_{a\in\{u,c,t\}} \frac{1}{16\pi^2}\sqrt{8}G_F \frac{2m_a(m_a^2-m_d^2)}{M_{H_2}^2}\xi\,\mathrm{Im}(e^{-i\alpha}V_L^{a1}V_R^{a1*}) \\
&\qquad \left[e_u\frac{3-4r_j'+r_j'^2+2\ln r_j'}{2(-1+r_j')^3} + e\frac{-1+r_j'^2-2r_j'\ln r_j'}{2(-1+r_j')^3}\right], \\
d_d^C &= \sum_{a\in\{u,c,t\}}\frac{g_s}{16\pi^2}\sqrt{8}G_F\frac{2m_a(m_a^2-m_d^2)}{M_{H_2}^2}\xi\,\mathrm{Im}(e^{-i\alpha}V_L^{a1}V_R^{a1*})\frac{3-4r_j'+r_j'^2+2\ln r_j'}{2(-1+r_j')^3},
\end{aligned}
\tag{3.13}
$$

in which

$$
r_j = \frac{M_{Dj}^2}{M_{H_2}^2}, \quad r_j' = \frac{M_{Uj}^2}{M_{H_2}^2},
\tag{3.14}
$$

Therefore, if the right-handed W-boson has a moderate mass, say, a few TeV, the contribution from H_2^+ to the quark EDM and CDM can be neglected in comparison to that from the right-handed gauge boson.

Actually, there are both long-distance and short-distance contributions from the one-loop diagrams in Fig. 3.2 and Fig. 3.3. The short-distance contributions come from the integration region where the internal momentum is around M_W; and the long-distance one from the loop momentum around the internal light quark masses. Due to asymptotic freedom of the strong interaction, the short-distance contributions can be calculated accurately using perturbation theory. The long-distance contributions, however, suffer from non-perturbative QCD effects, and the only known way to calculate it correctly is by Lattice QCD. In the matching calculation, the long distance contribution has to be subtracted to obtain the Wilson coefficients, which is shown in Fig. 3.4. This contribution can be calculated using a certain UV regulator, such as dimensional regulation or momentum cut-off or lattice regularization. Any regularization preserving a certain Fierz identity will give a zero answer as the loop integral involves only the photon or gluon external momentum. Other regularizations, such as naive dimensional regularization, will find a finite contribution. One must be careful though that the vanishing of long-distance contribution is only true at one-loop level: as soon as the QCD corrections are taken into account, the result becomes non-zero. Therefore, to the leading order, we can directly read off the Wilson coefficients of quark EDM and CDM operators from Eqs.(3.10), (3.11), and (3.12).

3.2.3 Weinberg Operator

In mLRSM, the Weinberg operator can be induced from diagrams in Fig. 3.5. Since the result is proportional to the quark masses, the leading contribution comes from the third generation of the quarks running in the loop. These are two-loop diagrams, the Weinberg operator comes out after one integrates out the internal quarks and bosons entirely. If one follows the effective theory approach, in which the top quark and the W-boson are first integrated out, the CDM operator of the bottom quark emerges and one can get its wilson coefficient from Eq. (3.11).

Then from Fig. 3.6, one gets the major contribution to the Weinberg three gluon vertex. Because this diagram would diverge quadratically in the infrared if the mass of the bottom quark was zero, this diagram should be proportional to $1/m_b^2$. However, chirality flipping is needed or otherwise the fermion loop will vanish, so the numerator of the diagram must be proportional to m_b. Combining the two effects together, this diagram is proportional to d_b^C/m_b, where d_b^C is the bottom quark CDM which is proportional to m_t. Therefore this diagram has an enhancement of a factor of m_t/m_b, about 40, which was first found in Ref. [60]. Detailed calculation gives the Wilson coefficient

$$C_g(m_b) = \frac{g_s^2(m_b)}{16\pi^2} \frac{d_b^C(m_b)}{m_b} \ . \tag{3.15}$$

This contribution is seemingly large, however, it is suppressed by a numerical factor, $1/(1 - m_t^2/M_1^2)^3 \simeq -0.02$ in Eq. (3.11). Therefore, the effect of the enhancement is totally canceled. Furthermore, the evolution also makes the contribution of this operator to be smaller at the low energy region [30]. Therefore, we safely neglect its

contribution to nEDM in the following calculations.

3.2.4 Wilson Coefficients at Hadronic Scale Through Leading-Order QCD Evolution

The coefficient functions above, and hence the quark-gluon operators, are calculated at the high-energy electroweak scale, which is not yet useful for practical calculations. We are going to remedy this by running down the scale in the composite operator by including the leading logarithmic pQCD corrections. When we change the scale, dimension-six operators will mix with each other and generate dimension-five operators, and dimension-five operators will also mix with each other. The Wilson coefficients for CP-odd four-quark operators are shown to the leading order approximation in Eq. (3.9). From Eq. (2.21) the renormalization group equations (RGE) keep this relation, and other CP-odd four-quark operators are not generated by the running. Then one can redefine the operators

$$
\begin{aligned}
O_1^{ab} &= O_{11}^{ab} - O_{12}^{ab} , \\
O_2^{ab} &= O_{21}^{ab} - O_{22}^{ab} ,
\end{aligned}
\tag{3.16}
$$

with the Wilson coefficients $C_1^{ab} = C_{11}^{ab}$ and $C_2^{ab} = C_{21}^{ab}$, respectively. Therefore, the RGEs of the Wilson coefficients of the dimension-six operators can be written as

$$
\begin{aligned}
\mu^2 \frac{d}{d\mu^2} C_1^{ab}(\mu) &= -8 \frac{\alpha_s(\mu)}{4\pi} C_1^{ab}(\mu) ; \\
\mu^2 \frac{d}{d\mu^2} C_2^{ab}(\mu) &= \frac{\alpha_s(\mu)}{4\pi} C_2^{ab}(\mu) ,
\end{aligned}
\tag{3.17}
$$

which shows that C_1 grows as the scale goes down, whereas C_2 does the opposite.

The RGE of the quark CDM operators are a little bit complicated. For d quark and s quark CDM operators, as we discussed before, the c quark internal line gives a large contribution. Therefore, the RGEs of d and s quark CDM operators can be written as [31]

$$
\begin{aligned}
\mu^2 \frac{d}{d\mu^2} d_{d,s}^C(\mu) &= -\frac{g_s^3(\mu)}{(16\pi)^2} m_c(\mu) \left(\frac{2}{3} \gamma_{31} C_2^{c(d,s)}(\mu) - 4\gamma_{32} C_1^{c(d,s)}(\mu) \right) \\
&\quad - \frac{g_s^2(\mu)}{16\pi^2} (\gamma_{33} + b_f/2 - \delta) d_{d,s}^C(\mu) \ .
\end{aligned} \tag{3.18}
$$

The Wilson coefficient of the up quark CDM operator is one order of magnitude smaller than that of the of d quark due to that $m_s/m_c \sim 1/10$. In the above formula, $\gamma_{31} = 5/2$, $\gamma_{32} = -1$, $\gamma_{33} = -14/3$, and $\delta = -4$ is the anomalous dimension of the quark mass. Detailed calculation gives, at m_c, the relevant Wilson coefficients are

$$
\begin{aligned}
C_1^{u(d,s)}(m_c) &= 3.0 C_1^{u(d,s)}(M_L) \ , \\
C_2^{u(d,s)}(m_c) &= 0.87 C_2^{u(d,s)}(M_L) \ , \\
d_{d,s}^C(m_c) &= 1.7 \frac{m_c}{16\pi^2} C_1^{c(d,s)}(M_L) + 0.34 \frac{m_c}{16\pi^2} C_2^{c(d,s)}(M_L) + 1.6 d_{d,s}^C(M_L) \ .
\end{aligned}
$$

$$
\tag{3.19}
$$

were M_L is the mass of the SM W-boson.

The CP-odd operators generate additional running of the quark EDM operators through the electromagnetic interaction. The RGE of the down quark EDM operator can be written as [31]

$$
\begin{aligned}
\mu^2 \frac{d}{d\mu^2} d_d^E(\mu) &= -\frac{2}{3} \frac{e m_c(\mu) g_s^2(\mu)}{(16\pi^2)^2} \gamma_{41} C_2^{cd}(\mu) - \frac{e g_s(\mu)}{16\pi^2} \gamma_{43} d_d^C(\mu) \\
&\quad - \frac{g_s^2(\mu)}{16\pi^2} (\gamma_{44} - \delta) d_d^E(\mu) \ ,
\end{aligned} \tag{3.20}
$$

where $\gamma_{41} = 16/3$, $\gamma_{43} = 16/9$, $\gamma_{44} = -16/3$, and similarly for the strange quark. The RGE of the electromagnetic coupling e does not depend on the strong coupling constant g_s up to one-loop, therefore, can be treated as a constant. At the charm quark mass scale, one can get

$$
\begin{aligned}
d_{d,s}^E(m_c) &= \frac{em_c}{16\pi^2}(0.07C_1^{c(d,s)}(M_L) + 0.34C_2^{c(d,s)}(M_L)) \\
&\quad + 0.17ed_{d,s}^C(M_L) + 0.83d_{d,s}^E(M_L) \,.
\end{aligned} \tag{3.21}
$$

which shows the explicit contributions from the running of the four-quark operators as well as CDM operators.

3.3   nEDM in mLRSM and Constraint on Left-right Symmetry scale

In this section, we carry out the last step of the nEDM calculation in mLRSM by incorporating the neutron matrix elements of hadronic operators. We collect the state-of-art results in the literature and use them to constrain the parameters in mLRSM. We find that in order to satisfy the current experimental bound on nEDM and the data on kaon-decay parameter ϵ, the right-handed gauge boson W_R might be as heavy as 10 ± 3 TeV. This bound is far higher than the bound obtained previously from the kaon mass difference, making it difficult to discover left-right symmetry at LHC.

3.3.1   Hadronic Matrix Elements

The most difficult part in calculating nEDM is to estimate the hadronic matrix elements. In the literature, many different approaches, such as the $SU(6)$ quark

model, bag models, QCD sum rules, and chiral perturbation theory have been used to make estimations. In this subsection, we summarize the results and get some idea about their uncertainties.

3.3.1.1 Contribution from Quark EDM

In the $SU(6)$ constituent quark model, the matrix elements of the quark tensor operators are simple and scale-independent [11, 12], leading to

$$d_N^{(1)} = -\frac{1}{3}d_u^E + \frac{4}{3}d_d^E . \tag{3.22}$$

Although it has been suggested that one should use the constituent quark masses in the formulas of quark EDM [12], this is incorrect from the point of view of factorization.

In the parton quark model discussed in [13], it was found,

$$d_N^{(1)} = -0.508d_u^E + 0.746d_d^E - 0.226d_s^E . \tag{3.23}$$

From the QCD sum rules, one gets [14]

$$d_N^{(1)} = (1 \pm 0.5) \times 0.7(-0.25d_u^E + d_d^E) . \tag{3.24}$$

Different approximations are largely consistent.

3.3.1.2 Contribution from Quark CDM

The contribution to nEDM from the quark CDM in the constituent quark model is [11]

$$d_N^{(2)} = \frac{4}{9}\frac{e}{g_s}d_u^C + \frac{8}{9}\frac{e}{g_s}d_d^C , \tag{3.25}$$

where g_s is the coupling of strong interaction at the energy scale where the model is applicable. In this calculation, the authors assumed first that the neutron is composed of constituent quarks, and then treated the gluon field inside the neutron as a background, neglecting its kinetic energy. Therefore, Eq. (3.25) can only be seen as an order-of-magnitude estimate.

Weinberg's naive dimensional analysis has also been used to estimate this contribution [29, 61, 62],

$$d_N^{(2)} \sim \frac{e}{4\pi} \left(O(1) d_u^C + O(1) d_d^C \right) . \tag{3.26}$$

In Ref. [63], the authors used the chiral perturbation theory to calculate the singular part of the long distance contribution,

$$d_N \simeq \frac{0.7e}{g_s} (d_u^C + d_d^C) . \tag{3.27}$$

And finally, QCD sum rules analysis in Ref. [14] gives

$$d_N^{(2)} = (1 \pm 0.5) \times \frac{0.55e}{g_s} (0.5 d_u^C + d_d^C) , \tag{3.28}$$

where g_s is the strong coupling constant at 1 GeV, about 2.5.

3.3.1.3 Contribution from Weinberg Operator

The contribution from the Weinberg's operator O_W can be estimated by Weinberg's naive dimensional analysis [29], which is an order-of-magnitude estimate

$$d_N^{(3)} \simeq eMC_g(\mu)/4\pi \approx 100 \text{ MeV } e\, C_g(1\text{GeV}) , \tag{3.29}$$

where $M = 4\pi F_\pi \simeq 1190$ MeV and μ is the hadronic scale taking as 1 GeV.

On the other hand, the estimate based on QCD sum rules gives [64]

$$d_N^{(3)} \simeq (10 - 30)\text{MeV} \, e \, C_g(1 \text{ GeV}) \, , \qquad (3.30)$$

which is considerably smaller. In any case, because of the small coefficient function, the Weinberg operator contribution can essentially be neglected.

3.3.1.4 Contribution from Four-Quark Operators

The hadronic matrix elements of the four-quark operators have been studied and reviewed in Ref. [65]. In this work we will take the results from that paper.

3.3.2 Numerical Results

As discussed in Ref. [3], combining with the kaon indirect CP-violation ϵ parameter, one can use nEDM to get the most stringent lower bound on the mass of the right-handed W boson in the context of the mLRSM. In Ref. [3], the authors used naive factorization [20] to estimate the contribution of four-quark operators. However, this method for baryons may not be valid even in the large-N_C limit, and the uncertainty is unknown. Therefore, we have assumed a very large error on their matrix elements and the resulting constraint on the left-right symmetry scale is not very strong. In a dedicated study of these matrix elements [65], we have gotten a much better understanding on their contribution. In Ref. [65], the contribution of four-quark operators to nEDM was separated into two parts, the direct contribution and the meson-condensate contribution. For the direct contribution, quark models were employed to calculate the hadronic matrix elements, which is only an

order-of-magnitude estimate be. However, for the meson-condensate contribution, the factorization method was used to calculate the meson matrix elements, which can be justified in the large-N_C limit. Since the meson-condensate contribution dominates over the direct one, we believe that we reached a factor-of-two accuracy in the matrix elements of four-quark operators.

In mLRSM, after neglecting the contributions from FCNH and the charged higgs boson exchange, nEDM depends only on three parameters, r, α, and M_{W_R}, where α is the new source of CP-violation. Therefore, if $\alpha = 0$, nEDM predicted by the mLRSM will be the same as that predicted by SM, about five orders of magnitude smaller than the upper bound given by the current experiment [4]. Whereas for ϵ, there are two new contributions in mLRSM [3], the Dirac phase in the righthanded CKM matrix inherited from the lefthanded CKM matrix, and the spontaneous phase α. The new contribution from the Dirac phase is enhanced compared to the similar contribution in SM due to the chiral enhancement in the hadronic matrix element (see Ref. [5] for a good review). The contribution of the spontaneous CP-phase α must be adjusted to cancel the contribution of the Dirac phase. Therefore, in mLRSM there is a tension between nEDM and ϵ that one cannot only adjust α to suppress all the new CP-violation sources, and a large M_{W_R} is needed. As a result, nEDM and ϵ together give a lower bound on M_{W_R}.

In this new study, we use the QCD sum rules to estimate the contribution of the quark EDM and CDM operators, and use the results in Ref. [65] for the contribution of the four-quark operators. Fig. 3.7 shows the contributions to nEDM from different operators at fixed M_{W_R} and r. The result from the Weinberg operator

is too small to be included in the figure. It is clear that the contributions from four-quark operators are much larger than from quark EDM and CDM operators. One way to understand this is that in mLRSM the quark EDM and CDM operators are generated in the same way as the four-quark operators. The quark EDM and CDM operators are generated through diagrams in Fig. 3.2 and the four-quark operators are generated through diagrams in Fig. 3.1. The Wilson coefficients roughly have the following relations

$$d_q^E \simeq \frac{e m_q A}{16\pi^2} C_4 \ ; \ d_q^C \simeq \frac{g_s m_q A'}{16\pi^2} C_4 \ , \tag{3.31}$$

where A and A' are two proportionality coefficients, C_4 is the Wilson coefficient of certain four-quark operators. Take the down quark EDM as an example, A can be written as $\sin^2\theta_C m_c/m_u \simeq 15$, where θ_C is the Cabibbo angle. From QCD sum rules, nEDM contributed by the down-quark EDM operator is approximately the down-quark EDM itself, whereas the nEDM contributed directly from the four-quark operator can be written as [65]

$$d_N^{\text{four}-\text{quark}} \simeq \frac{e}{16\pi^2} B_0 C_4 \ , \tag{3.32}$$

where $B_0 \simeq 2.2$ GeV is related to SSB of the chiral symmetry. Since $B_0 \gg A m_d$, nEDM directly from the four-quark operator $\bar{u} i\gamma_5 u \bar{d} d$ is much larger than the contribution from the down quark EDM operator. Indeed, this is a common phenomenon in left-right models and two-Higgs-doublet models, where the quark EDM and CDM operators are always generated by the triangle diagrams in Fig. 3.2, and the internal lines are always quarks. In other types of new physics models, the internal lines can be other kind of fermions. For example, in supersymmetric models, they can

be gauginos, and in extra dimension models, they can be KK-fermions, where the above relation between quark EDM operators and four-quark operators is no longer hold. In these models, quark EDM and CDM operators might be more important that four-quark operators.

Using the matrix elements in Ref. [65], we calculate the constraint from the nEDM and kaon-decay parameter ϵ on the allowed parameter space of mLRSM. The result is shown in Fig. 3.8. The allowed parameter region by the experimental upper bound on nEDM is shown as green dots. The constraints from ϵ-parameter depends strongly on the mass of the FCNH in the theory. We have shown two possible values of M_{H_0}, 50 TeV and ∞ for simplicity. We assume for ϵ the new contribution should not exceed 1/4 of the experimental value. From Fig. 3.8 one can see that the lower bound for the M_{W_R} from nEDM and ϵ is around 10 TeV. If we assume a factor of 2 uncertainty on the hadronic matrix elements, the actual bound is 10 ± 3 TeV. This will make a direct detection of the right-handed gauge boson very difficult at LHC if it exits.

3.4   Summary

In this chapter, we have studied nEDM in mLRSM systematically by using effective field theory approach. The formula for calculating nEDM is given in Eq. (3.5). The contribution of four-quark operators is found to be the most important. The contribution of Weinberg operator to nEDM has been discussed systematically. A numerical suppression is found which counteracts the infrared enhancement and

makes the contribution of this operator negligible. We have found a lower bound on the mass of W_R which is about (10 ± 3) TeV. This constraint is the most stringent one on the righthanded scale to date, which means in the framework of mLRSM, W_R cannot be detected at LHC.

In a more complicated non-supersymmetric scenario of LRSM, although the CP-violation pattern in the Higgs sector might be change, the tension between ϵ and nEDM discussed in Sec. IV still exists. Therefore, one can also use this analysis to set a lower bound on the righthanded scale. In the supersymmetric LRSM, there are new CP-violation sources from the soft terms, which can contribute to both nEDM and ϵ. Furthermore, in supersymmetric LRSM [66], the lefthanded and righthanded CKM matrices must be equal to each other up to a sign, therefore, if one assumes certain scenarios of the breaking mechanism of supersymmetry, ϵ itself can give a constraint on the righthanded scale [67].
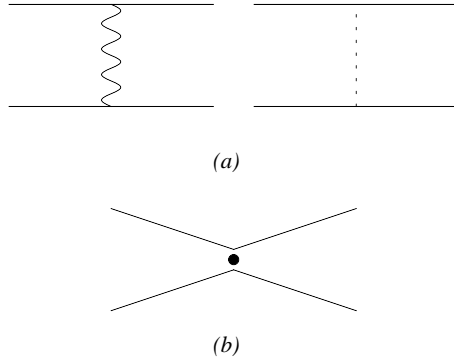
Figure 3.1: Effective four-quark operators generated by integrating out W_1-boson: (a) the diagrams in the full theory and (b) the effective operator.
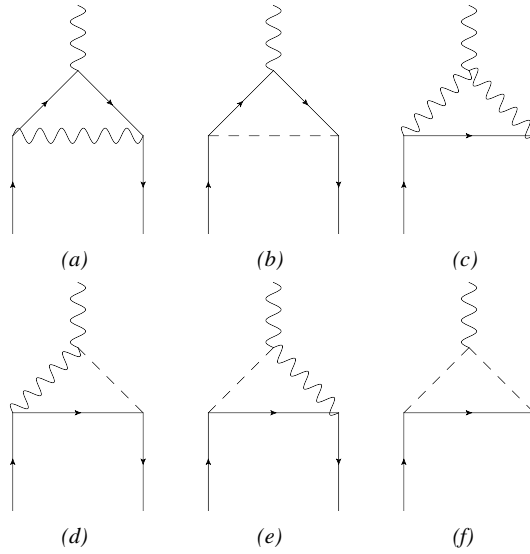
Figure 3.2: One-loop contribution to quark EDM. The internal wavy lines represent the W-boson contribution and the dashed lines the corresponding Goldstone bosons.
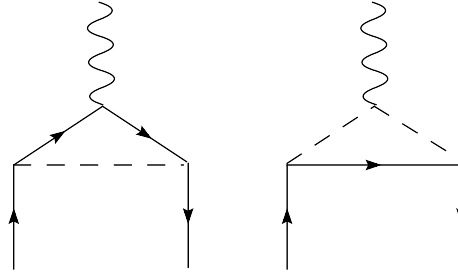
Figure 3.3: Higgs-induced quark EDM. The dashed lines here represents the Higgs bosons.
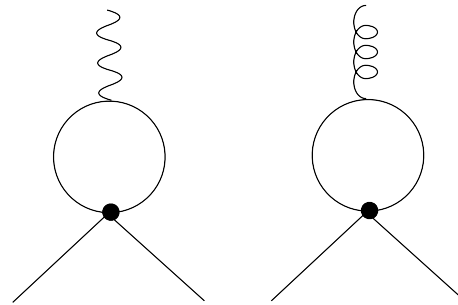
Figure 3.4: Long-distance contributions to quark EDM and CDM through CP-odd four-quark operators.
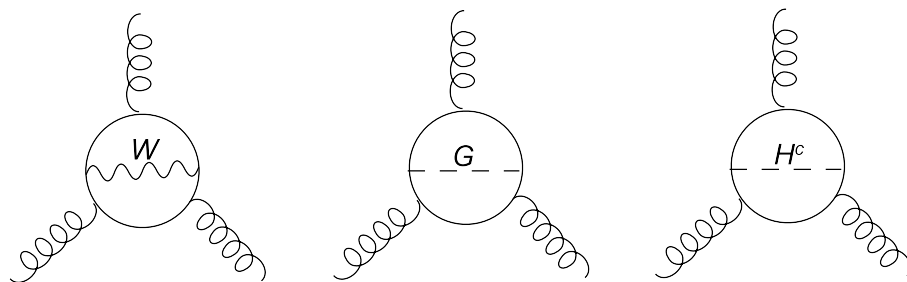
Figure 3.5: Diagrams contributing to Weinberg operator in mLRSM. The first diagram is induced by the W-boson exchange, the second by Goldstone exchange and the third by the charged Higgs boson.
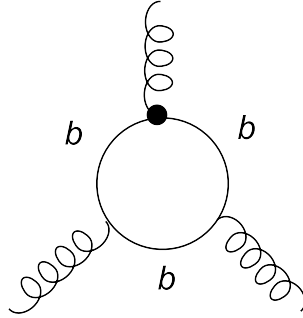
Figure 3.6: Contribution to the three-gluon vertex after integrating out the top quark, the Higgs boson and the W-bosons. The black dot labels the bottom quark CDM operator.
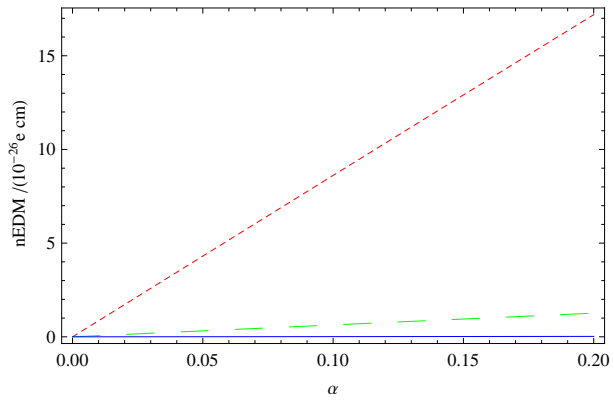
Figure 3.7: nEDM contributed from operators, $\bar{u}i\gamma_5 u\bar{d}d$ (short dashed red line), $\bar{u}i\gamma_5 u\bar{s}s$ (long dashed green line), down quark EDM and CDM operators (solid blue line).
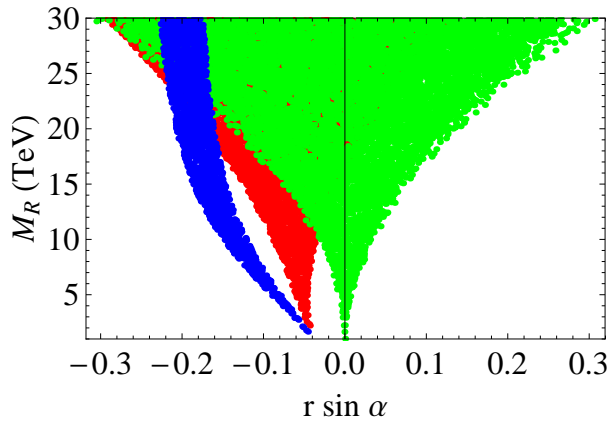
Figure 3.8: Constraints on the mass of W_R and the spontaneous CP-violating parameter α from the kaon decay parameter ϵ ($M_{H_0} = \infty$, red dots; $M_{H_0} = 50$ TeV, blue dots) and nEDM (green dots). For nEDM, we use the current experimental upper bound as the constraint and for ϵ we use the criteria that the beyond-SM-physics contribution should not exceed $1/4$ of the experimental value.

Chapter 4

Collider Constraints On Low Mass Dark Matter

4.1 Introduction

If the mass of WIMP is around or less than 15 GeV and the cross section between WIMP and nucleons is as large as 10^{-41} cm^2, it might probably be generated in colliders. The Tevatron constraints of direct detection signal has been studied in Refs. [68, 69] in an effective theory approach. The authors studied the process

$$p\bar{p} \rightarrow \text{mono} - \text{jet} \ + \ \text{missing energy} \ . \qquad (4.1)$$

At Tevatron, this process with the cuts that the leading jet $E_T > 80$ GeV, missing $E_T > 80$ GeV, second jet with $p_T < 30$ GeV and vetoing any third jet with $E_T > 20$ GeV has been studied in order to constrain large extra dimension model [70]. $1.0\,\text{fb}^{-1}$ of data was analyzed with 8449 events observed. On the other hand the expected value of SM background is 8663±332, therefore following Ref. [68, 69], the 2σ limit on the new physics can be set as $\sigma_{\text{new}} < 0.664$ pb. In Ref. [68], both the hard processes and soft ones have been simulated as well as the collider effects. It has been shown that the correction from the soft processes and the collider effects do not change much of the cross section of the hard processes. Therefore, in the following discussions, we only simulate the parton level processes.

In Tevatron, the center-of-mass energy of the incoming proton and anti-proton is 1.96 TeV. If the mass of mediator conducting the interaction between dark matter and SM particles is around or less than a few hundred GeV, it can be produced on-shell so that one cannot use contact operators to study Tevatron constraints. On the other hand, if the mass of mediator is so large that it cannot be produced on-shell at Tevatron, we show in Sec. 6.3 that the Tevatron constraint cannot be saturated in perturbative region. Furthermore, if the signal of CoGeNT or CRESST-II are induced by SI and momentum-independent (MI) interaction between WIMP and nuclei, the effective four-fermion interaction between quarks and WIMP (assuming dark matter is a fermion) can be estimated as

$$G^{(4)} \equiv \frac{g_{SM} g_D}{M_{\text{mediator}}^2} \approx \left(\frac{1}{(1 \sim 3) \text{ TeV}} \right)^2, \qquad (4.2)$$

where g_{SM} and g_D are the couplings of the mediator to quarks and MD, respectively. Therefore, at the Large Hadron Collider (LHC), since the center-of-mass energy of proton pairs is as large as 14 TeV, in the process $pp \rightarrow$ jets + missing energy, the mediator could not be integrating out or the unitary condition would be violated.

Another well known property of DM is its relic abundance, $\Omega h^2 \approx 0.11$ [71]. It can be generated in several ways. One is through thermal freezing out. The relic density of DM can also be produced by late-decays of the thermal relics of long living particles, for example, superWIMP models [72]. It can also be produced asymmetrically in analogy to baryogenesis, and this idea was first proposed in Ref. [73]. Usually, in late-decay scenarios, direct detection signal is difficult to be produced. On the other hand, if the annihilation interaction of DM is strong

so that the thermal produced relic abundance is much smaller than the observed value, asymmetric production can be turned on to solve this problem. Therefore, in this work, we use the observed relic abundance of DM as a lower bound for the thermal relic abundance, which gives lower bounds on the interaction between DM and SM particles. If there is a relationship between g_q and g_l, where g_q and g_l are the couplings of the mediator to quarks and leptons respectively, there are stringent constraints from the Linear Electron-Positron Collider (LEP) [74] and Tevatron [75]. Therefore, the constraint from relic abundance cannot be alleviated by increasing the thermal annihilation of channel of DM to leptons.

Since the Yukawa sector of SM violates flavor symmetry, the mediator of the interaction between SM and DM particles may induce additional sources of flavor changing neutral current (FCNC) if it does not commute with the rotations of quarks from flavor eigenstates to mass eigenstates, and in this case, the mass differences of neutral meson systems, $K^0 - \bar{K}^0$, $D^0 - \bar{D}^0$, $B_d - \bar{B}_d$, and $B_s - \bar{B}_s$ can be used to constrain the parameter space of this interaction.

In most models, if DM is a WIMP, the spin of DM is 0 or 1/2, for example in supersymmetric models both sneutrino and neutrolino can be DM candidate. In extra-dimension models, the spin of DM can also be 1 [76]. Furthermore, DM can also be composite particles like nuclei or atoms [77], and in these cases, the spin structure of DM can be rather complicated. If the mediator between DM and SM particles is a vector particle, the interaction between DM with non-vanishing spin can interact with SM particles through multi-pole interactions. In this work, to get the main features of the interaction between DM and SM particles, we consider spin

114

0 complex scalar DM candidate and spin-1/2 Dirac spinor DM candidates which are labeled as ϕ and χ, respectively.

The annihilation of dark matter can be either through either S-channel or through T-channel. In the case of S-channel annihilation, the mediator is neutral under the symmetry transformation which keeps DM stable. And the direct detection signal in this case must be through T-channel. Furthermore, the thermal relic abundance determines that the mass of the mediator should not be around weak scale. In the case of T-channel annihilation, the interaction between DM and quarks must be conducted by new colored particles which shares the same quantum number as DM under the transformation of the symmetry keeps DM stable. In this chapter, we concentrate on the S-channel annihilation cases.

In SM, there are two natural candidates for the mediator, which are Z-boson and the Higgs boson. Since we are interested in low mass dark matter with mass around or smaller than 15 GeV. Therefore, the Z-width constraint force the coupling between DM and Z to be no larger than 0.02. For the mass of DM as low as being smaller than 15 GeV, thermal annihilation would leave too much dark matter and the universe would be over closed.

In the case of Higgs boson mediator, if DM is a fermion, for the reason that a low mass dark matter particle cannot annihilate into top quarks during thermal annihilation era, the annihilation rate between dark matter and anti-dark matter particles to SM particles is suppressed by the small Yukawa couplings between Higgs boson and light SM fermions. Therefore, the correct dark relic abundance cannot be generated in the perturbative region. However, if DM is a scalar, the coupling

115

between DM and Higgs is dimension one, therefore, during the thermal annihilation, the coupling can be seen as enhanced by a factor of M_h/M_D relative to the fermion DM case, where M_h is the Higgs mass, so that it is possible to reconcile light DM with relic abundance [78].

In this chapter, we concentrate on the new vector mediator case which we will call Z' throughout this chapter. The interaction between Z' and DM particles are listed in Table 4.1. This Z' particle also contributes to the $p\bar{p} \rightarrow jj$ at Tevatron which is studied both in CDF detector [79] and in D0 detector [80].

ϕ	$Z'_\mu(\phi^\dagger i\partial^\mu\phi - i\partial^\mu\phi^\dagger\phi)$
χ	$Z'_\mu\bar{\chi}\gamma^\mu\chi,\ Z'_\mu\bar{\chi}\gamma^\mu\gamma_5\chi,\ Z'_{\mu\nu}\bar{\chi}\sigma^{\mu\nu}\chi,\ Z'_{\mu\nu}\bar{\chi}i\gamma_5\sigma^{\mu\nu}\chi$

Table 4.1: Interaction between DM and mediator.

4.2   From Resonant to Contact Interaction

The propagator of the S-channel mediator can be written as

$$\frac{i}{s - M^2 - i\sqrt{s}\Gamma(s)} \ , \tag{4.3}$$

where s is the center-of-mass energy of the two incoming particles and $\Gamma(s)$ is the width of the mediator if its mass is $\sqrt{s}$. Therefore, we can get

$$\sigma \propto \frac{g_{SM}^2 g_D^2}{(s - M^2)^2 + s\Gamma^2(s)} \ , \tag{4.4}$$

where g_{SM} is the coupling between the mediator and the SM particles whereas g_D is the coupling between the mediator and DM.

Assuming $g_{SM} = g_D = g$, in the case that both SM quarks and DM are much lighter than the mediator, the cross section can be written as

$$\sigma \propto \frac{g^4}{(s - M^2)^2 + \left(\frac{ag^2}{8\pi}\right)^2 s^2} \ , \tag{4.5}$$

where a is proportional to the number of light degrees of freedom. In direct detection experiments, since the momentum transfer is small, it can only see a contact interaction and the cross section is determined by $M_0 = M/g$. Substitute this relation to Eq. (4.5) we can get that

$$\sigma \propto \frac{1}{\left(\frac{s}{g^2} - M_0^2\right)^2 + \left(\frac{a}{8\pi}\right)^2 s^2} \ . \tag{4.6}$$

Therefore, in the case that $s/g_0^2 \ll M_0^2$ and $(a/(8\pi))^2 s^2 \ll M_0^4$, the contact interaction treatment is a good approximation.

On the other hand, if the mediator can be produced on shell, the enhancement of the cross section is quite large. In Fig. 4.1, it is demonstrated that
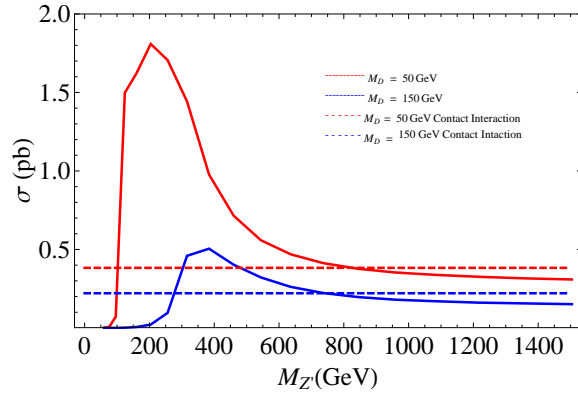
Figure 4.1: Transition from resonant case to contact interaction.

4.3 Tevatron Constraints on Z' Mediator

In this section, we study the constraint from the process in Eq. (4.1) on the couplings and masses of the mediator in different cases. The couplings between mediators and quarks are assumed to be universal. If they were not, there would be large tree-level flavor changing neutral currents induced by quark mixings which is discussed in Sec V.

4.3.1 Constraint from monojet plus missing energy

4.3.1.1 Vector-like Interaction

The interacting Lagrangian of vector-like interaction can be written as

$$\mathcal{L}_{\text{vector}} = Z'_\mu \left[\bar{q} \left(g_{Z'}^{(1)} \gamma_\mu + g_{Z'5}^{(1)} \gamma_\mu \gamma_5 \right) q + \bar{\chi} \left(g_D^{(1)} \gamma_\mu + g_{D5}^{(1)} \gamma_\mu \gamma_5 \right) \chi \right] . \qquad (4.7)$$

Since we are concentrating on low mass dark matter case, the produced dark matter particles in Tevatron are relativistic, therefore, the total cross section depends very weakly on whether the mediator couples to vector currents or axial vector currents. As a consequence, we concentrate on vector coupling cases.

Using CalcHEP2.5.7 [81] we simulate the $p\bar{p} \to \chi\bar{\chi} +$ one jet process, assuming Z' couples only to DM and quarks. The constraints on $g_{Z'}$ and $M_{Z'}/\sqrt{g_{Z'}g_D}$ for $M_{Z'} > 20$ GeV are shown in Fig. 4.2, where the mass of dark matter is fixed to 5 GeV. We can see that the bound on $M_{Z'}/\sqrt{g_{Z'}g_D}$ gets lower for smaller dark matter masses. The reason is that, in this region, Z' is on shell, and the process $p\bar{p} \to \chi\bar{\chi} +$ one jet can be divided into two processes, namely, $p\bar{p} \to Z'$ j and

$Z' \to \chi\bar{\chi}$. Furthermore, in small $M_{Z'}$ region, the cross section of $p\bar{p} \to Z'$ j changes very little with $M_{Z'}$, and the branching ratio of Z' decaying to $\chi\bar{\chi}$ also does not change much with $M_{Z'}$ since $M_{Z'}^2$ remains much larger than m_b^2, where m_b is the mass of bottom quark. Therefore, with fixed $g_{Z'}$ and g_D, the total cross section almost does not change with $M_{Z'}$. Therefore, as we can see from (a) of Fig. 4.2, with the fixed total cross section which is the Tevatron bound, the lower bound on $M_{Z'}/\sqrt{g_{Z'}g_D}$ gets smaller with smaller $M_{Z'}$.

In Fig. 4.2, the red, orange, yellow, green, and blue curves correspond to $g_D = 0.5, 1, 2, 3,$ and 5, respectively. We can see that in the small mass region, the upper bound on $g_{Z'}$ does not depend on g_D. The reason is that the total cross section depends only on the cross section of $p\bar{p} \to Z'$ j and the branching ratio of $Z' \to \chi\bar{\chi}$, and in small $M_{Z'}$ region, the upper bound on $g_{Z'}$ is much smaller than g_D so that the branching ratio of $Z' \to \chi\bar{\chi} \approx 1$. Therefore, the upper bound of $g_{Z'}$ does not change with g_D. As a result, in small $M_{Z'}$ region, the dependence of $M_{Z'}/\sqrt{g_{Z'}g_D}$ on g_D can be factorized out. Furthermore, this factorization property is applicable to more general cases.

From Fig. 4.2a, one can see that the coupling gets much larger when $M_{Z'}$ approaches certain value for each g_D. Furthermore, since Z' couples universally to SM quarks, the width of Z' is enhanced by a factor of 18. Neglecting the effect of top quark mass, the width of $M_{Z'}$ can be written as

$$\Gamma_{Z'}(M_{Z'}) \approx \frac{3}{2\pi}g_{Z'}^2 M_{Z'} + \frac{1}{12\pi}g_D^2 M_{Z'} \ . \tag{4.8}$$

Therefore, we can see that the loop factor is canceled by the degrees of freedom

(a)   (b)
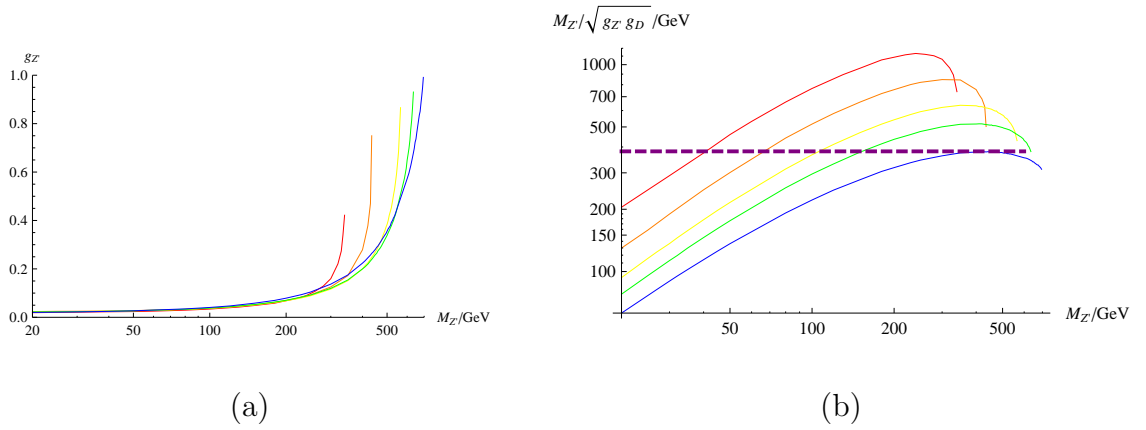
Figure 4.2: The red, orange, yellow, green, and blue curves show the upper bounds on the combination $g_{Z'}$ in (a) and lower bound on $M_{Z'}/\sqrt{g_{Z'}g_D}$ in (b) for cases in which g_D is fixed to 0.5, 1, 2, 3 and 5, respectively. In (b), the horizontal dashed purple line shows the upper bound in the case of contact operator.
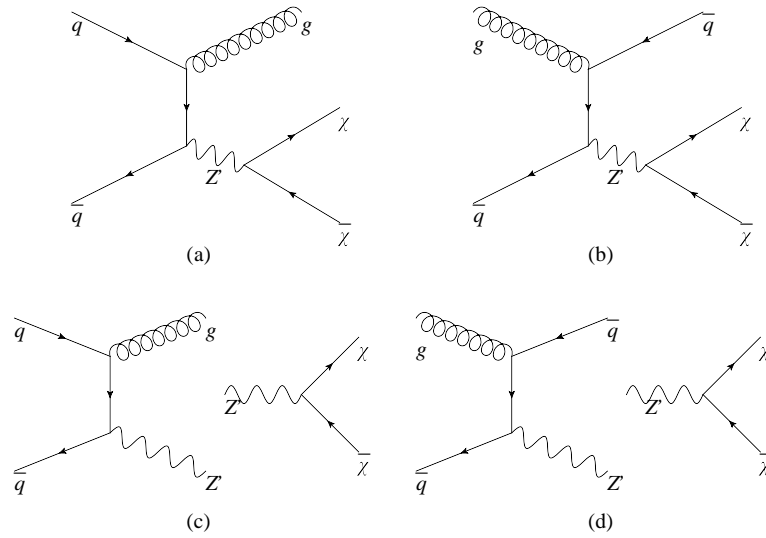
Figure 4.3: Typical hard processes for $p\bar{p} \to \chi\bar{\chi} + $ jet, where diagrams (c) and (d) show divided processes for (a) and (b), respectively.

120

of quarks. Therefore, for large $g_{Z'}$ the effect of width is important, and the total cross section gets smaller for larger $g_{Z'}$. Fig. 4.4 shows the total cross section of the hard process of $p\bar{p} \rightarrow \chi\bar{\chi} + \mathrm{j}$ where the mediator masses is chosen to be 430 (green), 450 (purple), 480 (red) and 500 (blue) GeV in the case of $g_D = 1$. The solid black horizontal line is the Tevatron bound. We can see that in the case that $g_D = 1$ if $M_{Z'} \geq 480$ GeV, the Tevatron bound cannot be achieved. Therefore, for each g_D a parameter M_* can be defined beyond which the collider constraint cannot be saturated in perturbative region. One can get M_* from Fig. 4.2a by looking at the sharp rising of each curve, and one can get $M_* \approx 340, 430, 560, 630, 690$ GeV for $g_D = 0.5, 1, 2, 3, 5$, respectively.
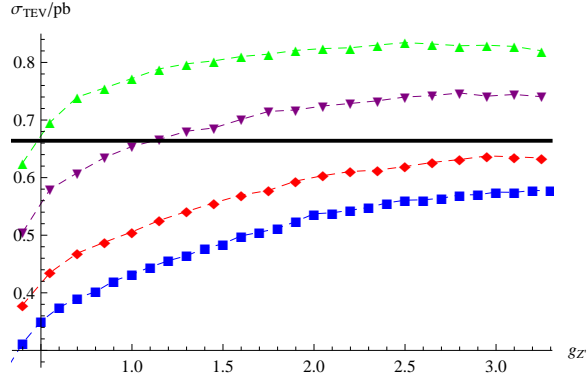
Figure 4.4: Cross section of hard process of $p\bar{p} \rightarrow \chi\bar{\chi} + \mathrm{j}$ with the cut that the transverse energy of the jet should be larger 80 GeV and $g_{Z'}$ fixed to 1. The green upward triangle, purple downward triangle, red diamond triangle, and blue square triangle are for 430, 450, 480, 500 GeV $M_{Z'}$, respectively. The solid black horizontal line is the Tevatron bound for this process.

Fig. 4.5 shows the comparison between 5 GeV and 15 GeV DM. From the

plots, we can see that at $M_{Z'} > 30$ GeV, the two curves coincide with each other, which means the bound does not depend on the mass of DM. And in the case of $M_{Z'} < 2M_\chi$, the constraint on $g_{Z'}$ gets much looser due to that the phase space of three-body final state is much smaller than the two-body one. Furthermore, in this region, a plateau appears indicating that the bound on $g_{Z'}$ does not depend on the mass of the mediator. The reason is that the denominator of the Z' propagator is completely off-shell and the width of Z' can be neglected. Therefore, on the plateau, the cross section of the process in Eq. (4.1) depends solely on the product $g_{Z'}g_D$, and the upper bound of $g_{Z'}$ goes like $1/g_D$. From Fig. 4.5a, we can see that the height of the plateau depends slightly on the mass of dark matter. The dependance of the upper bound of $g_{SM}g_D$ on the mass of DM in this case is shown as the red curve in Fig. 4.6a.

(a)   (b)
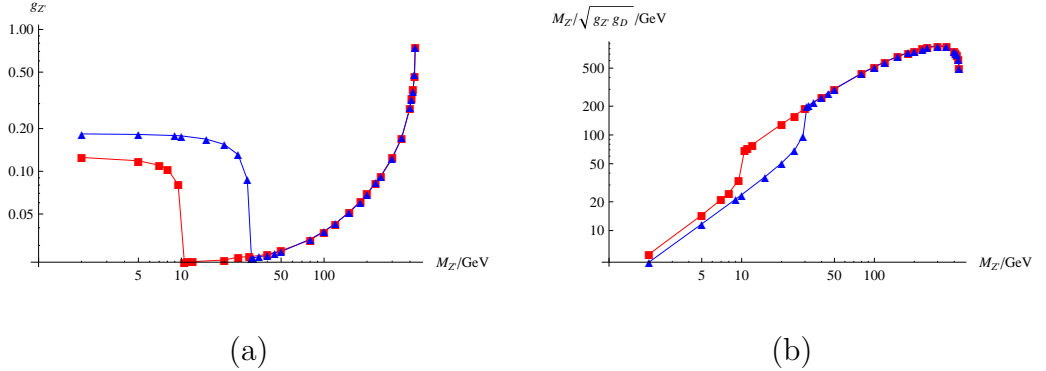
Figure 4.5: Comparison between upper bounds on $g_{Z'}$ (a) and lower bounds on $M_{Z'}/\sqrt{g_{Z'}g_D}$ (b) in the cases of 5 GeV (red square) and 15 GeV (blue triangle) DM mass. In both cases, $g_D = 1$.

If the coupling contains both the vector part and the axial-vector part, the constraint shown in Fig. 4.2 can be seen as on the combination $M_{Z'}/[(g_{Z'}^2 + g_{Z'5}^2)(g_D^2 +$
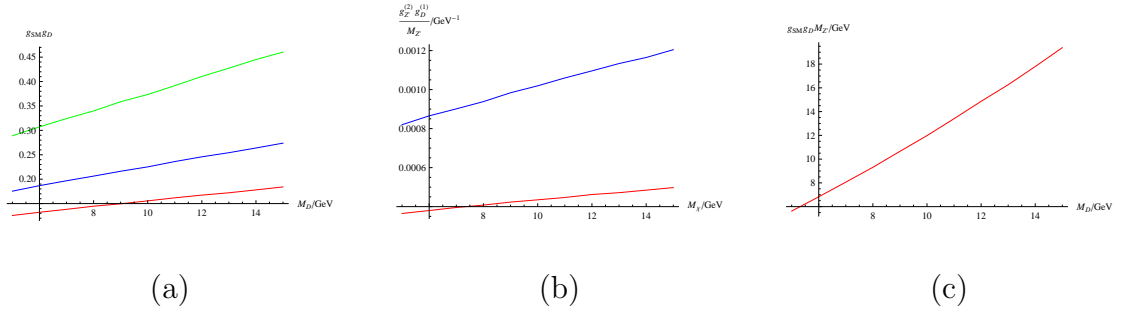
Figure 4.6: (a) shows upper bounds on $g_{SM}g_D$ from Tevatron in the case that $M_{\text{mediator}} \ll M_{DM}$, where the red curve is for vector coupling with fermion dark matter, the green one vector coupling with scalar dark matter, the blue one scalar mediator with fermion dark matter. In the first two cases the coupling between Z' to fermions are assumed to be vector-like. (b) shows upper bounds on $g_{Z'}^{(2)}g_D^{(1)}/M_{Z'}$, where the coupling between Z' and quarks is assumed to be dipole and the coupling between Z' and DM is vector-like. The red curve is for fermion dark matter whereas the blue one is for scalar dark matter. (c) shows upper bound of $g_{H'}g_D M_{H'}$ in the case of scalar mediator and scalar DM.

$g_{D5}^2)]^{1/4}$, instead of $M_{Z'}/\sqrt{g_{Z'}g_D}$.

In the case that dark matter particle is a scalar, the interacting Lagrangian can be written as

$$\mathcal{L}_{\text{vector}} = Z'_\mu \left[\bar{q} \left(g^{(1)}_{Z'} \gamma_\mu + g^{(1)}_{Z'5} \gamma_\mu \gamma_5 \right) q + g^{(1)}_D \left(\phi^\dagger i \partial^\mu \phi - i \partial^\mu \phi^\dagger \phi \right) \right] . \qquad (4.9)$$

The analysis is parallel to the fermion dark matter case and the constraints for 5 GeV dark matter is shown in Fig. 4.7. If parity violating interaction is invoked, the bounds should be seen as to $M_{Z'}/\sqrt{(g_{Z'}^2 + g_{Z'5}^2)^{1/2} g_D}$ instead of to $M_{Z'}/\sqrt{g_{Z'}g_D}$. From Fig. 4.7a, one can see that in this case M_* is around 340 GeV. In the case that $M_{Z'} < 2M_\phi$, the upper bound on $g_{Z'}g_D$ is similar as in Fig. 4.5a, and the height of the plateau is shown in Fig. 4.6a.

(a)   (b)
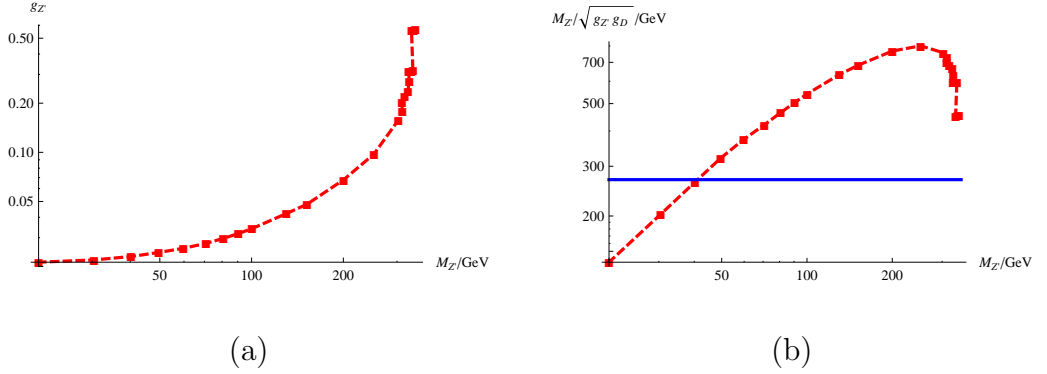
Figure 4.7: Lower bound on the combination $M_{Z'}/\sqrt{g_{Z'}g_D}$ (a) and upper bound on $g_{Z'}$ (b). The horizontal blue line is the upper bound in the case of contact operator. $M_\chi = 5$ GeV, $g_D = 1$. The horizontal blue line in (a) shows the corresponding bound in the case of contact operator.

In the case that Z' couples to the axial currents of SM fermions, an issue of anomaly occurs if the quantum numbers are assigned improperly. However, the

existence of anomaly only mean that the theory needs a cut-off at some energy scale. And for an anomalous U(1) gauge theory, the upper bound on the cut-off scale can be written as [94]

$$\Lambda < \frac{64\pi^3}{|g_{Z'}Q|^3} M_{Z'} \ , \tag{4.10}$$

where Q is the charge of chiral fermions. Therefore, we can see that even for GeV scale Z', the cut-off is far from the reach of Tevatron. Even if Z' couples only to vector currents of SM quarks, the chiral nature of electroweak interaction may induce the $SU(2)_L \& SU(2)_L \& U(1)_{Z'}$ anomaly, which means a cut-off is needed at the energy scale $4\pi M_{\text{weak}}/g_2^2$ where g_2 is the coupling of the weak interaction, therefore, we can see that in this case, the upper bound of the cut-off cannot be reached by Tevatron as well.

4.3.1.2 Dipole coupling between Z' and dark matter particle

The dipole interaction has recently be proposed to make CoGeNT and DAMA reconcile with other experiments [82, 83, 84, 85, 86]. In the case that dipole interaction dominates the interaction between DM particle and Z', the Lagrangian can be written as

$$\mathcal{L}_{\text{dipole}} = \frac{1}{M_{Z'}} \bar{\chi} \left(g_D^{(2)} \sigma^{\mu\nu} + g_{D5}^{(2)} i\gamma_5 \sigma^{\mu\nu} \right) \chi Z'_{\mu\nu} \ , \tag{4.11}$$

Generically, there are two ways the dipole operator can be induced. One is through strong dynamics in analogy to the anomalous magnetic moments of nucleons. The other is through perturbative interaction like the anomalous magnetic dipole of electron, which is induced by the diagrams shown in Fig. 4.8, and the dipole moment

125

can be estimated as

$$\frac{g_D^{(2)}}{M_{Z'}} \sim \frac{M_{\chi'}}{16\pi^2(M_{\chi'}^2 + M_{W'}^2)} \ . \tag{4.12}$$

where χ' and W' are some internal particles, which are shown in Fig. 4.8.
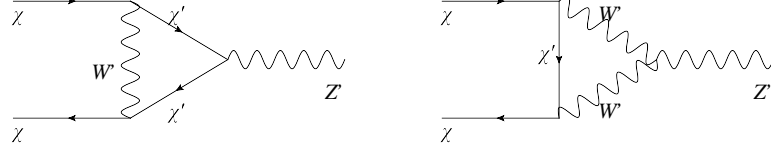
Figure 4.8: Triangle contribution to dipole moment.
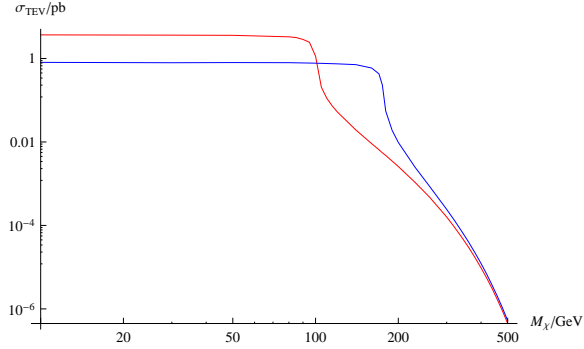
Figure 4.9: Total cross section of the hard process of $p\bar{p} \to \chi\bar{\chi} +$ jet in Tevatron requiring the transverse momentum of the jet larger than 80 GeV. The red and blue curves are for $M_{Z'} = 200$ GeV and 350 GeV, respectively. In both cases, $g_{Z'} = g_D = 1$.

In the perturbative scenario, in the case that $M_{Z'} < M_*$, Z' can be produced on shell. If $M_{Z'} > 2M_{\chi'}$ or $M_{Z'} > 2M_{W'}$, the process $p\bar{p} \to \chi'\bar{\chi}'+$jet or $p\bar{p} \to W'W'+$jet dominate over the process $p\bar{p} \to \chi\bar{\chi} +$ jet, and if the life-time of W' and χ' is long enough, they can fly out of the detector, and in this case, Tevatron constraints on single jet plus missing energy is similar to the vector-like coupling case. In order

126

for the dipole operator not to be destroyed by the decay of Z', $M_{Z'} < 2M_{\chi'}$ and

$M_{Z'} < 2M_{W'}$ should be imposed, and in this case, the partial decay width of Z' to

$\chi\bar{\chi}$ can be estimated as

$$\Gamma^{(2)}(Z' \to \chi\bar{\chi}) \approx \frac{M_{Z'}^3}{6\pi}\left(\frac{g_{Z'}^{(2)}}{M_{Z'}}\right)^2 = \frac{g_{Z'}^{(2)^2} M_{Z'}}{6\pi} \ . \tag{4.13}$$

The Tevatron bound on $g_{Z'}^{(1)}$ and the combination $M_{Z'}/(g_{Z'}^{(1)}g_D^{(2)})^{1/3}$ are shown in

Fig. 4.10. One can see in this case M_* is around 430 GeV. The factorization of the

dependance on g_D as discussed before for $M_{Z'} < 2M_\chi$ and $2M_\chi < M_{Z'} \ll M_*$ is still

applicable here. However, one should note that in this dipole coupling case, in this

case, it is the constraint on $g_{Z'}^{(1)}g_D^{(2)}/M_{Z'}$ does not depend on $M_{Z'}$. In this case, from

the simulation, it does not depend on M_χ as well, and the bound can be written as

$$\left.\frac{g_{Z'}^{(1)}g_D^{(2)}}{M_{Z'}}\right|_{M_{Z'}<2M_\chi} < 1.2 \times 10^{-3} \text{ GeV}^{-1} \ . \tag{4.14}$$

(a)   (b)
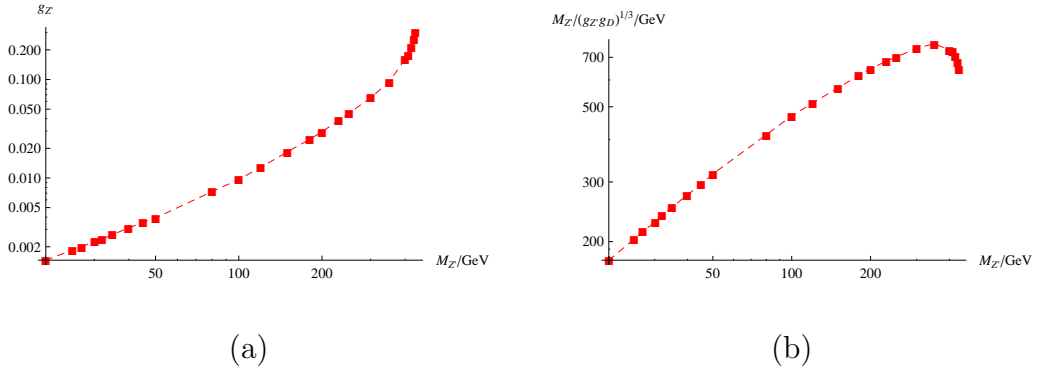
Figure 4.10: Lower bound on the combination $M_{Z'}/(g_D^{(2)}g_Z^{(1)})^{1/3}$ (a) and upper bound

on $g_{Z'}^{(1)}$ (b) for magnetic interaction between Z' and dark matter particle. $M_\chi = 5$

GeV, $g_D^{(2)} = 1$.

In the case of strong dynamics, just like in QCD, the intrinsic scale of the

strong interaction determines both the mass of the dark matter and its magnetic

moments. There, for low mass dark matter, Tevatron is energetic enough to break the composite dark matter particle and see the internal structure. Therefore, the hard process, in this case can be written as $q\bar{q} \to c_\chi \bar{c}_\chi + \text{jet}$, where c_χ is the constitute of the dark matter. In this case, the Tevatron bound is just like what is shown in Fig. 4.2.

4.3.2 Constraints from dijet final states

4.3.2.1 Fermion dark matter

The interacting Lagrangian is

$$\mathcal{L} = \bar{q}(g_{H'} + ig_{H'5}\gamma_5)qH' + \bar{\chi}(g_D + ig_{D5})\chi H' \; . \tag{4.15}$$

The constraints on $M_{H'}/(\sqrt{g_{H'}g_D})$ and $g_{H'}$ for 5 GeV dark matter and 15 GeV dark matter are shown in Fig. 4.11.

4.3.2.2 Scalar dark matter

The interacting Lagrangian is

$$\mathcal{L} = \bar{q}(g_{H'} + ig_{H'5}\gamma_5)qH' + g_D M_{H'}\phi^\dagger\phi H' \; . \tag{4.16}$$

In this case the low energy experiments and dark matter relic abundance depend only on the combination $M_{H'}/(\lambda_{Z'}\lambda_D)$ which is shown in Fig. 4.12, where we can see that in this case M_* is around 350 GeV.
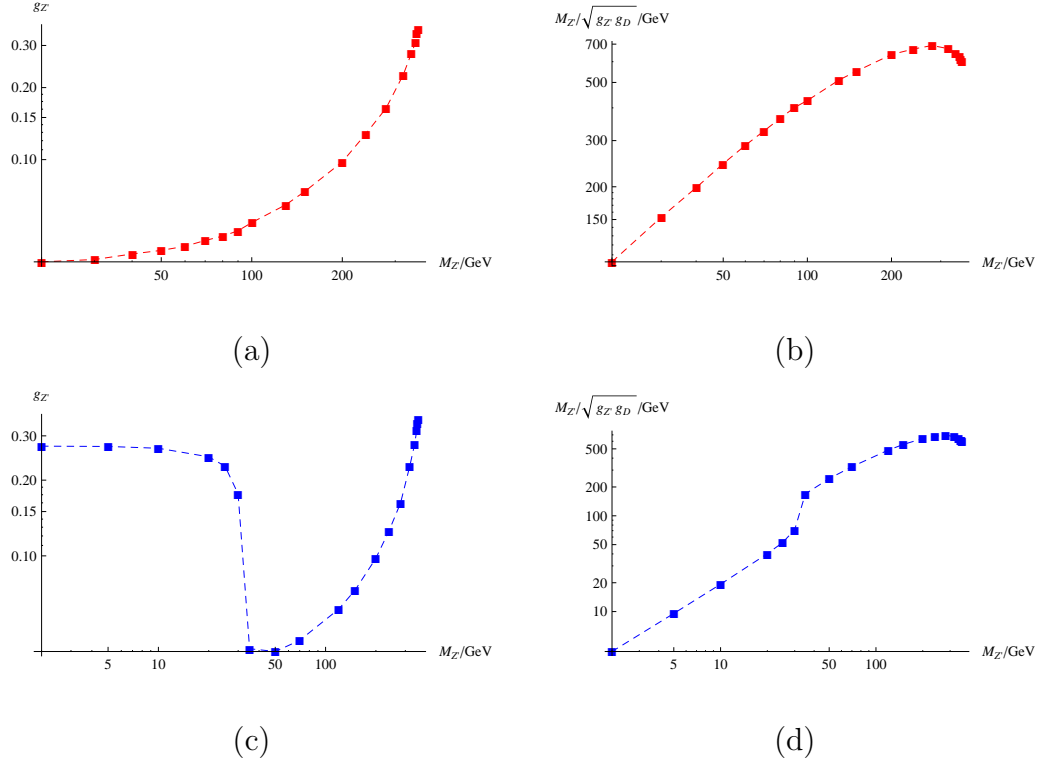
Figure 4.11: Upper bounds on the combination $g_{H'}$ (a), (c) and lower bounds on $M_{H'}/(g_{H'}g_D)$ (b), (d) in the case of scalar mediator and fermion DM. $M_\chi = 5$ GeV (a), (b) and 15 GeV (c), (d), respectively.
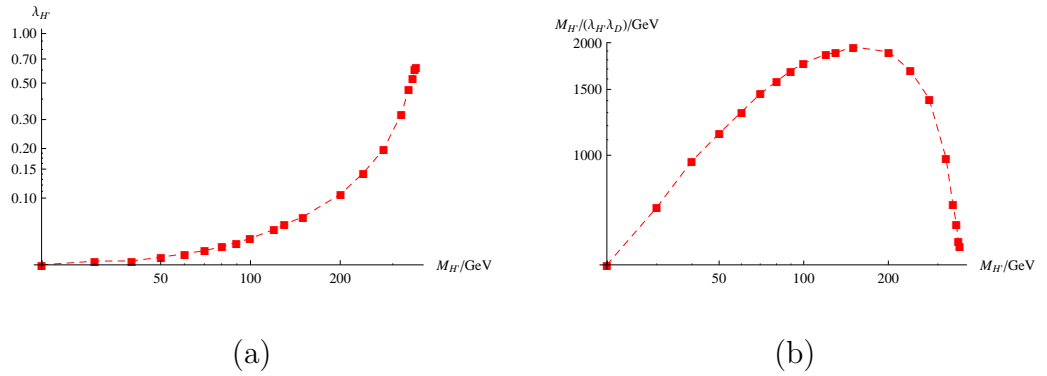
Figure 4.12: Upper bound on $\lambda_{H'}$ (a) and lower bound on the combination $M_{H'}/(\lambda_{Z'}\lambda_D)$ (b) in the case of scalar mediator and scalar dark matter particle. $M_\phi = 5$ GeV, $\lambda_D = 1$.

129

4.4 Detector Constraints on Dark Matter Direct Detection Signal

4.4.1 Effective Operator for Dark Matter Direct Detection Experiments

At the energy scale of direct detection, we should consider the interaction between mediator and the nucleons. Then a subtlety comes out that even if the Z' couples to u quark or d-quark through a vector-like coupling, that this vector-like might be canceled inside the nucleon, so that the leading order coupling becomes a dipole. This happens in models where the interaction between Z' and SM particles is induced by a kinetic mixing between Z' and photon. However, the target is composed by both protons and neutrons, and there is no way for the vector-like couplings to be canceled in proton and neutron at the same time. Therefore, if the vector-like coupling between Z' to u and d quarks is present, the vector-like interaction between Z' and the target nuclei dominates over the dipole interaction. However, if Z' couples only to heavy quarks, after integrating out the heavy quarks, a dipole interaction is induced [87] and the matching is calculated in Ref. [89]. The relevant hadronic matrix elements have been carefully discussed in detail in Ref. [90].

The non-relativistic (NR) effective operators for each couplings can be found in Ref. [90]. However, the magnetic interaction is different in our case. After integrating out Z', the four-fermion interaction should be written as $\partial_\mu(\bar{N}\sigma^{\mu\nu}N)\partial_\rho(\bar{\chi}\sigma^\rho_\nu\chi)$ and $\partial_\mu(\bar{N}i\gamma_5\sigma^{\mu\nu}N)\partial_\rho(\bar{\chi}\sigma^\rho_\nu\chi)$ for CP-even and CP-odd cases, respectively. There-fore, the leading order CP-even NR operator should be written as $(\vec{q}\times\vec{s}_N)\cdot(\vec{q}\times\vec{s}_\chi)$,

where $\vec{q}$ is the three-momentum transferred during the collision.

In direct detection experiment, the interactions between dark matter particle and the target nuclei is non-relativistic, and the velocity of dark matter is about 10^{-3}. Therefore, if the interaction is proportional to the momentum of dark matter particle, there is a suppression factor of 10^{-6} appearing in the cross section between nuclei and dark matter. Furthermore, the interaction should be separated into spin-dependent and spin-independent, since the energy transferred from dark matter to nuclei is smaller than the energy scale of nuclear structure, the dark matter particle interacts with nucleus as a whole, therefore the cross section of spin dependent interaction suffers from a factor of $1/A^2$ suppression relative to spin independent interaction, which is about a factor of 10^{-4}. Therefore, according to this power counting, we classify the operators as the following,

4.4.2 Tevatron Bounds on Direct Detection between Dark Matter and Nucleon ($M_{\text{mediator}} > 2M_{\text{dark matter}}$)

4.4.2.1 Z' mediator with fermion dark matter

The hadronic matrix elements are discussed in detail in Refs. [90, 91]. The CP-odd interaction $Z'_{\mu\nu}\bar{q}i\gamma_5\sigma^{\mu\nu}q$ can be seen as a Z' electric dipole moment (EDM), and the hadronic matrix elements can be calculated in the same way as calculating the quark EDM contribution to neutron EDM, which has been calculated in several ways. In this chapter, we use the result from QCD rum rules [14] that

$$d_{\text{neutron}}^E = (1 \pm 0.5) \times 0.7(-0.25 d_u^E + d_d^E) , \qquad (4.17)$$

	Operator	Structure	NR Cross Section
O_1	$\bar{N}\gamma^\mu N \bar{\chi}\gamma_\mu \chi$	SI, MI	$\frac{C^2 M_N^2 M_\chi^2}{\pi(M_N+M_\chi)^2}$
O_2	$\bar{N}\gamma^\mu N \bar{\chi}\gamma_\mu \gamma_5 \chi$	SI, MD	$\frac{C^2 M_N^4 M_\chi^2 v^2}{2\pi(M_N+M_\chi)^4}$
O_3	$\bar{N}\gamma^\mu \gamma_5 N \bar{\chi}\gamma_\mu \chi$	SD, MD	$\frac{C^2 M_N^2 M_\chi^2 [(M_N+M_\chi)^2+2M_N^2]v^2}{2\pi(M_N+M_\chi)^4}$
O_4	$\bar{N}\gamma^\mu \gamma_5 N \bar{\chi}\gamma_\mu \gamma_5 \chi$	SD, MI	$\frac{3C^2 M_N^2 M_\chi^2}{\pi(M_N+M_\chi)^2}$
O_5	$\bar{N}\gamma_\nu N \partial_\mu(\bar{\chi}\sigma^{\mu\nu}\chi)$		$\propto v^4$
O_6	$\bar{N}\gamma_\nu N \partial_\mu(\bar{\chi}i\gamma_5\sigma^{\mu\nu}\chi)$	SI, MD	$\frac{2C^2 M_N^4 M_\chi^4 v^2}{\pi(M_N+M_\chi)^4}$
O_7	$\bar{N}\gamma_\nu \gamma_5 N \partial_\mu(\bar{\chi}\sigma^{\mu\nu}\chi)$	SD, MD	$\frac{4C^2 M_N^4 M_\chi^4 v^2}{\pi(M_N+M_\chi)^4}$
O_8	$\partial_\mu(\bar{N}\sigma^{\mu\nu}N)\bar{\chi}\gamma_\nu \chi$		$\propto v^4$
O_9	$\partial_\mu(\bar{N}\sigma^{\mu\nu}N)\bar{\chi}\gamma_\nu \gamma_5 \chi$	SD, MD	$\frac{4C^2 M_N^4 M_\chi^4 v^2}{\pi(M_N+M_\chi)^4}$
O_{10}	$\partial_\mu(\bar{N}i\gamma_5\sigma^{\mu\nu}N)\bar{\chi}\gamma_\nu \chi$	SD, MD	$\frac{2C^2 M_N^4 M_\chi^4 v^2}{\pi(M_N+M_\chi)^4}$

Table 4.2: Effective operator between nucleon and dark matter, where C is the Wilson coefficient for each operator and v is the speed of dark matter particle.

	Operator	Structure	NR Cross Section
O_{11}	$g_{\mu\nu}\partial_\alpha(\bar{N}\sigma^{\mu\alpha}N)\partial_\beta(\bar{\chi}\sigma^{\nu\beta}\chi)$		$\propto v^4$
O_{12}	$g_{\mu\nu}\partial_\alpha(\bar{N}\sigma^{\mu\alpha}i\gamma_5 N)\partial_\nu(\bar{\chi}\sigma^{\nu\beta}\chi)$		$\propto v^6$
O_{13}	$g_{\mu\nu}\partial_\alpha(\bar{N}\sigma^{\mu\alpha}i\gamma_5 N)\partial_\nu(\bar{\chi}\sigma^{\nu\beta}\chi)$		$\propto v^6$
O_{14}	$g_{\mu\nu}\partial_\alpha(\bar{N}i\gamma_5\sigma^{\mu\alpha}N)\partial_\nu(\bar{\chi}i\gamma_5\sigma^{\nu\beta}\chi)$		$\propto v^4$
O_{15}	$\bar{N}\gamma_\mu N(\phi^\dagger i\partial^\mu\phi - i\partial^\mu\phi^\dagger\phi)$	SI, MI	$\frac{C^2 M_N^2 M_\chi^2}{\pi(M_N+M_\chi)^2}$
O_{16}	$\bar{N}\gamma_\mu\gamma_5 N(\phi^\dagger i\partial^\mu\phi - i\partial^\mu\phi^\dagger\phi)$	SD, MD	$\frac{C^2 M_N^2 M_\phi^2 v^2}{2\pi(M_N+M_\phi)^2}$
O_{17}	$\partial_\mu(\bar{N}\sigma^{\mu\nu}N)(\phi^\dagger i\partial^\mu\phi - i\partial^\mu\phi^\dagger\phi)$		$\propto v^4$
O_{18}	$\partial_\mu(\bar{N}i\gamma_5\sigma^{\mu\nu}N)(\phi^\dagger i\partial_\nu\phi - i\partial_\nu\phi^\dagger\phi)$	SD, MD	$\frac{2C^2 M_\phi^4 M_N^4 v^2}{\pi(M_N+M_\phi)^4}$
O_{19}	$\bar{N}N\bar{\chi}\chi$	SI, MI	$\frac{C^2 M_N^2 M_\chi^2}{\pi(M_N+M_\chi)^2}$
O_{20}	$\bar{N}N\bar{\chi}i\gamma_5\chi$	SI, MD	$\frac{C^2 M_N^4 M_\chi^2 v^2}{2\pi(M_\chi+M_N)^4}$
O_{21}	$\bar{N}i\gamma_5 N\bar{\chi}\chi$	SD, MD	$\frac{C^2 M_\chi^4 M_N^2 v^2}{2\pi(M_\chi+M_N)^4}$
O_{22}	$\bar{N}i\gamma_5 N\bar{\chi}i\gamma_5\chi$	SD, MD	$\propto v^4$
O_{23}	$\bar{N}N\phi^\dagger\phi$	SI, MI	$\frac{C^2 M_N^2}{4\pi(M_N+M_\chi)^2}$
O_{24}	$\bar{N}i\gamma_5 N\phi^\dagger\phi$	SD, MD	$\frac{C^2 M_\phi^2 M_N^2 v^2}{8\pi(M_N+M_\phi)^4}$

Table 4.3: Effective operator between nucleon and dark matter, where C is the Wilson coefficient for each operator and v is the speed of dark matter particle.

where d_u^E and d_d^E are the EDM of u and d quarks, respectively.

(a)

(b)

(c)

(d)
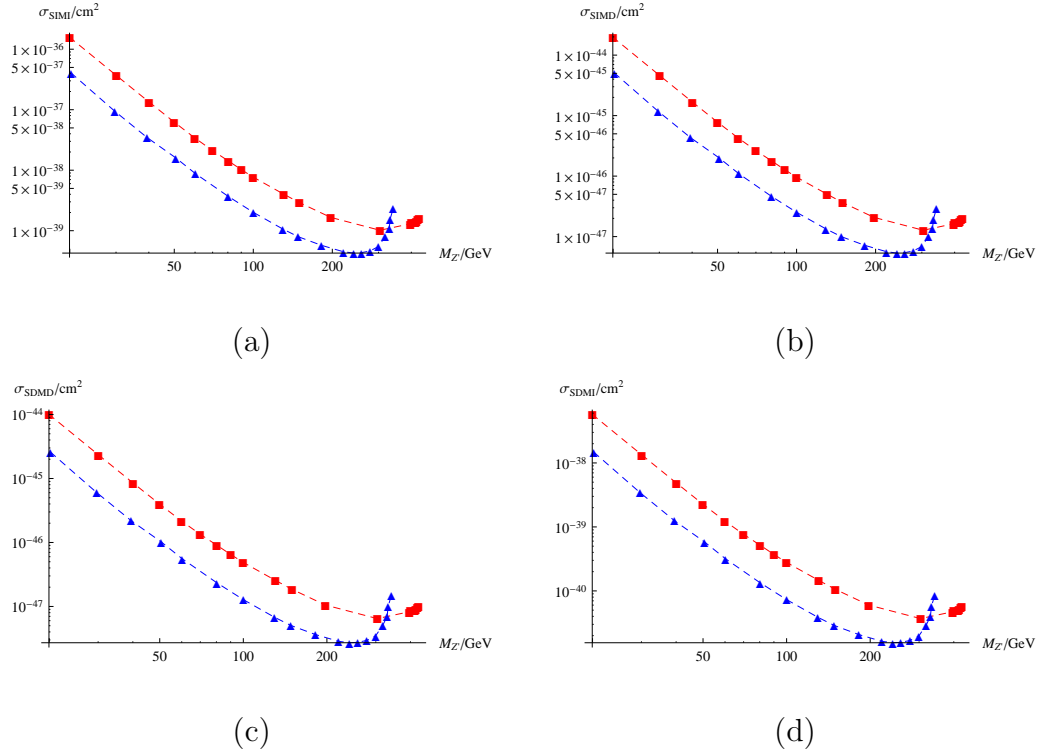
Figure 4.13: Tevatron constraints on cross sections between dark matter and nucleons for Z' mediator and fermion dark matter particle. Flavor universal coupling is assumed. The red and blue curves are cases for $g_D = 1$ and $g_D = 0.5$ cases, respectively. (a), (b), (c), and (d) are for effective operators O_1, O_2, O_3, and O_4, respectively.

If dark matter interacts with SM particles through the dipole of Z', either induced by the loop diagrams shown in Fig. 4.8 or by strong interactions, as discussed in last section, we need to classify the collider constraint into two cases.

First, if the mass of Z' is larger than twice of the intermediate particle like W' or χ' in Fig. 4.8, or larger than the intrinsic scale of the dark sector, the collider constraint is indeed on the process $p\bar{p}$ to intermediate particles or to constituents

of dark matter. Assuming Z' couples to intermediate particles or the constituents perturbatively. Then the loop contribution in Fig. 4.8 is suppressed by the loop factor, whereas in the case of strong interaction, in analogy to the anomalous magnetic dipole moments of proton and neutron, the induced dipole moment is order one and can be written as $d^{(2)} g_D / M_\chi$, where $d^{(2)}$ is an order 1 parameter which will be set to be 1. Tevatron constraints for this case is shown in Fig. 4.14.

(a)   (b)
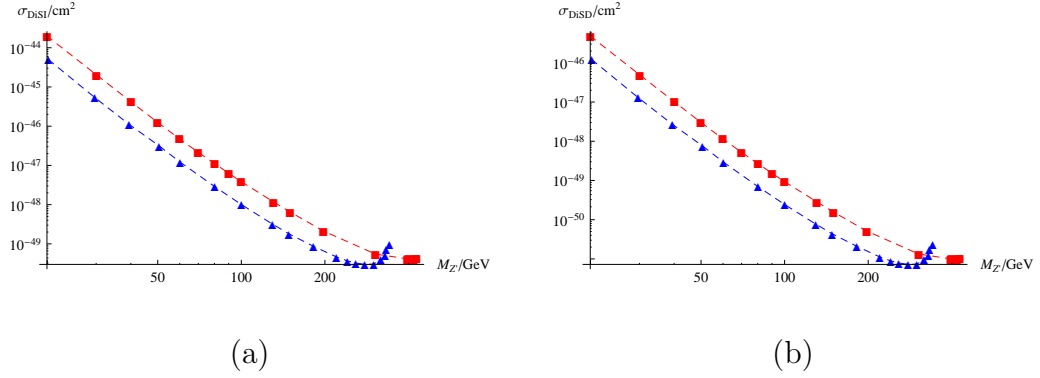
Figure 4.14: Tevatron constraints on cross section between dark matter and nucleons for Z' mediator, where the leading interaction between Z' and the dark matter particle is assumed to be dipole at the energy scale of direct detection and the decay of the Z' breaks the dipole structure. The interaction between Z' and the quarks are through vector-like and universal. (a) and (b) are for O_6 and O_7, respectively.

Second, if Z' cannot decay into any intermediate states, the bound on the combination of direct detection cross section can be calculated from Fig. 4.10, which is shown in Fig. 4.15.

If Z' couples to the quarks through a dipole interaction, the constraints on the direct detection cross section are shown in Fig. 4.16.
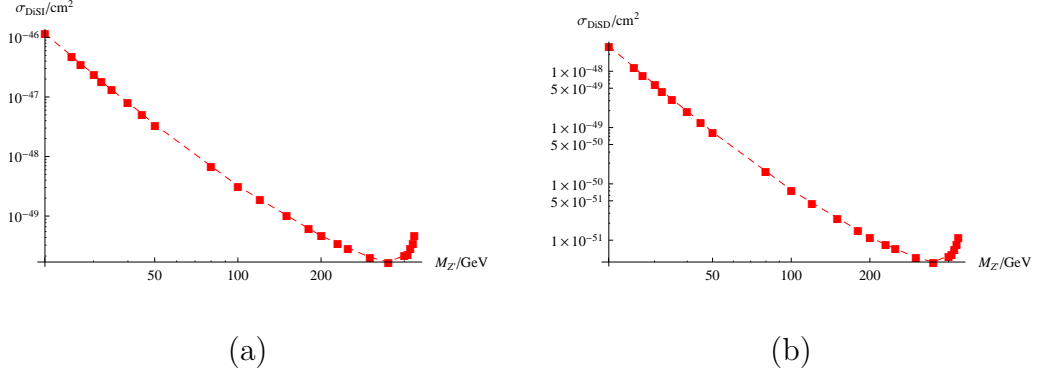
Figure 4.15: Tevatron constraints on cross section between dark matter and nucleons for Z' mediator, where the leading interaction between Z' and the dark matter particle is assumed to be dipole at the energy scale of direct detection and the decay of the Z' does not break the dipole structure. The interaction between Z' and the quarks are through vector-like and universal. (a) and (b) are for O_6 and O_7, respectively.
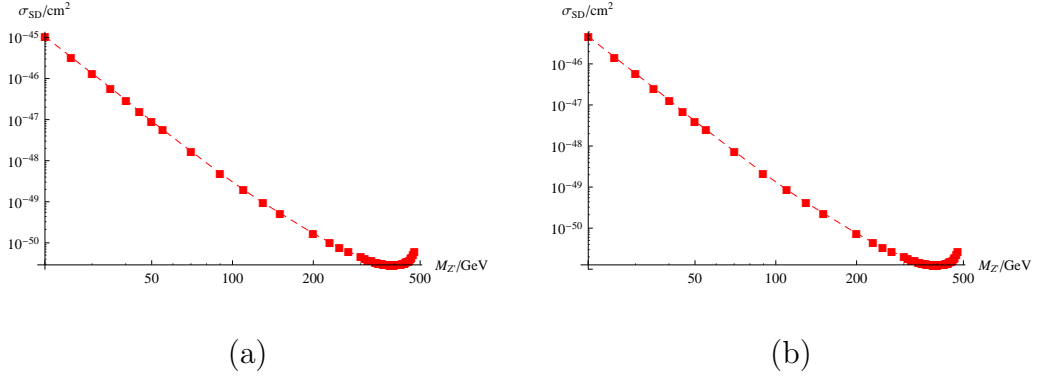
Figure 4.16: Tevatron constraints on cross section between dark matter and nucleons for Z' mediator, where the leading interaction between Z' and quarks is assumed to be dipole and universal. The interaction between Z' and the dark matter are through vector-like. (a) and (b) are for O_9 and O_{10}, respectively.

136

4.4.2.2 Z' mediator with scalar dark matter

In this case Tevatron constraint for direct detection cross section is shown in Fig. 4.17.

(a)   (b)   (c)
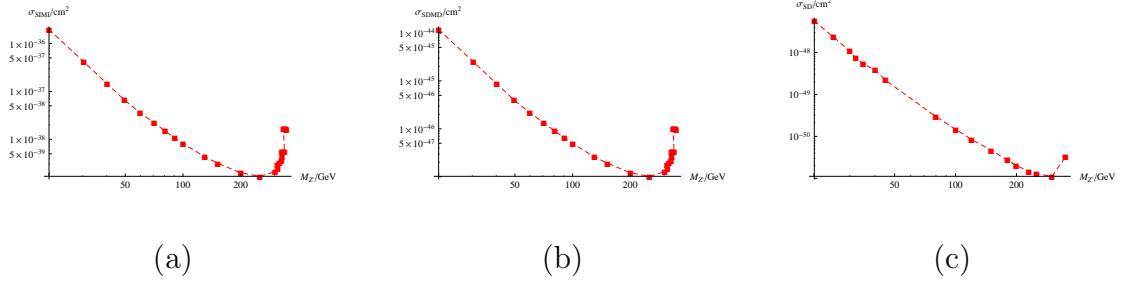
Figure 4.17: (a), (b) and (c) are for O_{15}, O_{16} and O_{18}, respectively.

4.4.2.3 H' mediator with fermion dark matter

In this case Tevatron constraint for direct detection cross section is shown in Fig. 4.18.

(a)   (b)   (c)
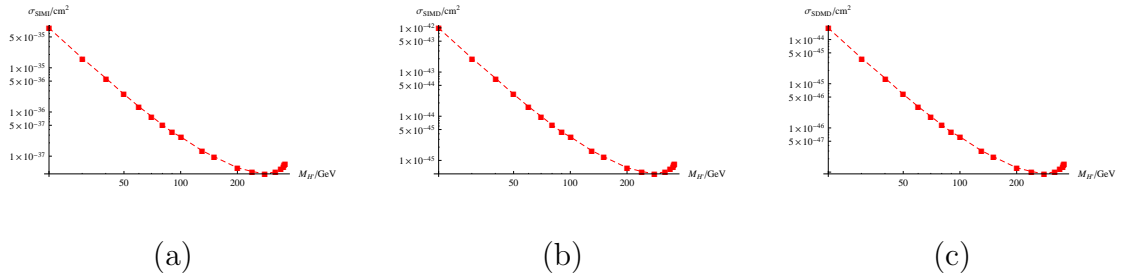
Figure 4.18: (a), (b) and (c) are for O_{19}, O_{20} and O_{21}, respectively.

4.4.2.4 H' mediator with scalar dark matter

In this case the collider constraint is shown in Fig. 4.19.
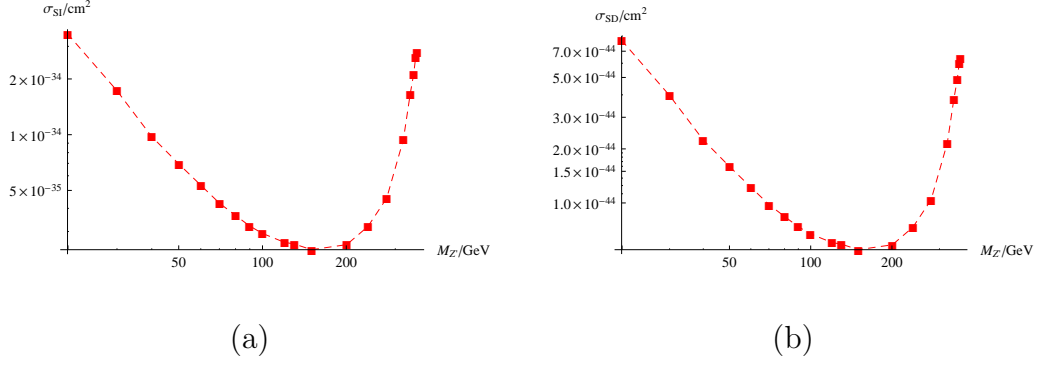
Figure 4.19: Tevatron constraints on cross section between scalar dark matter and nucleons for H' mediator. (a) and (b) are for O_{23} and O_{24}, respectively.

4.4.3 $M_{\mathrm{mediator}} < 2M_{\mathrm{DM}}$

The Tevatron bounds for direct detection cross section of 15 GeV dark matter are shown in Fig. 4.20 and Fig. 4.21 for Z' and H' mediator, respectively. We can see that at the region $M_{\mathrm{mediator}} < 2M_{\mathrm{dark\ matter}}$, due to that the phase space is smaller, the bound on direct detection cross section is about 2 orders of magnitude looser than the the case $M_{\mathrm{mediator}} > 2M_{\mathrm{dark\ matter}}$.

4.5 Constraint from Relic Abundance ($M_{\mathrm{mediator}}^2 \gg 4M_D^2$)

The relic abundance of dark matter is well determined that $\Omega h^2 = 0.11$. For the prototype models discussed in the above section, if the thermal relic abundance is smaller than the observed value, one can always introduce CP violation in the model and makes it to be asymmetric dark matter. However, if the calculated thermal relic abundance is larger than the observed value, there are no many methods to rescue. Therefore, the constraint from the the thermal relic abundance is that, the thermal relic abundance of DM generated by each prototype model should not over-close the
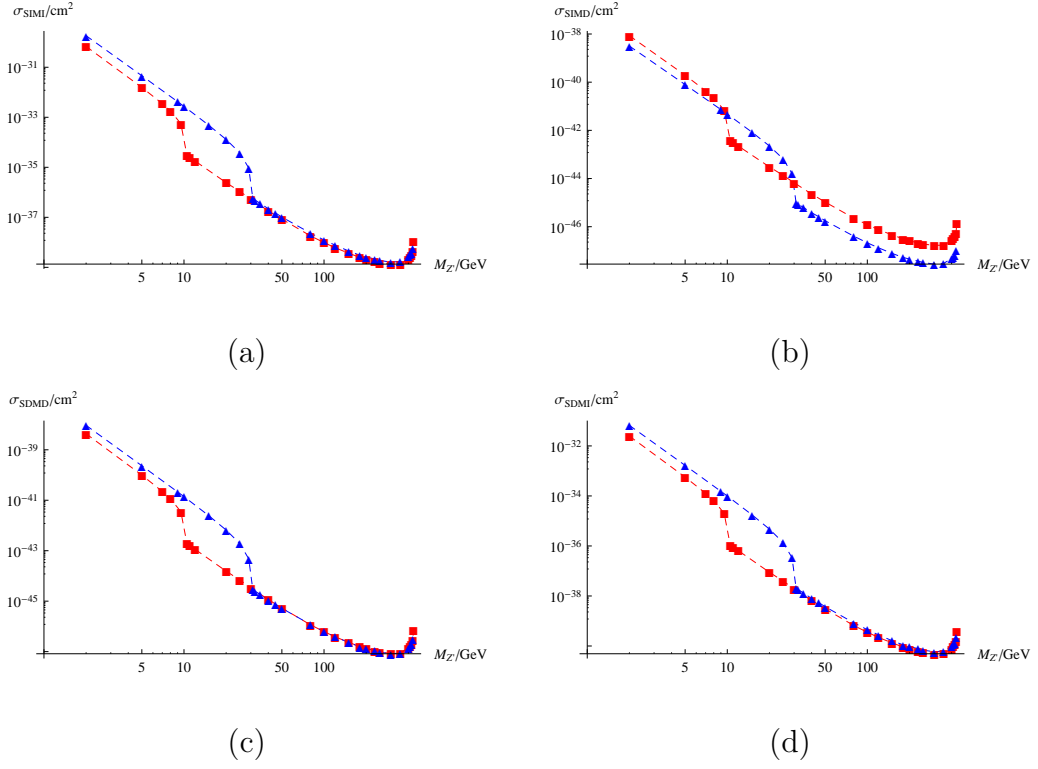
Figure 4.20: Tevatron constraints on cross section between fermion dark matter and nucleons for Z' mediator, where the leading interaction between Z' and quarks is assumed to be vector-like and universal. (a), (b), (c), (d) are for O_1, O_2, O_3, and O_4, respectively. The masses of DM are chosen to be 5 GeV (red square) and 15 GeV (blue triangle), respecttively.
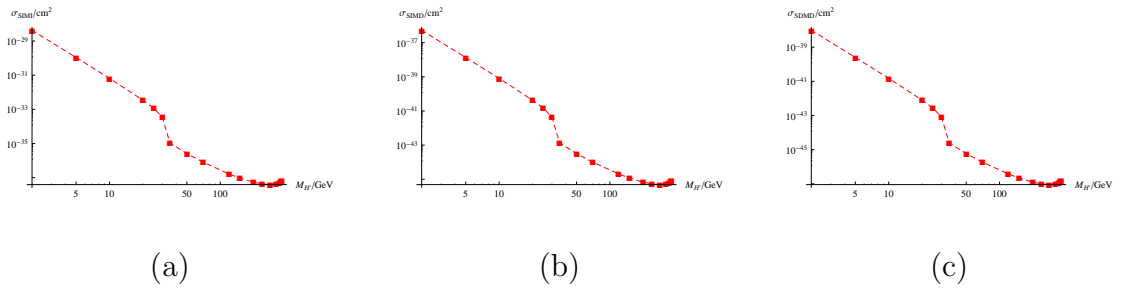
Figure 4.21: Tevatron constraints on cross section between fermion dark matter and nucleons for H' mediator. (a), (b) and (c) are for O_{19}, O_{20} and O_{21}, respectively. The mass of dark matter is 15 GeV.

universe. In this work, the relic abundance is simulated using MicrOmega2.4.O [93].

The relic abundance depends on the combination, $g_{SM} g_D / M^2_{\text{mediator}}$, and the Tevatron constraints on this combination is for different cases have been studied in Sec. III. From Fig. 4.2, we can see that the upper bound on this quantity depends on g_D, and too many parameters make the situation complicated. Therefore, we would like to study some benchmark scenario from which we can grasp the main feather of interactions between dark matter and SM particles. In this section, we focus on the $g_D = 1$ scenario. One case use the factorization properties discussed in Sec. III to get the constraint in the case of $M_{\text{mediator}} \ll M_*$.

4.5.1   Tevatron Constraint and Dark Matter Relic Abundance

In the above section, we can see that Tevatron strongly constrains on couplings between dark matter and SM particles. These interactions also determine the thermal relic abundance of dark matter. Therefore, from the Tevatron bound we can get lower bound on the dark matter relic abundance corresponding to each operator. The energy region of dark matter thermal annihilation is very different from Tevatron and direct detection experiments, and a specific effective theory needs to be introduced for each case. From Fig. 4.22 to Fig. 4.29, Tevatron constraints on the lower bound of relic abundance for each case is shown. The plots are explained in the following.

4.5.1.1   Annihilation at non-relativistic limit

In the era of dark matter thermal freezing-out, the ratio $M/T \approx 20$ [92], so the dark matter particle is non-relativistic during annihilation. Therefore, the annihilation cross section can be expanded in terms of v^2, where v is the speed of dark matter during and $v^2 \approx 0.1$. The mass of dark matter particle we are interested in is from 5 GeV to 15 GeV, in the case of universal coupling the annihilation channel of dark matter is mainly to light quarks. Therefore, the final states can be seen as massless particles.

In the case of Z' mediator, if the dark matter particle is a Dirac fermion and the interaction between dark matter and Z' is through a vector current,

$$\sigma_{\text{annihilation}} \propto \text{Tr}[(\not{p}_1 + M_D)\gamma^{\mu}(\not{p}_2 - M_D)\gamma^{\nu}]\text{Tr}[\not{k}_1\gamma_{\mu}\ \not{k}_2\gamma_{\nu}] \approx 128 M_D^4 \ , \qquad (4.18)$$

where p_1, p_2 and k_1, k_2 are the four-momentum for initial dark matter pairs and final quark pairs, respectively. However, if the interaction between dark matter and Z' is through a axial-vector current, the annihilation cross section can be written as

$$\sigma_{\text{annihilation}} \propto \text{Tr}[(\not{p}_1 + M_D)\gamma^{\mu}\gamma_5(\not{p}_2 - M_D)\gamma^{\nu}\gamma_5]\text{Tr}[\not{k}_1\gamma_{\mu}\ \not{k}_2\gamma_{\nu}] \approx 64 M_D^4 v^2(1 + \cos^2\theta) \ ,$$

$$(4.19)$$

where we can see that the cross section is suppressed by the v^2. In the case of Z' mediator and scalar dark matter the annihilation cross section can be written as

$$\sigma_{\text{annihilation}} \propto (p_1 - p_2)_{\mu}(p_1 - p_2)_{\nu}\text{Tr}[\not{k}_1\gamma^{\mu}\ \not{k}_2\gamma^{\nu}] \approx 32 M_D^4 v^2(1 - \cos^2\theta) \ . \qquad (4.20)$$

In the case of H' mediator, if the dark matter particle is a Dirac fermion and

141

the interaction between dark matter and H' is through a scalar vertex, we have

$$\sigma_{\text{annihilation}} \propto \text{Tr}[(\not{p}_1 + M_D)(\not{p}_2 - M_D)]\text{Tr}[\not{k}_1 \not{k}_2] \approx 64 M_D^4 v^2 \ , \qquad (4.21)$$

whereas if the interaction between H' and the fermion dark matter is through a pseudoscalar vertex, we can get

$$\sigma_{\text{annihilation}} \propto \text{Tr}[i\gamma_5(\not{p}_1 - M_D)i\gamma_5(\not{p}_2 + M_D)]\text{Tr}[\not{k}_1 \not{k}_2] \approx 64 M_D^2 \ . \qquad (4.22)$$

This non-relativistic suppression is clearly shown in Fig. 4.22, Fig. 4.26 and Fig. 4.28 where the Tevatron constraints on operators with v^2 suppression are much stronger than the ones without this suppression. Furthermore, we can see that inside the range of Tevatron ability, the interactions containing a v^2 suppression cannot satisfy Tevatron constraint and relic abundance constraint at the same time. Therefore, they cannot be the dominant interaction between dark matter and SM particles.

The physical reason for this suppression is that the ground state of a particle and anti-particle pair has certain parity. For spin-1/2 Direc fermions, J^{PC} of ground states can only be 0^{-+} and 1^{--}, and can be 0^{++} and 1^{+-} for first excited states ($L = 1$, where L is the orbital angular momentum). Therefore, in the case of scalar mediator, if the interaction is scalar-like, the χ-$\bar{\chi}$ cannot be in the ground state during annihilation, therefore, the annihilation amplitude must be proportional to the orbital angular momentum and the annihilation cross section must be proportional to v^2. The reason for the vector mediator case is a little bit more complicated. The suppression in the case of axial-vector like coupling is not only because of the J^{PC} structure but also due to the fact that the final states are massless so that the both

the vector current and the axial vector current of the final states are conserved at tree-level. Therefore, in the case that the mediator is a vector and the interaction is axial-vector like, the annihilation cross section must be proportional to v^2.

4.5.1.2 Dipole interactions

In the case of Z' mediation, in Tevatron, if Z' can be on shell, the energy scale of the Z' decay process to produce dark matter pairs is just $M_{Z'}$. However, in the process of dark matter annihilation during the thermal freezing-out epoch, the energy scalar is about $2M_D$, and in the case of $M_{Z'}^2 \gg 4M_D^2$, a suppression factor $(g^{(2)}M_D)^2/M_{Z'}^2$ appears in the cross section of the dipole interaction cases. From Fig. 4.23, Fig. 4.24, Fig. 4.25, and Fig. 4.27, we can see that in the range of Tevatron ability, if $M_{Z'} > 80$ GeV, dipole interactions cannot satisfy Tevatron constraint and relic abundance at the same time. Therefore, in this case, they cannot be the dominant interaction between dark matter and SM particles.

4.5.1.3 Scalar mediator with scalar dark matter

In the range of Tevatron ability to produce a real mediator particle, the energy flow inside the mediator is just the mass of the mediator. However, in the case of the dark matter annihilation during the thermal freezing-out epoch, the energy flow is around $2M_D$, therefore, in the case of dimension-1 coupling like the H' mediator with scalar dark matter case, compared to the dimensionless coupling cases, there is an enhancement factor $M_{H'}^2/M_D^2$ in the annihilation cross section. Therefore, in

143

Fig. 4.29, we see that the Tevatron constraint on the relic abundance is much lower than the observed value. This also explains why in the case of Higgs mediator low mass dark matter still survives the constraint from relic abundance.

4.5.1.4   Lepton Final States

A complication occurs when we are trying to calculate the relic abundance that Z' can also couple to leptons. However, if this is the case, the couplings between Z' and the SM particles suffer stringent constraint from LEP [74] as well as Tevatron with leptonic final states [75]. If $M_{Z'} > 209$ GeV, the LEP constraint on leptonic coupling of Z' model can be written as

$$\frac{M_{Z'}}{g_{Z'}} > 6.2 \ x \ \text{TeV} \ , \tag{4.23}$$

where x is the parameter in Lagrangian

$$\mathcal{L}_{Z'} = g_{Z'}(B - xL)\bar{\psi}\gamma^{\mu}\psi Z'_{\mu} \ , \tag{4.24}$$

where ψ labels SM fermions, B and L are baryon and lepton numbers, respectively. Whereas if the $M_{Z'} < 209$ GeV, the coupling between Z' and leptons should be smaller than or of order 10^{-2}. Assuming Z' couples only to the righthanded charged leptons universally, LEP constraint on relic abundance is shown in Fig. 4.30, where $g_D = 1$ is assumed. Approximately, the thermal relic abundance can be estimated as 0.1 pb/$\sigma_{\text{annihilation}}$, therefore, we can see that in the case of $M_{Z'} > 80$ GeV, the lepton channel contributes only less then 10% of the total annihilation cross section if Z' couples only to righthanded charged leptons. If Z' couples to lefthanded leptons
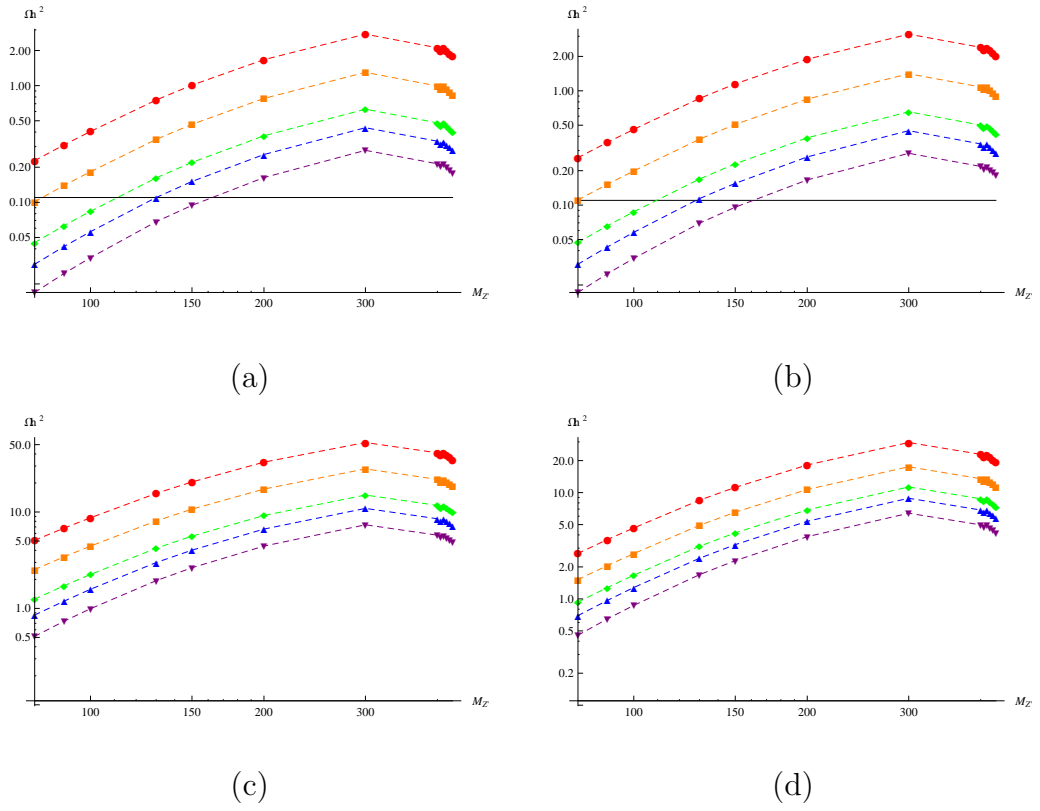
Figure 4.22: Tevatron constraints on lower bound of dark matter relic abundance for Z' mediator and fermion dark matter cases, where the leading interaction between Z' and quarks is assumed to be vector-like and universal, and the interaction between Z' and dark matter is also assumed to be vector-like. (a), (b), (c), (d) are for O_1, O_2, O_3, and O_4, respectively, with nucleons replaced by quarks. The red round circle, orange square, green diamond, blue upward triangle and purple downward triangle are for 5, 7, 10, 12, 15 GeV dark matter masses, respectively. The black horizontal line shows the observed value for Ωh^2.
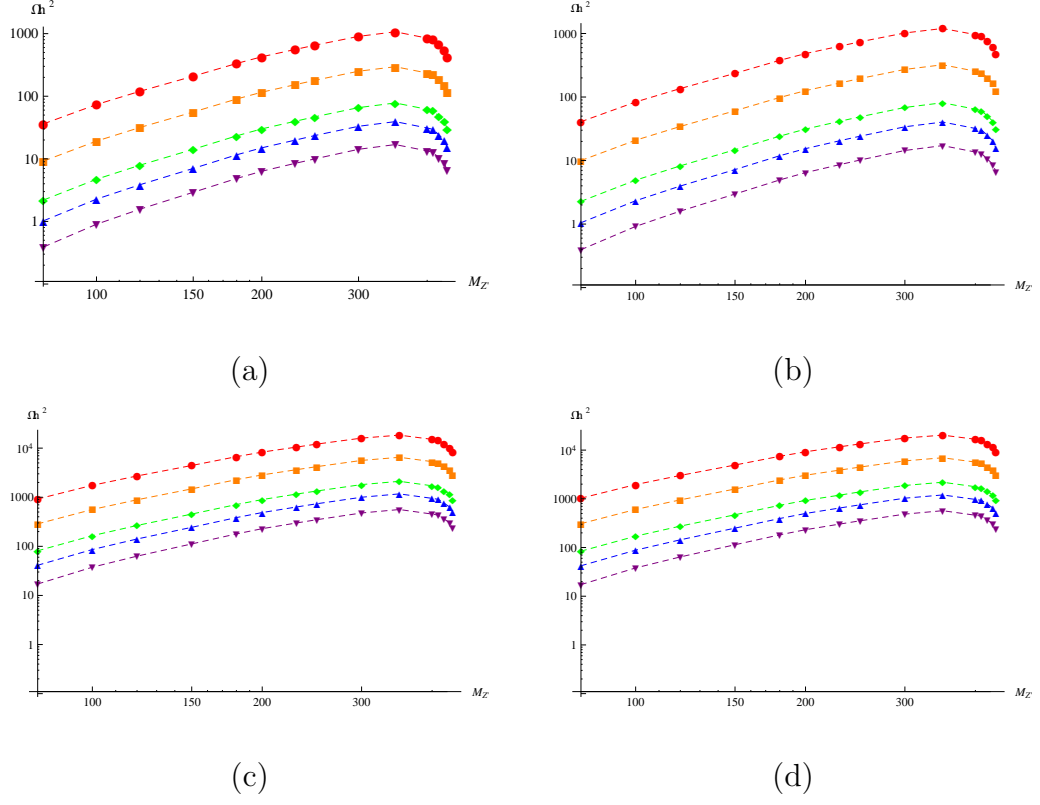
Figure 4.23: Tevatron constraints on lower bound of dark matter relic abundance for Z' mediator and fermion dark matter cases, where the leading interaction between Z' and quarks is assumed to be vector-like and universal, and the interaction between Z' and dark matter is also assumed to be dipole. (a), (b), (c), (d) are for $\{\bar{q}\gamma_\mu q \ , \ \bar{\chi}\sigma^{\mu\nu}\chi\}$, $\{\bar{q}\gamma_\mu\gamma_5 q \ , \ \bar{\chi}\sigma^{\mu\nu}\chi\}$, $\{\bar{q}\gamma_\mu q \ , \ \bar{\chi}i\gamma_5\sigma^{\mu\nu}\chi\}$, $\{\bar{q}\gamma_\mu\gamma_5 q \ , \ \bar{\chi}\sigma^{\mu\nu}i\gamma_5\chi\}$, respectively.
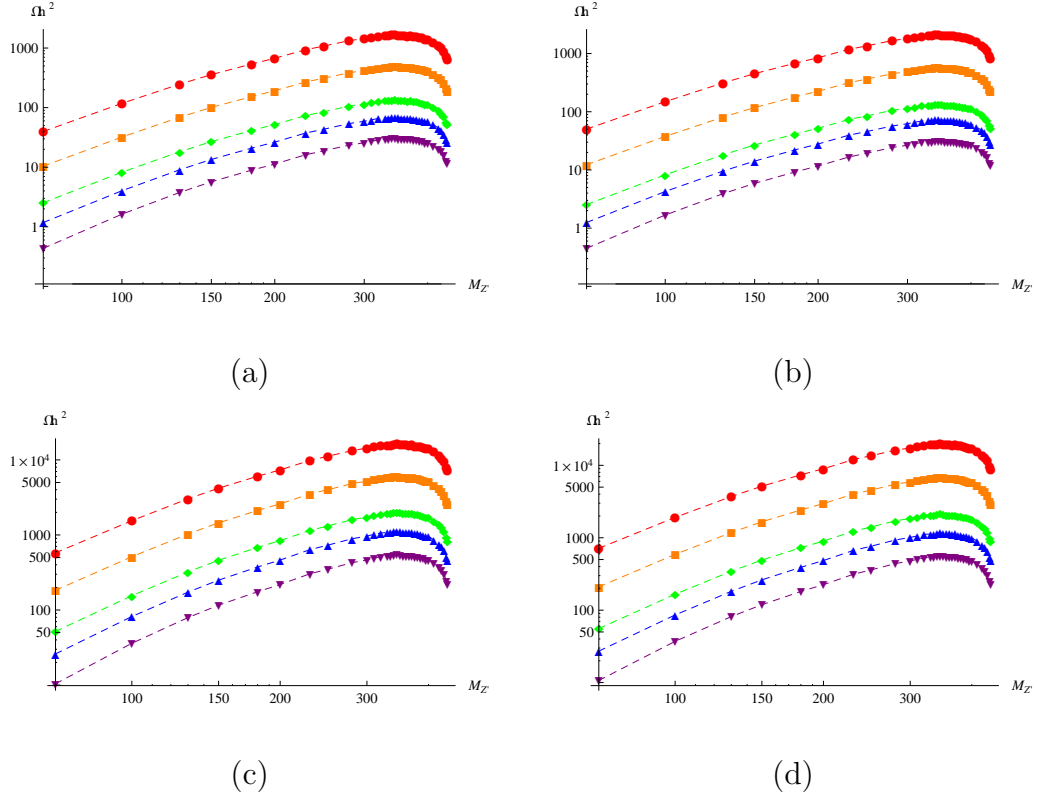
Figure 4.24: Tevatron constraints on lower bound of dark matter relic abundance for Z' mediator and fermion dark matter cases, where the leading interaction between Z' and quarks is assumed to be vector-like and universal, and the interaction between Z' and dark matter is also assumed to be dipole. (a), (b), (c), (d) are for $\{\bar{q}\sigma_{\mu\nu}q \ , \ \bar{\chi}\gamma_\mu\chi\}$, $\{\bar{q}i\gamma_5\sigma_{\mu\nu}q \ , \ \bar{\chi}\gamma_\mu\chi\}$, $\{\bar{q}\sigma_{\mu\nu}q \ , \ \bar{\chi}\gamma_\mu\gamma_5\chi\}$, $\{\bar{q}i\gamma_5\sigma_{\mu\nu}q \ , \ \bar{\chi}\gamma_\mu\gamma_5\chi\}$, respectively.
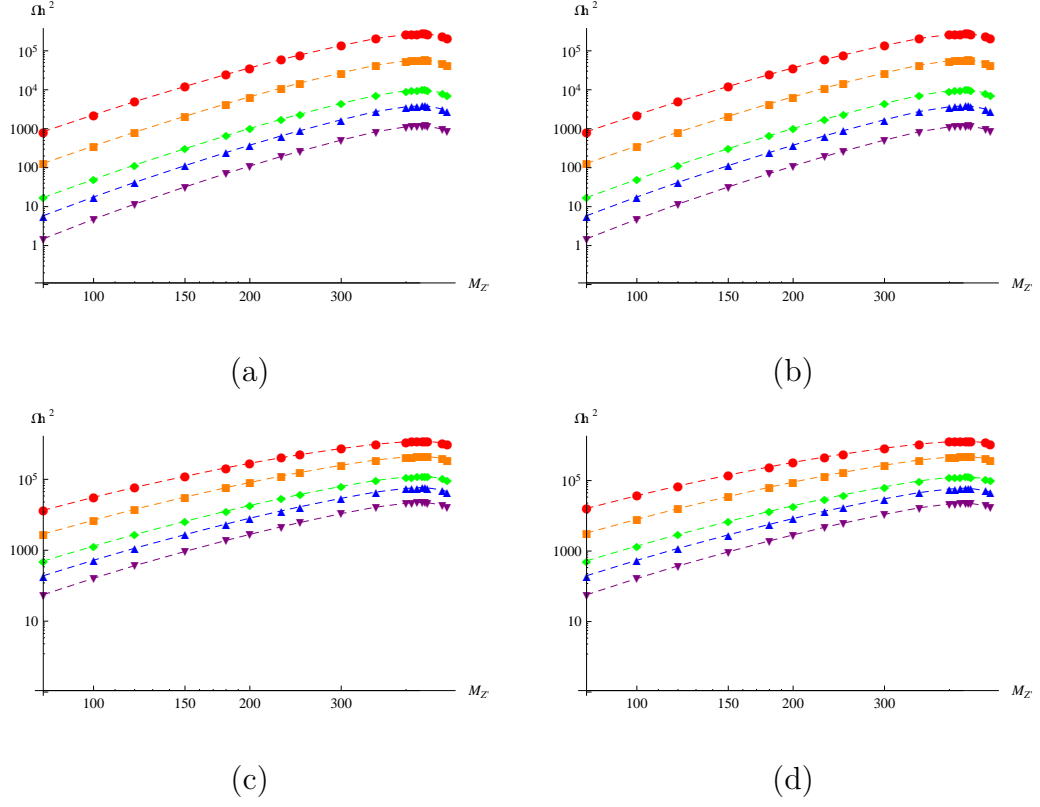
Figure 4.25: Tevatron constraints on lower bound of dark matter relic abundance for Z' mediator and fermion dark matter cases, where the leading interaction between Z' and quarks is assumed to be vector-like and universal, and the interaction between Z' and dark matter is also assumed to be dipole. (a), (b), (c), (d) are for $\{\bar{q}\sigma_{\mu\nu}q \ , \ \bar{\chi}\sigma^{\mu\nu}\chi\}$, $\{\bar{q}i\gamma_5\sigma_{\mu\nu}q \ , \ \bar{\chi}\sigma^{\mu\nu}\chi\}$, $\{\bar{q}\sigma_{\mu\nu}q \ , \ \bar{\chi}i\gamma_5\sigma^{\mu\nu}\chi\}$, $\{\bar{q}i\gamma_5\sigma_{\mu\nu}q \ , \ \bar{\chi}\sigma^{\mu\nu}i\gamma_5\chi\}$, respectively.

(a)   (b)
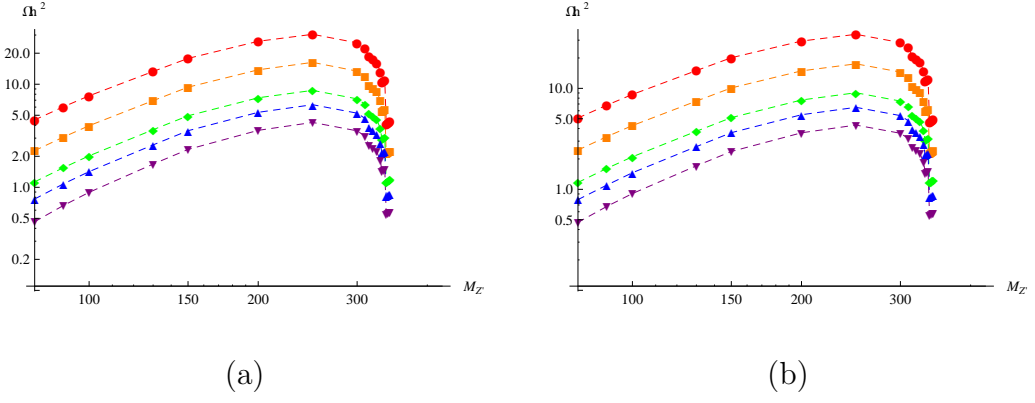
Figure 4.26: Tevatron constraints on lower bound of dark matter relic abundance for Z' mediator and fermion dark matter cases, where the leading interaction between Z' and quarks is assumed to be vector-like and universal, and the interaction between Z' and dark matter is also assumed to be dipole. (a), (b) are for $\{\bar{q}\gamma_\mu q \ , \ \phi^\dagger i\partial_\mu \phi - i\partial_\mu \phi^\dagger \phi\}$ and $\{\bar{q}\gamma_\mu \gamma_5 q \ , \ \phi^\dagger i\partial_\mu \phi - i\partial_\mu \phi^\dagger \phi\}$, respectively.

(a)   (b)
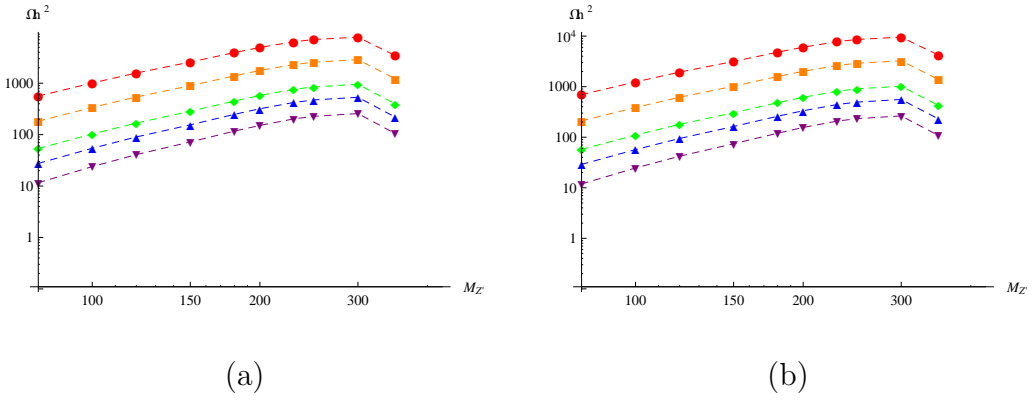
Figure 4.27: Tevatron constraints on lower bound of dark matter relic abundance for Z' mediator and fermion dark matter cases, where the leading interaction between Z' and quarks is assumed to be vector-like and universal, and the interaction between Z' and dark matter is also assumed to be dipole. (a), (b) are for $\{\bar{q}\sigma_{\mu\nu} q \ , \ \phi^\dagger i\partial_\mu \phi - i\partial_\mu \phi^\dagger \phi\}$ and $\{\bar{q}i\gamma_5 \sigma_{\mu\nu} q \ , \ \phi^\dagger i\partial_\mu \phi - i\partial_\mu \phi^\dagger \phi\}$, respectively.

149
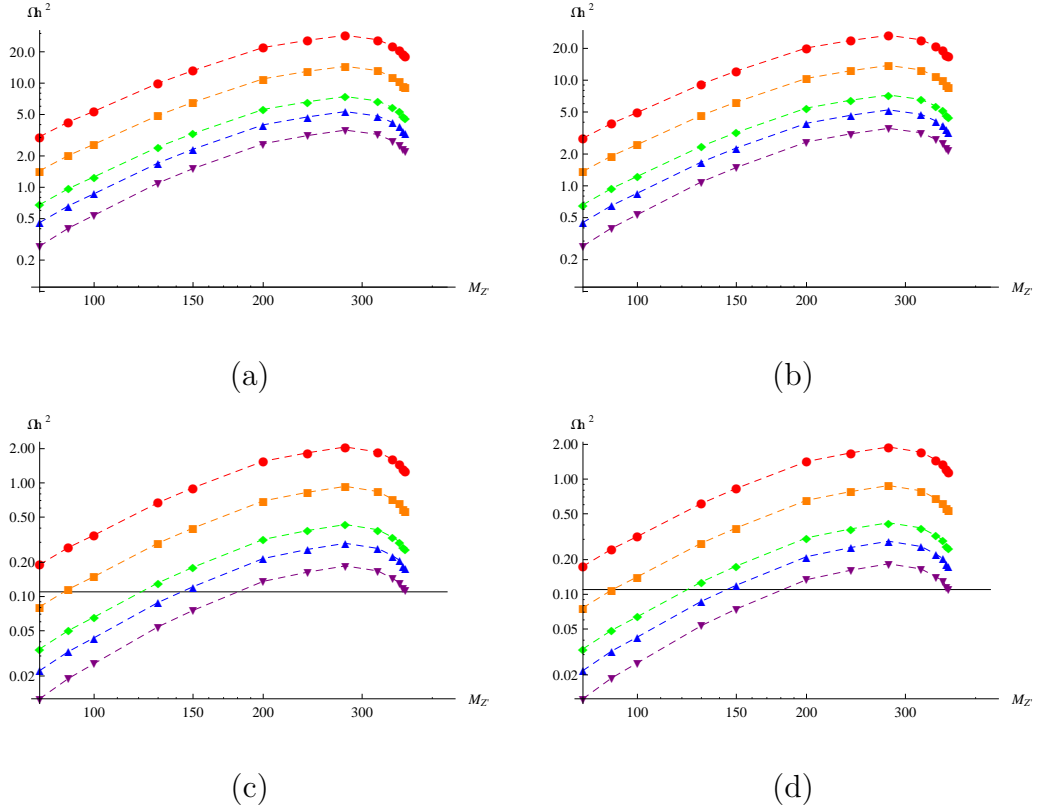
Figure 4.28: Tevatron constraints on lower bound of dark matter relic abundance for Z' mediator and fermion dark matter cases, where the leading interaction between H' and quarks is assumed to be universal. (a), (b), (c), (d) are for $\{\bar{q}q \ , \ \bar{\chi}\chi\}$, $\{\bar{q}i\gamma_5 q \ , \ \bar{\chi}\chi\}$, $\{\bar{q}q \ , \ \bar{\chi}i\gamma_5\chi\}$, $\{\bar{q}i\gamma_5 q \ , \ \bar{\chi}i\gamma_5\chi\}$, respectively.
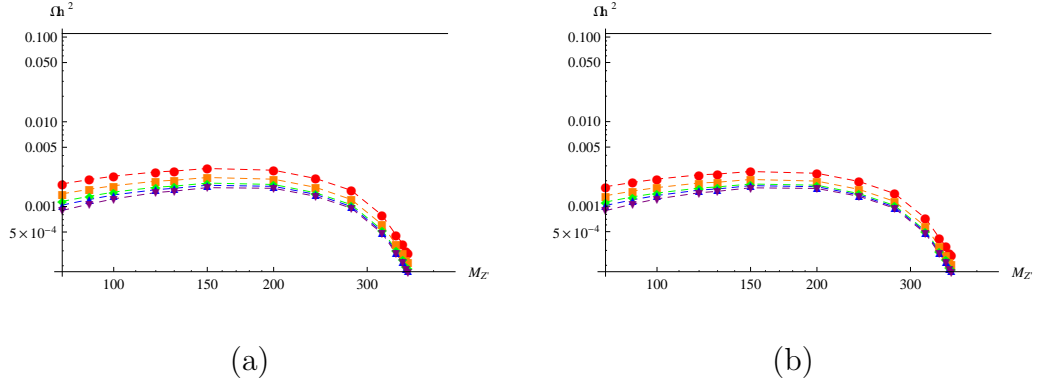
Figure 4.29: Tevatron constraints on lower bound of dark matter relic abundance for H' mediator and fermion dark matter cases, where the leading interaction between H' and quarks is assumed to be vector-like and universal, and the interaction between Z' and dark matter is also assumed to be dipole. (a), (b) are for $\{\bar{q}q \ , \ \phi^\dagger\phi\}$ and $\{\bar{q}i\gamma_5 q \ , \ \phi^\dagger\phi\}$, respectively.

Z' mediator:	$\{\bar{\chi}\gamma_\mu\chi \ , \ \bar{q}\gamma_\mu q\} \ , \ \{\bar{\chi}\gamma_\mu\chi \ , \ \bar{q}\gamma_\mu\gamma_5 q\}$
H' mediator:	$\{\bar{\chi}i\gamma_5\chi \ , \ \bar{q}q\} \ , \ \{\bar{\chi}i\gamma_5\chi \ , \ \bar{q}i\gamma_5 q\} \ , \ \{\phi^\dagger\phi \ , \ \bar{q}q\} \ , \ \{\phi^\dagger\phi \ , \ \bar{q}i\gamma_5 q\}$

Table 4.4: Possible interactions dominate the thermal annihilation of dark matter in the case of $M_{\text{mediator}} \gg 2M_D$.

as well, the lepton channel can at best contribute as large as 30% of the total annihilation cross section. Therefore, in the case $g_D = 1$, $M_{Z'} > 80$ GeV, the leptonic channel does not change much of the constraint.

From the above analysis, we can see that, in order to satisfy the bounds from Tevatron and relic abundance at the same time, the thermal annihilation must be dominated by interactions listed in Table 4.4.
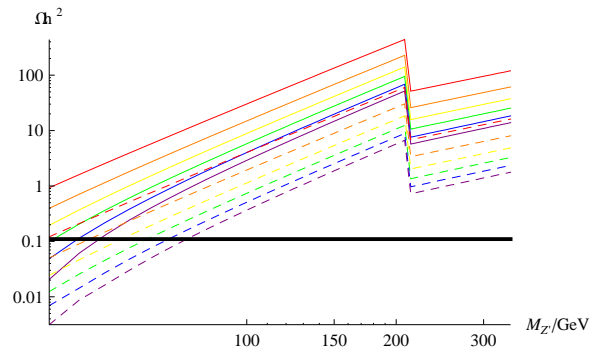
Figure 4.30: LEP constraint on dark matter thermal relic abundance, assuming Z' couples to righthanded charged leptons universally. The Red, Orange, Yellow, Green, Blue and Purple curves are lower bounds for 5, 7, 9, 11, 13 and 15 GeV dark matters, respectively. The dark matter particle is assumed to be Dirac fermion and g_D is assumed to be 1 for solid curves and 3 for dashed curves. The thick black line shows the observed value of the relic abundance of dark matter.

4.5.2 Combining Relic Abundance with Direct Detections

4.5.2.1 Z' mediator

For heavy mediator cases ($M_{Z'}^2 \gg 4M_D^2$), from Table 4.4, to generate the observed relic abundance, the dominant coupling between Z' and dark matter particle can only be like $Z'_\mu \chi \gamma^\mu \chi$. Therefore, if there is no Parity violation in the coupling, the interaction between nuclei and dark matter is spin-independent in the direct detection experiments. If the reported CoGeNT result is generated by collisions between dark matter and nuclei, one can calculate the range of $M_{Z'}/\sqrt{g_D g_{Z'}}$, and then one can calculate the lower bound of the relic abundance.

A complication occurs when we are trying to calculate the relic abundance that Z' can also couple to leptons. However, if this is the case, the couplings between Z' and the SM particles suffer stringent constraint from LEP [74] as well as Tevatron with leptonic final states [75]. If $M_{Z'} > 209$ GeV, the LEP constraint on leptonic coupling of Z' model can be written as

$$\frac{M_{Z'}}{g_{Z'}} > 6.2 \ x \ \text{TeV} \ , \tag{4.25}$$

where x is the parameter in Lagrangian

$$\mathcal{L}_{Z'} = g_{Z'}(B - xL)\bar{\psi}\gamma^\mu \psi Z'_\mu \ , \tag{4.26}$$

where ψ labels SM fermions, B and L are baryon and lepton numbers, respectively. Whereas if the $M_{Z'} < 209$ GeV, the coupling between Z' and leptons should be smaller than or of order 10^{-2}. In this model, constraint from thermal relic abundance and CoGeNT is shown in Fig. 4.31, where 5, 7, 9, 11, 13, 15 GeV dark matter masses

are considered, with x calculated from Eq. 4.25. One can see that a tension exists between direct detection experiments and thermal relic abundance. Therefore, to satisfy the relic abundance and direct detection at the same time, parity violation in the coupling between Z' and SM quarks must be introduced. The Lagrangian can be written as

$$\mathcal{L} = g_D Z'_\mu \bar{\chi} \gamma^\mu \chi + g_{Z'} Z'_\mu \bar{q} \gamma^\mu (\cos\theta + \sin\theta \gamma_5) q \ . \tag{4.27}$$

From Tables 4.2 and 4.3, we can see that the parity-odd part generates a SD&MD interaction, and the direct detection cross section is suppressed by $v^2 \sim 10^{-6}$, also, compared with SI interaction, the cross section between dark matter particle and nuclei is suppressed further at least by a factor of 10^{-2}. Therefore, as long as $\tan^2\theta \ll 10^8$, the contribution from parity-odd part to direct detection signal is negligible. The lower bound on $\tan\theta$ for different masses is shown in Fig. 4.32, where we can see that in the context of Z' mediator if CoGeNT signal is induced by dark matter, the coupling between Z' and quarks is axial-vector like. From XENON100 constraint, we can also see that if the coupling between quarks and Z' is axial-vector like for relatively heavy dark matter. In this case, the axial-vector coupling between Z' and quarks can induce non-vanishing gauge anomaly. Therefore, spectator fields must be introduced so that anomaly can be canceled. According to Ref. [94], for an anomalous Abelian gauge theory in four dimensions there is a fundamental cut-off, which can be written as

$$\Lambda < \frac{64\pi^3}{|g_{Z'}|^3} M_{Z'} \ , \tag{4.28}$$

which can be seen as the upper bound of the mass of the mediator. Therefore, in

154

our case, this bound cannot be reached by Tevatron.

(a)   (b)   (c)
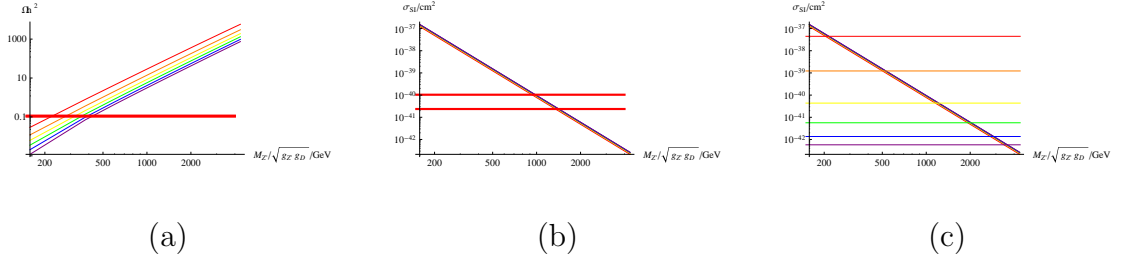
Figure 4.31: Z' mediator, no Parity-violation or CP-violation, no coupling to leptons, universally couple to quarks. The red, orange, yellow, green, blue, purple lines are for 5, 7, 9, 11, 13, 15 GeV dark matter particles, respectively. Plot (a) shows the relic abundance as a function of $M_{Z'}/\sqrt{g_{Z'}g_D}$, the thick red line shows the observed thermal relic abundance of cold dark matter. Plot (b) shows the spin-independent WIMP-nucleon cross section as a function of the same combination, and the region between the two red thick straight lines is the region favored by CoGeNT. The difference from the above plots is that, here the leptonic channels are opened in the context of $B - xL$ scenario, and the bound in x is calculated from Eq. (4.25). The horizontal lines in (c) show the XENON100 constraints for different dark matter masses.

4.5.2.2 H' mediator with fermion dark matter

In the case of H' mediator, the leading interaction is SI&MD, and for $M_{H'} > 80$ GeV, the collider constraint on direct detection cross section is about 3×10^{-43} cm^2 as shown in Fig. 4.18, which is much lower than XENON100 bound. However, if CoGeNT signal is due to dark matter collision, in this case, the SI&MI channel must be opened, but its contribution to thermal annihilation must be dominated over by

155
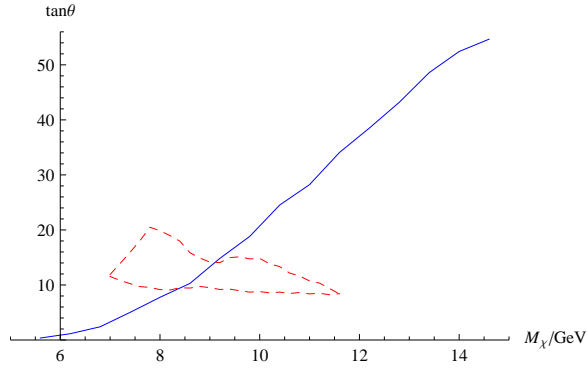
Figure 4.32: Lower bound on Parity-violating angle in Z' model from relic abundance and direct detection experiments. The blue curve is the lower bound constrained by XENON100 and the region enclosed in the red dashed curve is the region favored by CoGeNT.

the contribution from SI&MD interaction. In order to generate CoGeNT signal and correct relic abundance, the Lagrangian should be written as

$$\mathcal{L} = \bar{\chi}(g_D + ig_{D5}\gamma_5)\chi \ , \tag{4.29}$$

with $g_D/g_{D5} \approx 10^{-3}$.

4.5.3 Tension between Relic Abundance and FCNC

In the above discussion, the coupling between Z' or H' is assumed to be universal to all families of quarks, so that there is no flavor changing neutral current (FCNC) issue in the case of Z' mediator. However, in the case of H' mediator, even in this universal coupling case, after the diagonalization of quark masses, tree-level FCNC is difficult to be avoided.

In SM, the Yukawa coupling can be written as

$$\mathcal{L}_{\text{Yukawa}} = -\bar{Q} Y_U H u - \bar{Q} Y_D \tilde{H} d \ , \tag{4.30}$$

where H is the Higgs boson in SM and the $\tilde{H} \equiv -i\sigma_2 H^*$, Q, u and d are quark fields in flavor eigenstates. Rotating quarks into mass eigenstates, we can get that

$$u_L \to V_u^L u_L \ , \ \ u_R \to V_u^R u_R \ , \ \ d_L \to V_d^L d_L \ , \ \ d_R \to V_d^R d_R \ , \tag{4.31}$$

where $(u,d)_{L,R}$ are chiral quarks. The Cabibbo-Kobayashi-Maskawa (CKM) matrix is given by

$$V_{CKM} \equiv V_u^{L\dagger} V_d^L \ , \tag{4.32}$$

which can be parameterized as

$$V_{CKM} = \begin{pmatrix} 1 - \lambda^2/2 & \lambda & A\lambda^3(\rho - i\eta) \\ -\lambda & 1 - \lambda^2/2 & A\lambda^2 \\ A\lambda^3(1 - \rho - i\eta) & -A\lambda^2 & 1 \end{pmatrix} \ , \tag{4.33}$$

where $\lambda = 0.22$ is $\sin\theta_C$ and θ_C is the Cabibbo angle, other parameters are order one. All the known information of the quark rotations are involved in V_{CKM}, however, to avoid large fine-tuning, the off-diagonal elements of V_u^L and V_d^L should be of the same order of V_{CKM}.

On the other hand, mass differences of neutral meson systems are well-measured and can be used to constrain new FCNC contributions. In the case of H' mediator, the relevant Lagrangian can be written as

$$\mathcal{L}_{H'}^{\text{FCNC}} = -\frac{g_{H'}^2}{2M_{H'}^2} \left(a_L^{qq'} \bar{q}_L q_R' + a_R^{qq'} \bar{q}_R q_L' \right)^2 + \text{h.c.} \ , \tag{4.34}$$

157

where q and q' are different quarks with the same charge of electromagnetic interaction. Whereas in the case of Z' mediator, the corresponding Lagrangian can be written as

$$\mathcal{L}_{Z'}^{\text{FCNC}} = -\frac{g_{Z'}^2}{2M_{Z'}^2} \left(a_L^{qq'} \bar{q}_L \gamma_\mu q_L' + a_R^{qq'} \bar{q}_R \gamma_\mu q_R' \right)^2 + \text{h.c.} \ . \tag{4.35}$$

In the case of $K^0 - \bar{K}^0$ system, since the SM calculation suffers from a large uncertainty from long-distance contribution, we are using the criteria that the contribution from new physics should not exceed the experimental value. Therefore, we can get that

$$\frac{g_{H'(Z')} a^{ds}}{M_{H'(Z')}} < 2 \times 10^{-7} \ \text{GeV}^{-1} \ . \tag{4.36}$$

In the same way, we can get the constraint from $D^0 - \bar{D}^0$ system, that

$$\frac{g_{H'(Z')} a^{uc}}{M_{H'(Z')}} < 5 \times 10^{-7} \ \text{GeV}^{-1} \ . \tag{4.37}$$

In the case of B_d and B_s systems, the contribution from beyond SM physics can be as large as 20% of the mass differences with running into conflict with the present SM calculations. Therefore we can get the constraints

$$\frac{g_{H'(Z')} a^{db}}{M_{H'(Z')}} < 10^{-6} \ \text{GeV}^{-1} \ , \quad \frac{g_{H'(Z')} a^{sb}}{M_{H'(Z')}} < 5 \times 10^{-6} \ \text{GeV}^{-1} \ . \tag{4.38}$$

4.5.3.1 H' with fermion dark matter

where g_{D5} is fixed to 1. Therefore, then one can get the bound on the constraint of the off-diagonal elements that

In the case of H' mediator with fermion dark matter, to get the correct relic abundance, in the case of universal coupling between H' and quarks, one can get

that

$$\frac{\sqrt{g_{H'}g_D}}{M_{H'}} > 1.5 \times 10^{-3} \text{ GeV}^{-1} \left(\frac{15 \text{ GeV}}{M_D}\right)^{1/2} ,\tag{4.39}$$

Therefore, together with Eqs. (4.36), (4.37) and (4.38), one can get

$$\begin{aligned}
a^{ds} &< 10^{-3} g_D \left(\frac{100 \text{ GeV}}{M_{H'}}\right)\left(\frac{M_D}{15 \text{ GeV}}\right) , \\
a^{uc} &< 2 \times 10^{-3} g_D \left(\frac{100 \text{ GeV}}{M_{H'}}\right)\left(\frac{M_D}{15 \text{ GeV}}\right) , \\
a^{db} &< 4 \times 10^{-3} g_D \left(\frac{100 \text{ GeV}}{M_{H'}}\right)\left(\frac{M_D}{15 \text{ GeV}}\right) , \\
a^{sb} &< 2 \times 10^{-2} g_D \left(\frac{100 \text{ GeV}}{M_{H'}}\right)\left(\frac{M_D}{15 \text{ GeV}}\right) .
\end{aligned}\tag{4.40}$$

In the case of universal coupling between H' and quarks, after rotating the quarks to mass eigenstates, without fine-tuning, a^{ds} and a^{uc} should be at least around λ. Therefore, we can see that there is a tension between the relic abundance and FCNC.

4.5.3.2 H' mediator with scalar dark matter

As discussed in Sec. V.A, if the relic abundance is enhanced by a factor of $(M_{H'}/M_D)^2$ due to that the coupling between H' and DM is dimension 1. Therefore, as soon as the leptonic channel is opened, there should be no constraint from relic abundance.

4.5.3.3 Z' non-universally coupled to quarks

In the above discussions, Z' is assumed to be universally coupled to quarks. A tension between relic abundance and direct detection if the coupling between dark matter and Z' is vector-like. However, if Z' couples only to the second and third

generations of quarks, this constraint can be well alleviated. However, since the Yukawa couplings in SM also violate flavor symmetry, the rotation of quarks from flavor eigenstates to mass eigenstates induces off-diagonal couplings between Z' and the quarks, which are also strongly constrained from FCNC [95, 96].

The discussion is in parallel to the case of H' mediator. In the case that Z' couples only to the second and third families of quarks, from the relic abundance assuming hadronic channels dominate the thermal annihilation, we can get that

$$\frac{\sqrt{g_{Z'}g_D}}{M_{Z'}} > 1.5 \times 10^{-3} \text{ GeV} \left(\frac{15 \text{ GeV}}{M_D}\right)^{1/2} . \tag{4.41}$$

Therefore, together with the $FCNC$ constraints on can get that

$$
\begin{aligned}
a^{ds} &< 10^{-3} g_D \left(\frac{100 \text{ GeV}}{M_{Z'}}\right)\left(\frac{M_D}{15 \text{ GeV}}\right) , \\
a^{uc} &< 2 \times 10^{-3} g_D \left(\frac{100 \text{ GeV}}{M_{Z'}}\right)\left(\frac{M_D}{15 \text{ GeV}}\right) , \\
a^{db} &< 4 \times 10^{-3} g_D \left(\frac{100 \text{ GeV}}{M_{Z'}}\right)\left(\frac{M_D}{15 \text{ GeV}}\right) , \\
a^{sb} &< 2 \times 10^{-2} g_D \left(\frac{100 \text{ GeV}}{M_{Z'}}\right)\left(\frac{M_D}{15 \text{ GeV}}\right) .
\end{aligned} \tag{4.42}
$$

On the other hand, from quark rotation matrix, the off-diagonal elements can be written as

$$a_u^{12} \sim \lambda , \quad a_d^{12} \sim \lambda , \quad a_d^{13} \sim \lambda^4 , a_d^{23} \sim \lambda^4 . \tag{4.43}$$

In this case, since the mixing in lepton sector is large [97], rotating leptons from flavor eigenstates to mass eigenstates may generate a large coupling between Z' and the first generation of leptons, therefore, the coupling between Z' and leptons may still suffer from stringent constraint from LEP. Therefore, generally, in this

case the annihilation channel of dark matter is similar to the universal coupling case. Following the same procedure as in the discussion of the case of H' mediator, one can show that there is a strong tension between relic abundance and FCNC in $K^0 - \bar{K}^0$ and $D^0 - \bar{D}^0$ systems as well.

If Z' couples only to the third generation of SM fermions, from the relic abundance and assuming DM dominantly annihilates to hadrons, we can get

$$\frac{\sqrt{g_{Z'}g_D}}{M_{Z'}} > 2 \times 10^{-3} \text{ GeV} \left(\frac{15 \text{ GeV}}{M_D}\right)^{1/2} . \tag{4.44}$$

Therefore, the constraints on off-diagonal matrix elements can be written as

$$
\begin{aligned}
a^{ds} &< 5 \times 10^{-4} g_D \left(\frac{100 \text{ GeV}}{M_{Z'}}\right) \left(\frac{M_D}{15 \text{ GeV}}\right) , \\
a^{uc} &< 10^{-3} g_D \left(\frac{100 \text{ GeV}}{M_{Z'}}\right) \left(\frac{M_D}{15 \text{ GeV}}\right) , \\
a^{db} &< 2 \times 10^{-3} g_D \left(\frac{100 \text{ GeV}}{M_{Z'}}\right) \left(\frac{M_D}{15 \text{ GeV}}\right) , \\
a^{sb} &< 10^{-2} g_D \left(\frac{100 \text{ GeV}}{M_{Z'}}\right) \left(\frac{M_D}{15 \text{ GeV}}\right) .
\end{aligned} \tag{4.45}
$$

On the other hand, after rotating quarks to mass eigenstates, we can get that

$$a^{uc} \sim a^{ds} \sim \lambda^5 , \; a^{db} \sim \lambda^3 , \; a^{sb} \sim \lambda^2 . \tag{4.46}$$

We can see that the tension gets weakened in this case.

We need to note that the CKM matrix is related only to V_u^L and V_d^L, and the structure of V_u^R and V_d^R might be completely different from their lefthanded counterparts. Therefore, the off-diagonal elements of the righthanded quark matrices might be much smaller than the lefthanded ones, so that if Z' couples only to righthanded quarks the FCNC constraints can be avoided.

161

4.6   Low Mass Mediator

4.6.1   Resonant Thermal Annihilation

In last Sec. V, we have seen that in Z' mediator case, if the coupling between dark matter and Z' is vector-like, there is tension between relic abundance and direct detection in heavy mediator case. However, if the mass of mediator is about twice of DM, the annihilation of DM to SM particles is strongly enhanced. As shown in the Fig. 4.33, the red, blue and green curves show relic abundance constraint on the direct detection cross section between DM and nucleons. We can see that in the resonant annihilation region, the tension between relic abundance and direct detection can be alleviated.

4.6.2   Very Light Mediator

A sharp drop-down appears on the righthand side of each curve in Fig. 4.33 which is due to the newly opened annihilation channel of

$$\chi\bar{\chi} \to Z'Z' , \tag{4.47}$$

when M_χ approaches $M_{Z'}$, and the relic abundance cannot serve as a constraint anymore.

As discussed in Sec. IV, in the heavy mediator region, there is a tension between Tevatron constraint and the CoGeNT result for MD interactions due to that the cross section predicted by MD interaction is much smaller than CoGeNT favored region. However, there is no such a tension in the light mediator region due
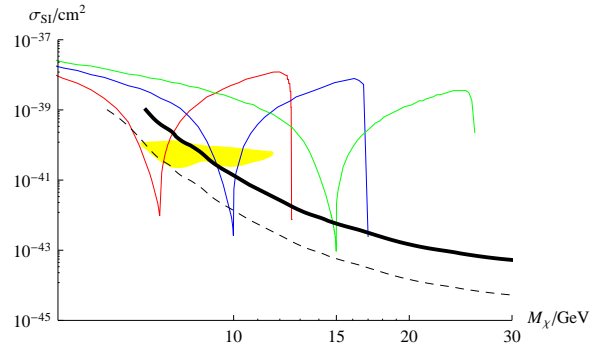
Figure 4.33: Z' mediator, the couplings between Z' to both quarks and DM are vector-like. The red, blue and green curves show the constraint from relic abundance on direct detection cross section between DM and nucleons for 15, 20, and 30 GeV $M_{Z'}$, respectively. The yellow region is favored by CoGeNT result. The solid black curve shows the constraint from XENON100 result and the dashed black curve shows the constraint from new XENON100 result which will be published soon assuming the non WIMP events being found and the detecting power increased by a factor of 10.

to that the mass in the denominator of the propagator is negligible.

The favored region of SD WIMP-nucleon cross section for CoGeNT is studied in Ref. [98]: the favored WIMP mass range is from 5 GeV to 10 GeV, and the SD cross section is about $10^{-33} \sim 10^{-32}$ cm^2 if WIMP only interacts with proton and $10^{-35} \sim 10^{-34}$ cm^2 if WIMP only interacts with neutron. Therefore, together with the SI region, one can get the GoGeNT favored range of $M_{Z'}$ for each interaction. Generally, the value for $M_{Z'}$ to fit the CoGeNT result for SI&MD&v^4 interaction and SD&MD&v^2 interaction is about $0.1 \sim 1$ GeV.

A subtlety occurs when one try to estimate $M_{Z'}$ from a dipole interaction since the dipole can be destroyed in the collider processes. In this case, one needs to first get the collider constraint on $g_{Z'} g_D$ from Fig. 4.6a and then translate the constraint into the dipole coupling.

4.7   Summary

In this chapter we use Tevatron constraints, DM relic abundance, direct detection experiments as well as results from low energy flavor physics to study the parameter space of light DM with a mass around or smaller than 15 GeV. During the study we concentrate on the s-channel Z' and H' mediators. The Tevatron constraints can be clearly separated into three parts, $M_{\text{mediator}} < 2M_{DM}$, $2M_{DM} < M_{\text{mediator}} < M_*$ and $M_{\text{meditor}} > M_*$. In this chapter, we have concentrated on the first two cases, whereas for the third case, the Tevatron constraint cannot be saturated in perturbative region. In the first two cases, the dependance of the direct detection cross

section between DM and nucleon on g_D can be factorized out, which makes the analysis simpler. Combining the constraints from relic abundance and Tevatron, one can see that the parameter space for $2M_{DM} \ll M_{Z'} < M_*$ is strongly limited, whereas in the region $M_{Z'} \ll 2M_{DM}$ the dipole interactions become possible.

In the case of MD interactions, indeed, in the direct detection, the speed of DM cannot be factorized out from the convolution of the differential detecting rate which can be written as

$$\frac{dR}{dE_r} = N_T \frac{\rho_0}{M_D} \int_{v_{\min}}^{v_{\max}} \frac{d\sigma}{dE_r} v f(v, v_{\rm e}) d^3\mathbf{v} \; , \qquad (4.48)$$

where ρ is the local DM density in the solar system, $f(v, v_{\rm e})$ is the distribution of DM velocity and v is the velocity with respect to the Earth, N_T is the number of target nuclei in the detector. $v_{\min}$ is the minimal energy can induce nuclear recoil energy E_r and $v_{\max}$ is the escape velocity in our galaxy. In the case MD interaction, the dependence of $d\sigma/dE_r$ on v is different from in the case of MI interaction. Therefore, the constraint from direct detection experiments will be slightly changed. However, to make an order-of-magnitude estimation, we simply factorize the additional velocity out and replace it with the average velocity which is about 10^{-3}.

There are many details needed to be studied, like in the dipole interaction. If the mass difference between χ and χ' is about a few keV, the collision between DM and nuclei can be inelastic which would change the pattern of direct detection signals and the Tevatron signal would be changed as well.

Chapter 5

Discussions

In this thesis, we have discussed the low energy constraints on minimal left-right symmetric model, the constraints from neutron EDM together with the indirect CP-violation give the most stringent constraint on M_{W_R} to date.

However, in many other cases, the constraint can be relaxed. For example, in the case of the supersymmetric (SUSY) version of LRSM, the CP-violation pattern is forced to be manifest so that the contribution to nEDM is much smaller than in mLRSM. Furthermore, the contributions to ΔM_K and ϵ from SUSY box diagrams by exchanging gluino or chargino fields can partially cancel with the major new contribution from LRSM, and the lower bound on M_{W_R} can be as low as around 2 TeV [67].

There is another kind of left-right symmetric model called the $\mathcal{C}$ version [99, 100]. In this model, the building blocks are the same as in mLRSM, however, instead of impose Parity to the Lagrangian, in the $\mathcal{C}$ version, the Lagrangian is invariant under the following transformation,

$$
\mathcal{C} \; : \; \begin{cases} Q_L \leftrightarrow (Q_R)^c \\ \Phi \leftrightarrow \Phi^T \end{cases} , \tag{5.1}
$$

where $(Q_R)^c$ is the charge conjugate of Q_R. In this case the Yukawa coupling ma-

trices are required to be symmetric instead of hermitian as in the case of mLRSM. Therefore, more phases are allowed in the Yukawa couplings, and there are parameter spaces that contributions to all the CP-violation observables can be canceled. Therefore the most stringent constraint on M_{W_R} still comes from the mass difference between K_L and K_S, which is about 2.5 TeV.

In nEDM calculation, quark models have been used to calculate the hadronic matrix elements. However, these models were invented to understand the mass spectrum of the baryons which are not effective theories. A model good at one aspect of phenomenology may not work in the other. Although the Feinberg-Weinberg-Kabir theorem is employed to control the uncertainty, we still need an effective theory, for example Lattice QCD, where the error bar can be systematically defined.

In mLRSM, from Ref. [3], we can see that the dominating part of the new contribution to the direct CP-violation parameter ϵ' is also proportional to the spontaneous CP phase α. Therefore, these is also a tension between the constraints from ϵ and ϵ'. A detailed calculation of ϵ' can be found in Ref. [101]. However, the constraint from nEDM is stronger.

The updated upper bound on the EDM of ^{199}Hg atom [102] can also be used to constrain the right handed scale in mLRSM. The EDM of a diamagnetic atom such as Hg can be written as

$$d_{\text{dia}} = d_{\text{dia}}(S[\bar{g}_{\pi NN}, d_N], C_S, C_P, C_T, d_e) , \qquad (5.2)$$

where S is the Schiff moment of the nucleus which depends on the P-odd and CP-odd nucleon-pion couplings and the EDM of nucleons; d_e is the EDM of electron;

167

and C_S, C_P, C_T are Wilson coefficients of P-odd and CP-odd electron-nucleon four-fermion operators [17]. Putting in the results of numerical studies, the EDM of Hg can be written as

$$d_{\text{Hg}} = -(1.8 \times 10^{-4}\text{GeV}^{-1})e\bar{g}_{\pi NN}^{(1)} + 10^{-2}d_e + (3.5 \times 10^{-3}\text{GeV})eC_S^{(0)} \, , \qquad (5.3)$$

where $\bar{g}_{\pi NN}^{(1)}$ is the P-odd and CP-odd isospin-vector nucleon-pion coupling, $C_S^{(0)}$ is the Wilson coefficient of the operator $\bar{e}i\gamma_5 e\bar{N}N$. Of course, the isospin-scalar and tensor parts also contribute to the Schiff moment, but they are numerically suppressed according to the same reference.

The operator $\bar{e}i\gamma_5 e\bar{N}N$ can be induced from four-fermion operators $\bar{e}i\gamma_5 e\bar{q}q$, where q labels light quarks. In mLRSM, this kind of operators cannot be generated by integrating out a heavy gauge boson at tree-level since neutral currents never violate CP whereas charged currents always violate flavor. Therefore, the leading order contribution to this operator is from integrating out Higgs bosons. Furthermore, since in this model quarks only couple to the bi-doublet higgs whose vevs induce the masses of the quarks and charged leptons. Therefore, the Wilson coefficient of this operator must be proportional to the mass of electron and the mass of the light quark. Therefore, $C_S^{(0)}$ can be estimated as $(m_e m_u)/(\text{TeV}^4)$ which is about ten orders of magnitude smaller than the Wilson coefficient of the four-quark operators which is induced by integrating out the W-boson. Therefore, it is not difficult to see that d_{Hg} generated by $C_S^{(0)}$ is not as competitive as nEDM in mLRSM.

In mLRSM, the coupling between leptons and triplet Higgs bosons involve new CP-violating parameters which complicates the calculation of electron EDM.

Therefore, it is difficult to constrain the righthanded scale using electron EDM. If we assume there is no cancelation between the contribution from the Schiff moment and the contribution from the electron EDM, we can get a constraint on $\bar{g}_{\pi NN}^{(1)}$ from d_{Hg} that

$$\bar{g}_{\pi NN}^{(1)} < 10^{-11} \ . \tag{5.4}$$

The neutron EDM generated by $\bar{g}_{\pi NN}^{(1)}$ can be estimated as [65]

$$d_N \approx \frac{3\bar{g}_{\pi NN}^{(1)}}{2} \frac{\kappa_n e}{16\pi^2} \frac{D+F}{F_\pi} \approx 0.3 e \bar{g}_{\pi NN}^{(1)} \mathrm{GeV}^{-1} \ . \tag{5.5}$$

Then using the experimental upper bound $d_N < 2.9 \times 10^{-26} e$ cm, one can get

$$\bar{g}_{\pi NN}^{(1)} < 5 \times 10^{-12} \ , \tag{5.6}$$

Since the uncertainty of the hadronic matrix elements is about a factor of two, if we assume there is no cancelation between the electron EDM contribution and the Schiff moment contribution, we can say that the constraint from d_{Hg} is as competitive as the constraint from d_N. However, we also see that the constraint from neutron EDM is cleaner since only two phases are involved and there is no way to cancel it after the constraint from ϵ is considered.

Appendix A

Notations and Conventions

The metric tensor is defined as

$$g_{\mu\nu} = g^{\mu\nu} = \begin{pmatrix} 1 & 0 & 0 & 0 \\ 0 & -1 & 0 & 0 \\ 0 & 0 & -1 & 0 \\ 0 & 0 & 0 & -1 \end{pmatrix} . \tag{A.1}$$

The Pauli matrices are defined as

$$\vec{\sigma} = (\sigma_1, \ \sigma_2 \ , \sigma_3) \ , \tag{A.2}$$

where

$$\sigma_1 = \begin{pmatrix} 0 & 1 \\ 1 & 0 \end{pmatrix} \quad \sigma_2 = \begin{pmatrix} 0 & -i \\ i & 0 \end{pmatrix} \quad \sigma_3 = \begin{pmatrix} 1 & 0 \\ 0 & -1 \end{pmatrix} . \tag{A.3}$$

The Dirac Notation of the gamma matrices are defined as

$$\gamma^0 = \begin{pmatrix} 1 & 0 \\ 0 & -1 \end{pmatrix} \quad \vec{\gamma} = \begin{pmatrix} 0 & \vec{\sigma} \\ -\vec{\sigma} & 0 \end{pmatrix} \quad \gamma_5 = i\gamma^0\gamma^1\gamma^2\gamma^3 = \begin{pmatrix} 0 & 1 \\ 1 & 0 \end{pmatrix} . \tag{A.4}$$

The left and right-handed projectors are defined as

$$\mathbb{P}_L = (1 - \gamma_5)/2 \ , \quad \mathbb{P}_R = (1 + \gamma_5)/2 \ , \tag{A.5}$$

respectively.

The total symmetric tensor is defined as $\epsilon^{0123} = 1$.

Appendix B

Proof of the Completeness and Independence of Operators in χPT

The chiral operators in different irreducible representations are shown in Table 2.4. We need to prove that the operators in each set are complete and independent with each other. The proof is tedious and the outline is given in this Appendix.

The building blocks of these operators are $\xi B \xi$, $\xi^\dagger \bar{B} \xi^\dagger$, the spurions fields, U, and $U^\dagger$. We need to use these building blocks to construct singlets of the the chiral symmetry group. Since we consider only the tree-level matching, the operators we need should contain one B, one $\bar{B}$ and exactly the same spurions as in the corresponding quark operator.

The irreducible representation of $SU(3)$ group can be constructed using Young tableau. A good introduction to Young tableau can be found in Ref. [103]. To construct a singlet of $SU(3)$, each column of the Young-tableau needs to be filled with three boxes. For example, if all the three boxes are filled by U, using the total anti-symmetric properties of Young tableau, the constructed operator must be proportional to

$$\epsilon^{ijk} U_l^i U_m^j U_n^k = \det[U] \epsilon^{ijk} , \tag{B.1}$$

where ϵ^{ijk} is the total anti-symmetric tensor. Since U is an element of $SU(3)$, $\det[U] = 1$. The corresponding Young-tableau is reduced. Therefore, the number

of operators in each set of the group is finite. Using this method, the operators (without the tilde) we can get are listed in the following,

$$O_{31} = i\epsilon_{nkl}^{mij}A_m^n(\xi\bar{B}\xi)_i^k(\xi B\xi)_j^l + h.c.$$

$$O_{32} = i\mathrm{Tr}[\bar{B}B]\mathrm{Tr}[AU] + h.c.$$

$$O_{33} = i\mathrm{Tr}[A\xi^\dagger\bar{B}B\xi^\dagger] + h.c.$$

$$O_{34} = i\mathrm{Tr}[\bar{B}\xi^\dagger A\xi^\dagger B] + h.c.. \tag{B.2}$$

$$O_{61} = iT_{kl}^{ij}(\xi\bar{B}\xi)_i^k(\xi B\xi)_j^l + h.c.$$

$$O_{62} = iT_{kl}^{ij}(\xi\bar{B}B\xi)_i^k U_j^l + h.c.$$

$$O_{63} = iT_{kl}^{ij}(\bar{B}\xi)_i^m(\xi B)_m^k U_j^l + h.c.$$

$$O_{64} = i\mathrm{Tr}[\bar{B}B]T_{kl}^{ij}U_i^k U_j^l + h.c.$$

$$O_{65} = iT_{lr}^{uj}\epsilon_{kps}^{imu}U_s^l U_j^r(\xi^\dagger\bar{B}\xi)_k^i(\xi^\dagger B\xi)_p^m + h.c.. \tag{B.3}$$

$$O_1^8 = i\epsilon_{lmn}^{ijk}(\xi\bar{B}\xi)_l^i(\xi B\xi)_m^j U_q^p h_{1p}^k h_{2n}^q + h.c.$$

$$O_2^8 = i\epsilon_{lmn}^{ijk}(\xi\bar{B}\xi)_l^p(\xi B\xi)_m^j U_q^i h_{1p}^k h_{2n}^q + h.c.$$

$$O_3^8 = i\epsilon_{lmn}^{ijk}(\xi\bar{B}\xi)_l^i(\xi B\xi)_m^p U_q^j h_{1p}^k h_{2n}^q + h.c.$$

$$O_4^8 = i\epsilon_{lmn}^{ijk}(\xi\bar{B}\xi)_q^i(\xi B\xi)_m^j U_l^p h_{1p}^k h_{2n}^q + h.c.$$

$$O_5^8 = i\epsilon_{lmn}^{ijk}(\xi\bar{B}\xi)_l^i(\xi B\xi)_q^j U_m^p h_{1p}^k h_{2n}^q + h.c.$$

$$O_6^8 = i\epsilon_{lmn}^{ijk}(\xi^\dagger\bar{B}\xi^\dagger)_l^i(\xi^\dagger B\xi^\dagger)_m^j U_q^{\dagger p} h_{2p}^k h_{1n}^q + h.c.$$

$$O_7^8 = i\epsilon_{lmn}^{ijk}(\xi^\dagger\bar{B}\xi^\dagger)_l^p(\xi^\dagger B\xi^\dagger)_m^j U_q^{\dagger i} h_{2p}^k h_{1n}^q + h.c.$$

$$O_8^8 = i\epsilon_{lmn}^{ijk}(\xi^\dagger\bar{B}\xi^\dagger)_l^i(\xi^\dagger B\xi^\dagger)_m^p U_q^{\dagger j} h_{2p}^k h_{1n}^q + h.c.$$

$$O_9^8 = i\epsilon_{lmn}^{ijk}(\xi^\dagger\bar{B}\xi^\dagger)_q^i(\xi^\dagger B\xi^\dagger)_m^j U_l^{\dagger p} h_{2p}^k h_{1n}^q + h.c.$$

$$O_{10}^8 = i\epsilon_{lmn}^{ijk}(\xi^\dagger\bar{B}\xi^\dagger)_l^i(\xi^\dagger B\xi^\dagger)_q^j U_m^{\dagger p} h_{2p}^k h_{1n}^q + h.c.$$

$$O_{11}^8 = i\text{Tr}[\bar{B}B]\text{Tr}[U^\dagger h_1 U h_2] + h.c.$$

$$O_{12}^8 = i\text{Tr}[\xi^\dagger\bar{B}B\xi^\dagger h_1 U h_2] + h.c.$$

$$O_{13}^8 = i\text{Tr}[\bar{B}\xi^\dagger h_1 U h_2 \xi^\dagger B] + h.c.$$

$$O_{14}^8 = i\text{Tr}[\xi\bar{B}B\xi h_2 U^\dagger h1] + h.c. \quad O_{15}^8 = i\text{Tr}[\bar{B}\xi h_2 U_1 h_1 \xi B] + h.c.$$

$$O_{16}^8 = i\text{Tr}[\xi\bar{B}\xi^\dagger h_1]\text{Tr}[\xi^\dagger B\xi h_2] + h.c. \quad O_{17}^8 = i\text{Tr}[\xi^\dagger\bar{B}\xi h_2]\text{Tr}[\xi B\xi^\dagger h_1] + h.c.$$

$$O_{18}^8 = i\text{Tr}[\xi\bar{B}\xi h_2 \xi^\dagger B\xi^\dagger h_1] + h.c.$$

$$O_{19}^8 = i\text{Tr}[\xi^\dagger\bar{B}\xi^\dagger h_1 \xi B\xi h_2] + h.c.$$

$$O_{20}^8 = i\epsilon_{ikl}^{ipq}(\xi\bar{B}B\xi)_i^j U_r^k h_{2q}^r U_p^m h_{1m}^l + h.c.$$

$$O_{21}^8 = i\epsilon_{ikl}^{ipq}(\bar{B}\xi)_i^n(\xi B)_n^j U_r^k h_{2q}^r U_p^m h_{1m}^l + h.c. \tag{B.4}$$

where A, T, h_1 and h_2 are spurion fields for $(\bar{3}, 3)$, $(6, \bar{6})$, and $(8, 8)$ representations, respectively. However, these operators are not independent with each other. One can use the relation

$$\epsilon^{abc}_{def} \sim \delta^a_d \delta^b_e \delta^c_f + \delta^b_d \delta^c_e \delta^a_f + \delta^c_d \delta^a_e \delta^b_f - \delta^b_d \delta^a_e \delta^c_f - \delta^a_d \delta^c_e \delta^b_f - \delta^c_d \delta^b_e \delta^a_f ,\qquad (\text{B.5})$$

the number of operators can be reduced. First of all, by tedious calculation, it can be shown that O^3_1 can be constructed by a linear combination of the other three and O^6_5 can be constructed by the other four. Second, all the $(8, 8)$ operators can be constructed by O^8_{11}, O^8_{12}, O^8_{13}, O^8_{14}, O^8_{15}, O^8_{16}, O^8_{17}, O^8_{18}, O^8_{19}.

It turns out, however, the remaining nine $(8, 8)$ operators still have a linear relation. This can be seen in the following way. An important observation is that all these nine operators can be constructed from four matrices, which are B, $\bar{B}$, $\xi^\dagger h_1 \xi$ and $\xi h_2 \xi^\dagger$. All these four fields transform as 8-representation of the unbroken $SU(3)_V$ symmetry. However, the product of four 8-dimensional representations of $SU(3)_V$ group gives only eight singlet rather than nine.

$$8 \times 8 \times 8 \times 8 = (1 + 8 + 8 + 10 + \bar{10} + 27) \times (1 + 8 + 8 + 10 + \bar{10} + 27) . \quad (\text{B.6})$$

Therefore, one of the nine operators can written as a linear combination of the other eight.

Now, we have complete bases in each set. During the matching process in Chapter 2, we have shown that the solution for the matching equations in each case is unique. Therefore, the operators of each representation are complete and linearly independent with each other.

Appendix C

Discussions of the nEDM generated by θ-term and the contribution from η'

In the case of θ-term, the Lagrangian of QCD is

$$\mathcal{L}^{QCD} = \mathcal{L}_0^{QCD} - \bar{q}\mathcal{M}q - \theta m_*(\bar{u}i\gamma_5 u + \bar{d}i\gamma_5 d + \bar{s}i\gamma_5 s), \tag{C.1}$$

where m_* is the reduce quark mass defined as $m_u m_d m_s (m_u m_d + m_d m_s + m_s m_u)^{-1}$. With the θ-term, the quark mass matrics can be redefined as

$$M = \begin{pmatrix} m_u + i\theta m_* & & \\ & m_d + i\theta m_* & \\ & & m_s + i\theta m_* \end{pmatrix}. \tag{C.2}$$

Just as before, the vev of U is assumed to have the form of Eq. (D.9). And the potential of U is still can be written as in Eq. (D.8). In the case of small θ, it is easy to see that α and β should also be small, since they must be proportional to θ. The potential is

$$V = -F_\pi^2 B \left(m_u \cos\alpha + m_d \cos\beta + m_s \cos(\alpha + \beta) + m_*\theta(\sin\alpha + \sin\beta - \sin(\alpha + \beta)) \right) . \tag{C.3}$$

Expanding over α and β, we can get

$$
\begin{aligned}
V \;=\;\; & -F_\pi^2 B \left(m_u + m_d + m_s - \frac{1}{2} m_u \alpha^2 - \frac{1}{2} m_d \beta^2 \right. \\
& \left. - \frac{1}{2} m_s (\alpha + \beta)^2 + m_* \theta (\alpha + \beta - (\alpha + \beta)) \right) .
\end{aligned}
\tag{C.4}
$$

Therefore, we can see that the terms including θ canceled, which means the potential is not depends on θ and it is easy to see that the minimum happens at

$$
\alpha = \beta = 0.
\tag{C.5}
$$

Which means such a choice of θ vacuum will not generate the vev of goldstone bosons.

The θ-term has exactly the same chiral properties as the quark mass matrix, so we can combine them together. Therefore the spurion fields can be written as

$$
M = \mathcal{M} + diag(i\theta m_*, i\theta m_*, i\theta m_*).
\tag{C.6}
$$

Then, we can consider the leading order contribution of this spurion field to the nucleon-pion Lagrangian in chiral perturbation theory. The relevant terms in χPT are listed in Eqs. (2.45) and (2.46). In the presence of θ, the terms in Eq. (2.45) generate a CP-odd pion-nucleon coupling which can be written as

$$
\frac{4\theta m_*}{F_\pi} \left(c_2 \mathrm{Tr}[\Sigma \bar{B} B] + c_3 \mathrm{Tr}[\bar{B}\Sigma B] \right) ,
\tag{C.7}
$$

which is independent of c_1 since the Σ is traceless. c_2 and c_3 can be determined by the mass differences of baryons. The terms in Eq. (2.46) in the leading order generate CP-odd masses for baryons which can be written as

$$
2m_*(d_1 + d_2 + d_3)\mathrm{Tr}[\bar{B}i\gamma_5 B] ,
\tag{C.8}
$$

which term will turn the neutron magnetic dipole moment to the electric dipole moment as discussed in Chapter 2.

There is one more subtlety that there is another meson field η', which can be annihilated by the θ term. Therefore, it may have a vev, and generate new contributions to CP-violating processes. Therefore, we should add η' in Σ to get a meson nonet,

$$\Sigma = \begin{pmatrix} \frac{1}{2}\pi^0 + \frac{1}{2\sqrt{3}}\eta + \frac{1}{\sqrt{6}}\eta' & \frac{1}{\sqrt{2}}\pi^+ & \frac{1}{\sqrt{2}}K^+ \\ \frac{1}{\sqrt{2}}\pi^- & -\frac{1}{2}\pi^0 + \frac{1}{2\sqrt{3}}\eta + \frac{1}{\sqrt{6}}\eta' & \frac{1}{\sqrt{2}}K^0 \\ \frac{1}{\sqrt{2}}K^- & \frac{1}{\sqrt{2}}\bar{K}^0 & -\frac{1}{\sqrt{3}}\eta + \frac{1}{\sqrt{6}}\eta' \end{pmatrix}. \tag{C.9}$$

We know that the $U(1)_A$ symmetry is not only spontaneously broken by the quark condensate and explicitly broken by the small quark masses, it is broken by the chiral anomaly as well. Therefore, η' gets a unusual heavy mass. To realize the chiral anomaly in the chiral perturbation theory, we can add a special mass term for η', which can be written as [8]

$$\mathcal{L}_{U(1)_A} = -\frac{F_\pi^2}{4}\frac{a}{N_c}\left\{\frac{i}{2}\left[\log(\det U) - \log(\det U^\dagger)\right]\right\}^2, \tag{C.10}$$

where a can be related to vacuum susceptibility in the zero flavor case and N_c is the number of color. Then one can write down the potential of the neutral meson fields

$$\begin{aligned} V &= -F_\pi^2 B \left\{ m_u \cos\left[(\pi^0 + \frac{1}{\sqrt{3}}\eta + \frac{2}{\sqrt{6}}\eta')/F_\pi\right] \right. \\ &\quad +m_d \cos\left[(-\pi^0 + \frac{1}{\sqrt{3}}\eta + \frac{2}{\sqrt{6}}\eta')/F_\pi\right] + m_s \cos\left[(-\frac{2}{\sqrt{3}}\eta + \frac{2}{\sqrt{6}}\eta')/F_\pi\right]\right\} \\ &\quad -F_\pi^2 B m_* \theta \left\{ \sin\left[(\pi^0 + \frac{1}{\sqrt{3}}\eta + \frac{2}{\sqrt{6}}\eta')/F_\pi\right] \right. \\ &\quad + \sin\left[(-\pi^0 + \frac{1}{\sqrt{3}}\eta + \frac{2}{\sqrt{6}}\eta')/F_\pi\right] + \sin\left[(-\frac{2}{\sqrt{3}}\eta + \frac{2}{\sqrt{6}}\eta')/F_\pi\right]\right\} \\ &\quad +\frac{1}{2}\frac{N_f}{N_c}a^2\eta'^2, \end{aligned} \tag{C.11}$$

where the last term is induced by the anomaly and in the $N_f = N_c = 3$ case, a is just the mass of η'. Since θ is small, to get the vevs of meson fields one can expand the sine and cosine to the second order in θ, then, we can get

$$
\begin{aligned}
V &= -F_\pi^2 B(m_u + m_d + m_s) \\
&+ \frac{1}{2} B(m_u + m_d)\pi^{02} + \frac{1}{2} B\left[\frac{1}{3}(m_u + m_d + 4m_s)\eta^2\right] \\
&+ \frac{1}{2}\left[\frac{2}{3}B(m_u + m_d + m_s) + a^2\right]\eta'^2 \\
&+ B\left[\frac{1}{\sqrt{3}}(m_u - m_d)\pi^0\eta + \frac{2}{\sqrt{6}}(m_u - m_d)\pi^0\eta' \right. \\
&\left. + \left(\frac{\sqrt{2}}{3}(m_u + m_d) - \frac{2\sqrt{2}}{3}m_s\right)\eta\eta'\right] \\
&- \sqrt{6}F_\pi B m_* \theta\eta'.
\end{aligned}
\tag{C.12}
$$

We need to solve the minimum of the above potential to get the vevs of the meson fields. With the help of MATHEMATICA, one can get

$$
\begin{aligned}
\langle\pi^0\rangle &= -\frac{3\theta B F_\pi m_*(m_u - m_d)(1 - m_*/m_s)}{(m_u + m_d)(a^2 + 6Bm_*)} \\
\langle\eta\rangle &= \frac{\sqrt{3}\theta B F_\pi m_*(1 - 3m_*/m_s)}{a^2 + 6Bm_*} \\
\langle\eta'\rangle &= \frac{\sqrt{6}\theta B F_\pi m_*}{a^2 + 6Bm_*}.
\end{aligned}
\tag{C.13}
$$

The vevs are of the same order of magnitude as $\theta B F_\pi m_*/a^2$. Put the meson vevs in Eq. (2.45), we can get

$$
c\frac{m_q\theta B m_*}{F_\pi a^2}\text{Tr}[\bar{B}B\Sigma]\,,
\tag{C.14}
$$

where c is an order 1 parameter. Then, compared to the CP-odd vertex directly induced by the θ-term. This contribution is suppressed by $m_q B/a^2$, which is just the mass ratio between a usual pseudo-goldstone and the mass of η'. Therefore, in

the following, we will neglect the contribution of η' condensate. η' also appears in the CP-odd vertices and with an equal coupling to all the baryons. However, the loop generated by η' has no large log therefore, we will not consider η' in future discussion.

One interesting thing here is to consider the large N_c limit, in which $a^2 = 0$. Then, just like in the last section, a rotation of the baryon fields can kill all the CP-odd effects in Eq.(C.7) and (C.8). Therefore, one can see that all the physical effects must be multiplied by a factor of $1 - \mathcal{O}(m_\pi^2/a^2)$. To be precise, the factor is

$$\frac{a^2}{a^2 + \frac{2}{3}B(m_u + m_d + m_s)} \; . \tag{C.15}$$

Appendix D

Feinberg-Weinberg-Kabir theorem

In the case of two flavor quantum electrodynamics, the Lagrangian can be written as

$$\mathcal{L} = \sum_{ij} \bar{\psi}_i i \not{D} \psi_j - \sum_{ij} m_{ij} \bar{\psi}_i \psi_j \; , \tag{D.1}$$

where $D_\mu = \partial_\mu - ieA_\mu$, A_μ is $U(1)$ gauge field.

The theorem states that no flavor changing observed in this system. The reason is that all these mixings can be absorbed into the redefinition of the fields.

In the context of the chiral perturbation theory, it can be restate as CP-odd $(3, \bar{3})$ two-quark operators cannot generate CP-violation observables, the reason is that all these operators can be absorbed by redefinition of quark fields. In this Appendix, we show this property explicitly.

The QCD Lagrangian without any CP-violating sources, can be written as

$$\mathcal{L}^{QCD} = \mathcal{L}_0^{QCD} - \bar{q}\mathcal{M}q \; , \tag{D.2}$$

where $\mathcal{L}_0^{QCD}$ is the massless part which is invariant under the chiral $SU(3)_L \times SU(3)_R$ transformation, and $\mathcal{M} = diag\{m_u, m_d, m_s\}$ is the mass matrix of light quarks, which breaks the chiral symmetry explicitly. To introduce CP-violating two-quark operator, let's redefine the quark fields by the following transformation,

$$q = \exp[i\gamma_5 \theta t^3]q', \tag{D.3}$$

where $t^3 = \lambda^3/2$ is the third generator of the $SU(3)$ group. Therefore, the Lagrangian can be written as

$$\mathcal{L}^{QCD}[q'] = \mathcal{L}_0^{QCD}[q'] - \bar{q}' \exp[i\gamma_5\theta t^3]\mathcal{M}\exp[i\gamma_5\theta t^3]q' . \tag{D.4}$$

One can separate the left and right part of the fermion fields and then the mass term can be written as

$$-\bar{q}'_L\mathcal{M}e^{2i\theta t^3}q'_R - \bar{q}'_R\mathcal{M}e^{-2i\theta t^3}q'_L , \tag{D.5}$$

where the fact that t^3 commutes with $\mathcal{M}$ has been used. Therefore, the mass term can be further written as

$$-\bar{q}'_L M q'_R - \bar{q}'_R M^\dagger q'_L , \tag{D.6}$$

where $M = \mathcal{M}e^{2i\theta t^3}$. Then M can be seen as a spurion field, transforms as a $(3,\bar{3})$ operator, From which one can construct the effective Lagrangian in χPT.

In the meson sector, the leading order Lagrangian for meson fields can be written as

$$\mathcal{L} = \frac{1}{4}F_\pi^2\text{Tr}[\partial_\mu U^\dagger \partial^\mu U] + \frac{1}{2}F_\pi^2 B\text{Tr}[M^\dagger U + U^\dagger M] , \tag{D.7}$$

where U is defined in Chapter 2. Then, the potential up to leading order of the quark mass can be written as

$$V(U) = -\frac{1}{2}F_\pi^2 B\text{Tr}[M^\dagger U + U^\dagger M] . \tag{D.8}$$

Note that t^3 commutes with the electromagnetic symmetry generator which is $diag\{2/3, -1/3, -1/3\}$, so only the neutral fields can have a vev. Therefore, consid-

ering that $\det U = 1$, the vev of U can be written as

$$\langle U \rangle = \begin{pmatrix} e^{i\alpha} & & \\ & e^{i\beta} & \\ & & e^{-i(\alpha+\beta)} \end{pmatrix}. \tag{D.9}$$

Then the potential of meson fields becomes

$$V = -F_\pi^2 B[m_u \cos(\theta - \alpha) + m_d \cos(\theta + \beta) + m_s \cos(\alpha + \beta)]. \tag{D.10}$$

From the potential one can seen that the two-flavor case is equivalent to $m_s \to \infty$, which set $\alpha = -\beta$. And the minimum of the potential is at $\alpha = \theta$. In the three-flavor case, one can get the following equations

$$m_u \sin(\alpha - \theta) + m_s \sin(\alpha + \beta) = 0$$

$$m_d \sin(\theta + \beta) + m_s \sin(\alpha + \beta) = 0 \tag{D.11}$$

The analytical solution is

$$\alpha = \theta \quad \beta = -\theta. \tag{D.12}$$

Therefore, we can see that the CP-phases cause a non-vanishing vev of U, so that U can be parameterized as

$$U = \langle U \rangle U' , \tag{D.13}$$

and now the meson fields contained in U' are physical fields, which means that they have no vevs. After this reparametrization, the Lagrangian for meson fields can be written as

$$\mathcal{L} = \frac{1}{4}F_\pi^2 \mathrm{Tr}[\partial_\mu U'^\dagger \partial^\mu U'] + \frac{1}{2}F_\pi^2 B \mathrm{Tr}[\mathcal{M}U' + U'^\dagger \mathcal{M}]. \tag{D.14}$$

We can see that there is no CP-violation in the meson Lagrangian using the redefined meson fields. Now let's consider the baryon fields. The terms in the Lagrangian of baryon terms can be put in two groups, the first group is only generated by $\mathcal{L}^{QCD}$ which respects the chiral symmetry in the Lagrangian level, and the second group has the contribution from the quark mass term and breaks the chiral symmetry explicitly. Let's have an example of the operators in the first group which can be written, without loose of generality, as

$$O_1 = \text{Tr}[\partial_\mu U(\xi^\dagger \bar{B} \xi^\dagger) \partial^\mu U(\xi^\dagger B \xi^\dagger)], \tag{D.15}$$

where $\xi \equiv U^{1/2}$. From the potential of U we found that $U = \langle U \rangle U'$ and $U^\dagger \equiv U'^\dagger \langle U' \rangle$. Therefore, O_1 becomes

$$O_1 = \text{Tr}[\partial_\mu U'(\xi^\dagger \bar{B} \xi^\dagger) \langle U \rangle \partial^\mu U'(\xi^\dagger B \xi^\dagger) \langle U \rangle]. \tag{D.16}$$

Since $\xi = U^{1/2}$, we know that $\langle \xi \rangle = \langle U \rangle^{1/2}$. Since generically, $\langle U \rangle$ does not commute with U', it is very difficult to write down ξ' in terms of U'. However, we can always redefine the baryon field B to make that

$$\xi B \xi = \langle U \rangle \xi' B' \xi', \tag{D.17}$$

where $\xi' = U'^{1/2}$, and B' is a collection of physical baryon fields. From the above relation one can easily get that

$$\xi^\dagger \bar{B} \xi^\dagger = \xi'^\dagger \bar{B}' \xi'^\dagger \langle U \rangle^\dagger$$

$$\xi \bar{B} \xi = \langle U \rangle \xi' \bar{B}' \xi'$$

$$\xi^\dagger B \xi^\dagger = \xi'^\dagger B' \xi'^\dagger \langle U \rangle^\dagger \tag{D.18}$$

183

After this co-transformation of baryon fields, one can get

$$O_1 = \text{Tr}[\partial_\mu U'(\xi'^\dagger \bar{B}' \xi'^\dagger) \partial^\mu U'(\xi'^\dagger B' \xi'^\dagger)], \qquad (\text{D.19})$$

from which one can say that O_1 is not bothered by the vev of U if one applies a suitable co-transformation of B.

Now, let's consider the terms in the breaking the chiral symmetry explicitly. A typical operator in this group is

$$O_2 = C_2 \text{Tr}[M^\dagger \xi \bar{B} B \xi] + C_2 \text{Tr}[\xi^\dagger \bar{B} B \xi^\dagger M] \qquad (\text{D.20})$$

For the baryon field, we perform the above co-transformation, and it is easy to see that

$$\xi \bar{B} B \xi = \langle U \rangle \xi' \bar{B}' B' \xi' \qquad (\text{D.21})$$

Therefore, we can get

$$O_2 = C_2 \left(\text{Tr}[(M^\dagger \langle U \rangle) \xi' \bar{B}' B' \xi'] + \text{Tr}[\xi'^\dagger \bar{B}' B' \xi'^\dagger \langle U \rangle^\dagger M] \right). \qquad (\text{D.22})$$

And it is easy to see that

$$M^\dagger \langle U \rangle = \langle U \rangle^\dagger M = \mathcal{M}. \qquad (\text{D.23})$$

Therefore,

$$O_2 = C_2 \text{Tr}[\mathcal{M}(\xi' \bar{B}' B' \xi' + \xi'^\dagger \bar{B}' B' \xi'^\dagger)] \qquad (\text{D.24})$$

from which one can see that there is no CP-violation in the redefined Lagrangian. The redefinition of the meson field is by no doubt due to the meson condensate. Therefore, in another way the meson condensate contribution cancels the direct matching contribution so that there is no CP-violation observable in the system.

Bibliography

[1] R. N. Mohapatra and J. C. Pati, Phys. Rev. D **11**, 566 (1975); R. N. Mohapatra and J. C. Pati, Phys. Rev. D **11**, 2558 (1975); R. N. Mohapatra and G. Senjanovic, Phys. Rev. Lett. **44**, 912 (1980). G. Senjanovic and R. N. Mohapatra, Phys. Rev. D **12**, 1502 (1975); Phys. Rev. D **23**, 165 (1981); For a review, Rabindra N. Mohapatra, *CP Violation*, World Scientific Publ. Co., C. Jarlskog, Ed., 1989.

[2] T. D. Lee, talk given at the Center for High-Energy Physics, Peking University, Nov. 2006.

[3] Y. Zhang, H. An, X. Ji and R. N. Mohapatra, Phys. Rev. D **76**, 091301 (2007) [arXiv:0704.1662 [hep-ph]]; Y. Zhang, H. An, X. Ji and R. N. Mohapatra, arXiv:0712.4218 [hep-ph].

[4] E. P. Shabalin, Sov. J. Nucl. Phys. **28**, 75 (1978) [Yad. Fiz. **28**, 151 (1978)]. A. Czarnecki and B. Krause, Phys. Rev. Lett. **78**, 4339 (1997) [arXiv:hep-ph/9704355]. D. V. Nanopoulos, A. Yildiz and P. H. Cox, Phys. Lett. B **87**, 53 (1979).

[5] I. I. Y. Bigi and A. I. Sanda, Camb. Monogr. Part. Phys. Nucl. Phys. Cosmol. **9**, 1 (2000).

[6] V. Baluni, Phys. Rev. D **19**, 2227 (1979).

[7] R. J. Crewther, P. Di Vecchia, G. Veneziano and E. Witten, Phys. Lett. B **88**, 123 (1979) [Erratum-ibid. B **91**, 487 (1980)].

[8] A. Pich and E. de Rafael, Nucl. Phys. B **367**, 313 (1991).

[9] M. Pospelov and A. Ritz, Phys. Rev. Lett. **83**, 2526 (1999) [arXiv:hep-ph/9904483].

[10] M. Pospelov and A. Ritz, Nucl. Phys. B **573**, 177 (2000) [arXiv:hep-ph/9908508].

[11] X. G. He, B. H. J. McKellar and S. Pakvasa, Int. J. Mod. Phys. A **4**, 5011 (1989) [Erratum-ibid. A **6**, 1063 (1991)].

[12] G. Beall and A. Soni, Phys. Rev. Lett. **47**, 552 (1981).

[13] S. Abel and S. Khalil, Phys. Lett. B **618**, 201 (2005) [arXiv:hep-ph/0412344].

[14] M. Pospelov and A. Ritz, Phys. Rev. D **63**, 073015 (2001) [arXiv:hep-ph/0010037].

[15] W. H. Hockings and U. van Kolck, Phys. Lett. B **605**, 273 (2005) [arXiv:nucl-th/0508012].

[16] J. Erler and M. J. Ramsey-Musolf, Prog. Part. Nucl. Phys. **54**, 351 (2005) [arXiv:hep-ph/0404291].

[17] M. Pospelov and A. Ritz, Annals Phys. **318**, 119 (2005) [arXiv:hep-ph/0504231].

[18] V. M. Khatsimovsky, I. B. Khriplovich and A. S. Yelkhovsky, Annals Phys. **186**, 1 (1988).

[19] G. Valencia, Phys. Rev. D **41**, 1562 (1990).

[20] X. G. He and B. McKellar, Phys. Rev. D **47**, 4055 (1993).

[21] R. Babich, N. Garron, C. Hoelbling, J. Howard, L. Lellouch and C. Rebbi, Phys. Rev. D **74**, 073009 (2006) [arXiv:hep-lat/0605016].

[22] S. Scherer, Adv. Nucl. Phys. **27**, 277 (2003) [arXiv:hep-ph/0210398].

[23] V. Bernard, N. Kaiser and U. G. Meissner, Int. J. Mod. Phys. E **4**, 193 (1995) [arXiv:hep-ph/9501384].

[24] S. N. Gninenko, M. M. Kirsanov, N. V. Krasnikov and V. A. Matveev, Phys. Atom. Nucl. **70**, 441 (2007).

[25] C. E. Aalseth *et al.* [CoGeNT collaboration], arXiv:1002.4703 [astro-ph.CO].

[26] W.Seidel *et. al.* [CRESST collaboration], Talk given at IDM2010, July 2010.

[27] E. Aprile *et al.* [XENON100 Collaboration], Phys. Rev. Lett. **105**, 131302 (2010) [arXiv:1005.0380 [astro-ph.CO]].

[28] R. D. C. Miller and B. H. J. McKellar, Phys. Rept. **106**, 169 (1984).

[29] S. Weinberg, Phys. Rev. Lett. **63**, 2333 (1989).

[30] E. Braaten, C. S. Li and T. C. Yuan, Phys. Rev. Lett. **64**, 1709 (1990).

[31] J. M. Frere, J. Galand, A. Le Yaouanc, L. Oliver, O. Pene and J. C. Raynal, Phys. Rev. D **45**, 259 (1992).

[32] M. A. Shifman, A. I. Vainshtein and V. I. Zakharov, Phys. Rev. D **18**, 2583 (1978) [Erratum-ibid. D **19**, 2815 (1979)].

[33] C. A. Baker *et al.*, Phys. Rev. Lett. **97**, 131801 (2006) [arXiv:hep-ex/0602020].

[34] K. S. Babu, B. Dutta and R. N. Mohapatra, Phys. Rev. D **65**, 016005 (2002) [arXiv:hep-ph/0107100]. R. N. Mohapatra, A. Rasin and G. Senjanovic, Phys. Rev. Lett. **79**, 4744 (1997) [arXiv:hep-ph/9707281]. R. N. Mohapatra and A. Rasin, Phys. Rev. Lett. **76**, 3490 (1996) [arXiv:hep-ph/9511391]. K. S. Babu and R. N. Mohapatra, Phys. Rev. D **41**, 1286 (1990). R. N. Mohapatra and G. Senjanovic, Z. Phys. C **20**, 365 (1983).

[35] R. D. Peccei and H. R. Quinn, Phys. Rev. Lett. **38**, 1440 (1977). R. D. Peccei and H. R. Quinn, Phys. Rev. D **16**, 1791 (1977).

[36] S. Weinberg, Phys. Rev. D **11**, 3583 (1975).

[37] J. E. Kim, Phys. Rev. Lett. **43**, 103 (1979).

[38] M. A. Shifman, A. I. Vainshtein and V. I. Zakharov, Nucl. Phys. B **166**, 493 (1980).

[39] T. Falk, K. A. Olive, M. Pospelov and R. Roiban, Nucl. Phys. B **560**, 3 (1999) [arXiv:hep-ph/9904393].

[40] S. L. Adler, Phys. Rev. **177**, 2426 (1969). J. S. Bell and R. Jackiw, Nuovo Cim. A **60**, 47 (1969).

[41] G. 't Hooft, Nucl. Phys. B **72**, 461 (1974).

[42] A. V. Manohar, arXiv:hep-ph/9802419.

[43] A. Manohar and H. Georgi, Nucl. Phys. B **234**, 189 (1984).

[44] O. W. Greenberg, Phys. Rev. Lett. **13**, 598 (1964).

[45] D. Faiman and A. W. Hendry, Phys. Rev. **173**, 1720 (1968).

[46] J. F. Donoghue and G. Karl, Phys. Rev. D **24**, 230 (1981) [Erratum-ibid. D **26**, 1804 (1982)].

[47] R. Koniuk and N. Isgur, Phys. Rev. D **21**, 1868 (1980) [Erratum-ibid. D **23**, 818 (1981)].

[48] J. F. Donoghue, E. Golowich and B. R. Holstein, Camb. Monogr. Part. Phys. Nucl. Phys. Cosmol. **2**, 1 (1992).

[49] A. Chodos, R. L. Jaffe, K. Johnson, C. B. Thorn and V. F. Weisskopf, Phys. Rev. D **9**, 3471 (1974).

[50] K. Johnson, Phys. Lett. B **78**, 259 (1978).

[51] A. Chodos, R. L. Jaffe, K. Johnson and C. B. Thorn, Phys. Rev. D **10**, 2599 (1974).

[52] T. A. DeGrand, R. L. Jaffe, K. Johnson and J. E. Kiskis, Phys. Rev. D **12**, 2060 (1975).

[53] G. Ecker, W. Grimus and H. Neufeld, Nucl. Phys. B **229**, 421 (1983).

[54] C. Amsler *et al.* [Particle Data Group], Phys. Lett. B **667**, 1 (2008).

[55] J. L. Goity, R. Lewis, M. Schvellinger and L. Z. Zhang, Phys. Lett. B **454**, 115 (1999) [arXiv:hep-ph/9901374].

[56] V. Bernard, N. Kaiser and U. G. Meissner, Z. Phys. C **70**, 483 (1996) [arXiv:hep-ph/9411287].

[57] J. F. Donoghue and B. R. Holstein, Phys. Rev. D **33**, 2717 (1986).

[58] G. Feinberg, P. Kabir and S. Weinberg, Phys. Rev. Lett. **3**, 527 (1959).

[59] K. Kiers, J. Kolb, J. Lee, A. Soni and G. H. Wu, Phys. Rev. D **66**, 095002 (2002) [arXiv:hep-ph/0205082].

[60] D. Chang, C. S. Li and T. C. Yuan, Phys. Rev. D **42**, 867 (1990).

[61] R. L. Arnowitt, J. L. Lopez and D. V. Nanopoulos, Phys. Rev. D **42**, 2423 (1990).

[62] R. L. Arnowitt, M. J. Duff and K. S. Stelle, Phys. Rev. D **43**, 3085 (1991).

[63] V. M. Khatsymovsky and I. B. Khriplovich, Phys. Lett. B **296**, 219 (1992).

[64] D. A. Demir, M. Pospelov and A. Ritz, Phys. Rev. D **67**, 015007 (2003) [arXiv:hep-ph/0208257].

[65] H. An, X. Ji and F. Xu, arXiv:0908.2420 [hep-ph].

[66] C. S. Aulakh, K. Benakli and G. Senjanovic, Phys. Rev. Lett. **79**, 2188 (1997) [arXiv:hep-ph/9703434]. C. S. Aulakh, A. Melfo, A. Rasin and G. Senjanovic, Phys. Rev. D **58**, 115007 (1998) [arXiv:hep-ph/9712551]. R. N. Mohapatra and A. Rasin, Nucl. Phys. Proc. Suppl. **52A**, 182 (1997).

[67] Y. Zhang, H. An and X. d. Ji, Phys. Rev. D **78**, 035006 (2008) [arXiv:0710.1454 [hep-ph]].

[68] J. Goodman, M. Ibe, A. Rajaraman, W. Shepherd, T. M. P. Tait and H. B. P. Yu, arXiv:1005.1286 [hep-ph]. J. Goodman, M. Ibe, A. Rajaraman, W. Shepherd, T. M. P. Tait and H. B. P. Yu, arXiv:1008.1783 [hep-ph].

[69] Y. Bai, P. J. Fox and R. Harnik, arXiv:1005.3797 [hep-ph].

[70] T. Aaltonen *et al.* [CDF Collaboration], Phys. Rev. Lett. **101**, 181602 (2008) [arXiv:0807.3132 [hep-ex]].

[71] K. Nakamura *et al.* [Particle Data Group], J. Phys. G **37**, 075021 (2010).

[72] J. L. Feng, A. Rajaraman and F. Takayama, Phys. Rev. Lett. **91**, 011302 (2003) [arXiv:hep-ph/0302215].

[73] S. Nussinov, Phys. Lett. B **165**, 55 (1985).

[74] J. Alcaraz *et al.* [ALEPH Collaboration and DELPHI Collaboration and L3 Collaboration and], arXiv:hep-ex/0612034.

[75] M. S. Carena, A. Daleo, B. A. Dobrescu and T. M. P. Tait, Phys. Rev. D **70**, 093009 (2004) [arXiv:hep-ph/0408098].

[76] H. C. Cheng, J. L. Feng and K. T. Matchev, Phys. Rev. Lett. **89**, 211301 (2002) [arXiv:hep-ph/0207125].

[77] D. E. Kaplan, G. Z. Krnjaic, K. R. Rehermann and C. M. Wells, JCAP **1005**, 021 (2010) [arXiv:0909.0753 [hep-ph]].

[78] X. G. He, S. Y. Ho, J. Tandean and H. C. Tsai, Phys. Rev. D **82**, 035016 (2010) [arXiv:1004.3464 [hep-ph]].

[79] T. Aaltonen *et al.* [CDF Collaboration], Phys. Rev. **D79**, 112002 (2009). [arXiv:0812.4036 [hep-ex]].

[80] V. M. Abazov *et al.* [D0 Collaboration], [arXiv:1009.2444 [hep-ex]].

[81] A. Pukhov, arXiv:hep-ph/0412191.

[82] H. An, S. L. Chen, R. N. Mohapatra, S. Nussinov and Y. Zhang, Phys. Rev. D **82**, 023533 (2010) [arXiv:1004.3296 [hep-ph]].

[83] S. Chang, N. Weiner and I. Yavin, arXiv:1007.4200 [hep-ph].

[84] V. Barger, W. Y. Keung and D. Marfatia, arXiv:1007.4345 [hep-ph].

[85] A. L. Fitzpatrick and K. M. Zurek, Phys. Rev. D **82**, 075004 (2010) [arXiv:1007.5325 [hep-ph]].

[86] T. Banks, J. F. Fortin and S. Thomas, arXiv:1007.5515 [hep-ph].

[87] D. B. Kaplan and A. Manohar, Nucl. Phys. B **310**, 527 (1988).

[88] M. A. Shifman, A. I. Vainshtein and V. I. Zakharov, Phys. Lett. B **78**, 443 (1978).

[89] X. d. Ji and D. Toublan, Phys. Lett. B **647**, 361 (2007) [arXiv:hep-ph/0605055].

[90] J. Fan, M. Reece and L. T. Wang, arXiv:1008.1591 [hep-ph].

[91] G. Belanger, F. Boudjema, A. Pukhov and A. Semenov, Comput. Phys. Commun. **180**, 747 (2009) [arXiv:0803.2360 [hep-ph]].

[92] E. W. . Kolb and M. S. . Turner, *REDWOOD CITY, USA: ADDISON-WESLEY (1988) 719 P. (FRONTIERS IN PHYSICS, 70)*

[93] G. Belanger, F. Boudjema, P. Brun, A. Pukhov, S. Rosier-Lees, P. Salati and A. Semenov, arXiv:1004.1092 [hep-ph].

[94] J. Preskill, Annals Phys. **210**, 323 (1991).

[95] P. Langacker and M. Plumacher, Phys. Rev. D **62**, 013006 (2000) [arXiv:hep-ph/0001204].

[96] R. S. Chivukula and E. H. Simmons, Phys. Rev. D **66**, 015006 (2002) [arXiv:hep-ph/0205064].

[97] P. F. Harrison, D. H. Perkins and W. G. Scott, Phys. Lett. B **530**, 167 (2002) [arXiv:hep-ph/0202074].

[98] J. Kopp, T. Schwetz and J. Zupan, JCAP **1002**, 014 (2010) [arXiv:0912.4264 [hep-ph]].

[99] B. Bajc, M. Nemevsek and G. Senjanovic, Phys. Lett. B **684**, 231 (2010) [arXiv:0911.1323 [hep-ph]].

[100] A. Maiezza, M. Nemevsek, F. Nesti and G. Senjanovic, Phys. Rev. D **82**, 055022 (2010) [arXiv:1005.5160 [hep-ph]].

[101] P. Chen, H. Ke and X. Ji, Phys. Lett. B **677**, 157 (2009) [arXiv:0810.2576 [hep-ph]].

[102] W. C. Griffith, M. D. Swallows, T. H. Loftus, M. V. Romalis, B. R. Heckel and E. N. Fortson, Phys. Rev. Lett. **102**, 101601 (2009).

[103] Z. Q. Ma, *"Group Theory for Physicists"*, World Scientific, (2007).